Argonne National Laboratory

REACTOR DEVELOPMENT PROGRAM PROGRESS REPORT

March 1971

Printed in the United States of America
Available from
National Technical Information Service
U.S. Department of Commerce
5285 Port Royal Road
Springfield, Virginia 22151
Price: Printed Copy $3.00; Microfiche $0.95

NOTICE

This issue of the Reactor Development Program Progress Report inaugurates a new format. Instead of the budget-oriented arrangement used before, the accounts are now divided into nine major sections, corresponding to the nine areas of the Laboratory's reactor program. However, the "189a" numbers that identify the "funding item" for each narrative account are retained for the benefit of readers concerned with this matter. Further, a listing of 189a numbers, together with an indication of the items reported and the section in which each appears, is included in the front matter. The Highlights are also presented by program area, although it is not intended that there be Highlights for all sections every month.

We hope that this new arrangement proves helpful to our readers.

ANL-7798
Reactor Technology

ARGONNE NATIONAL LABORATORY
9700 South Cass Avenue
Argonne, Illinois 60439

REACTOR DEVELOPMENT PROGRAM PROGRESS REPORT

March 1971

Robert B. Duffield, Laboratory Director
Robert V. Laney, Associate Laboratory Director

	Program Area	Lead Division	Division Director/ Program Manager
I	EBR-II	EBR-II	M. Levenson
II	LMFBR Design Support	ETD	S. A. Davis
III	Instrumentation and Control	ETD	S. A. Davis
IV	Sodium Technology	CEN	R. C. Vogel/L. Burris
V	Fuels and Materials Development	MSD	P. G. Shewmon
VI	Fuel Cycle	CEN	R. C. Vogel/D. S. Webster
VII	Reactor Physics	AP	R. Avery
VIII	Reactor Safety	RAS	W. R. Simmons
IX	Environmental Studies	CES	L. E. Link

Report Coordinator: M. Weber

Issued: April 19, 1971

FOREWORD

The Reactor Development Program Progress Report describes current activities, technical progress, and technical problems in the program at Argonne National Laboratory sponsored by the USAEC Division of Reactor Development and Technology. Not all projects are reported every month, but a running account of each project is maintained in the series of reports.

The last six reports
in this series are:

September 1970	ANL-7742
October 1970	ANL-7753
November 1970	ANL-7758
December 1970	ANL-7765
January 1971	ANL-7776
February 1971	ANL-7783

REACTOR DEVELOPMENT PROGRAM

Highlights of Project Activities for March 1971

EBR-II

EBR-II was started up March 2 and reached full power of 62.5 MWt on March 4. From startup through March 15, it operated for 505 MWd in Run 47B, bringing its accumulated operational total to 42,321 MWd. Careful monitoring of noise and performance of the intermediate heat exchanger (IHX) and both primary pumps shows that their operation is satisfactory. During the maintenance shutdown, the IHX 1-in.-dia drain tube, which was found to be loose and causing the unusual noise reported earlier, had been removed. Also during the shutdown, the No. 1 primary pump had been removed from the primary tank, disassembled, cleaned, inspected, given minor repair, reassembled, and reinstalled. The pump had been immersed continuously in hot sodium for more than seven years.

LMFBR DESIGN SUPPORT

Flowtesting of FFTF Mark-II Fuel Assembly

On March 23, 1971, the FFTF Mark-II fuel assembly was removed from the Core Component Test Loop (CCTL) after 6287 hr of flowtesting in sodium at full flow (525 gpm) and temperature (1100°F). Loop downtime during the test was only 15.8 hr, yielding an operating factor greater than 99%. The fuel assembly will be examined by FFTF staff at Hanford.

INSTRUMENTATION AND CONTROL

Long-term High-temperature Stability of Permanent-magnet Materials

Long-term high-temperature stability of permanent-magnet materials is a key factor in several sensors being developed to monitor sodium flow in an LMFBR. Intermediate test results at 3200 hr indicate that the maximum long-term operating temperature (without irreversible degradation of magnetic properties) is between 1000 and 1100°F for Alnico V, and between 1100 and 1200°F for Alnico VIII.

Radiation Tolerance of Lithium Niobate

Lithium niobate crystalline material is a leading candidate for high-temperature, radiation-resistant piezoelectric components in accelerometers and ultrasonic detectors for the LMFBR Program. Irradiations by 2-MeV Van de Graaff electrons and by ^{60}Co gamma photons show that lithium niobate has exceptional radiation stability, comparable to close-packed oxides such as sapphire.

SODIUM TECHNOLOGY

Argonne has the responsibility of certifying sampling and analytical methods for use throughout the sodium-technology program. To meet near-term needs, a set of interim standard methods has been established with the aid of an advisory group representing both reactor and nonreactor laboratories. Procedural details of these methods are described in a manual titled Interim Methods for the Analysis of Sodium and Cover Gas, being published as ANL/ST-6.

FUEL CYCLE

Apparatus has been constructed for demonstrating a continuous fluid-bed denitration process for converting uranium/plutonium nitrate solutions to mixed-oxide powders suitable for fabricating LMFBR fuel shapes. Because of the growing concern over the shipment of plutonium as nitrate solution, ready conversion of plutonium-containing solutions to a solid form is important. In the selection of the feed composition for the fluid-bed denitration process, solubility limits of uranium/plutonium nitrate solutions are being measured to allow use of high plutonium concentrations while yet avoiding precipitation of plutonium compounds. Results indicate that the substitution of plutonium for uranium in a nitrate solution lowers the crystallization temperature, allowing relatively concentrated actinide solutions to be processed: A feed solution with a composition of 1.44M uranyl nitrate, 0.36M plutonium nitrate, and 2.0M nitric acid can safely be used at room temperature for making powders containing 20% PuO_2. The crystallization temperature for this solution is ~13°C.

REACTOR PHYSICS

The Engineering Mockup Critical (EMC) for the FTR (ZPR-9 Assembly 27), simulating the fissile mass, volume, and test-loop and control-rod locations of that reactor at end of cycle (EOC), attained initial criticality on March 4. A modified reactor (EOC-2), changed to accommodate subsequent major FFTF core-map design changes, was made critical on March 18.

A calculation of the isothermal Doppler coefficient in FTR at the beginning of its equilibrium cycle shows it to be negative and well-approximated by the Doppler effect in ^{238}U.

Consistent with previous observation, calculated central reaction-rate ratios for fissile and fertile isotopes in FTR-2 (ZPPR Assembly 1) and FTR-3 (ZPR-9 Assembly 26) are smaller than measured values.

Radial reactivity worths of Na, Pu, ^{238}U, SS, and Ta were determined in a single-zone plutonium-fueled reference assembly (ZPR-6 Assembly 7) with the use of a calibrated autorod. Preliminary studies of the sensitivity of k_{eff}, reaction rates, and spectra to cross-section variation in this assembly have begun.

REACTOR SAFETY

In the coolant-dynamics program, incipient-boiling superheat data obtained with sodium from EBR-II continue to demonstrate the key influence of (1) the system pressure-temperature history and (2) the partial pressure of inert gas in the surface cavities. Data from tests in which an e-m pump applied pressure to the sodium (thus, no inert gas was introduced) show considerable scatter, unless the pressure-temperature history is reestablished for at least 20 min between test runs. Tests in which an argon cover gas was used to apply pressure to the system demonstrate again that inert gas in the surface cavities significantly reduces the incipient-boiling superheat. With certain assumptions, the pressure-temperature-history model and the experimental data agree excellently.

ENVIRONMENTAL STUDIES

Eleven temperature recorders were set on the bottom of Lake Michigan within the area of influence of the thermal discharge of the Point Beach, Wisconsin, nuclear-power plant. The instruments will record lake-bottom water temperatures for two months. The purpose of the experiment is to observe whether a sinking thermal plume will have a significant effect on the water temperature near the lake bottom. The problem is related to the potential for premature hatching of fish eggs.

TABLE OF CONTENTS

TABLE OF CONTENTS

TABLE OF CONTENTS

TABLE OF CONTENTS

TABLE OF CONTENTS

TABLE OF CONTENTS

TABLE OF CONTENTS

Listing of Reportable
ANL Reactor Development Program Projects
in 189a Order

189a No.	Reported This Month in Section	189a Title	RDT Branch
02-005	V	Oxide Fuel Studies	RT-FM
02-009		General Fast Reactor Physics	RT-PH
02-010		Fast Critical Experiments; Theoretical Support--Idaho	RT-PH
02-011		Fast Critical Experiments; Experimental Support--Idaho	RT-PH
02-012		Fast Critical Experiments; Industrial Appointments	RT-PH
02-013	VII	Fast Critical Experiments; Experimental Support--Illinois	RT-PH
02-015	VII	Planning and Evaluation of FFTF Critical Assembly Experiments	RT-PH
02-019		Production of Materials for ZPR Experiments	RE-FE
02-020		ZPR Materials Procurement	RE-FE
02-021	IV	Monitoring and Sampling Systems Development and Reactor Proof-test	RT-CC
02-024	III	Instrumentation Development for Instrumented Subassembly	PE-IC
02-025	III	FFTF Instrumentation Development	PE-IC
02-026	II	Core Component Test Loop (CCTL)	RE-CD
02-045		Equipment--Fuel Related	RE-FH
02-046		New Subassemblies and Experimental Support	RE-CD
02-048	I	Instrumented Subassemblies	RE-CD
02-051	I	Coolant Chemistry	RT-CC
02-053	I	Experimental Irradiation and Testing	RT-FM
02-061		Nuclear Instrument Test Facility	PE-IC
02-063	I	Materials-Coolant Compatibility	RT-CC
02-068	I	Systems Engineering	PE-LS
02-073	I	Fuel and Hardware Procurement	RE-FE
02-075	I	Reactor Operations	PE-LS
02-076	I	Fuels and Examination Facility (FEF)	RE-FE
02-081	VII	Theoretical Reactor Physics	RT-PH
02-082		Cross-section Measurements	RT-PH
02-083		Burnup Analysis and Fission Yields for Fast Reactors	RT-PH
02-084		Determination of Nuclear Constants	RT-PH
02-085	VII	Reactor Code Center	RT-PH
02-086	V	Behavior of Reactor Materials	RT-FM
02-087		Chemistry of Irradiated Fuel Materials	RT-FM
02-088		Thermodynamics of Carbide Fuel	FT-FM
02-091		Creep, Fracture, and Fatigue Studies on Stainless Steel	RT-FM

189a No.	Reported This Month in Section	189a Title	RDT Branch
02-092	V	Nondestructive Testing Research and Development	RT-FM
02-094	V	High-temperature Properties of Ceramic Fuels	RT-FM
02-096	III	Advanced Technology Instrument Development	RT-ST
02-097		Heat Transfer and Fluid Flow	RT-ST
02-099		Engineering Mechanics	RT-ST
02-112		Accident Analysis and Safety Evaluation	NS-FS
02-114	VIII	Coolant Dynamics	NS-FS
02-115	VIII	Core Structural Safety	NS-FS
02-116	VIII	Fuel-element Failure Propagation	NS-FS
02-117	VIII	Fuel Dynamics Studies in TREAT	NS-FS
02-119	VIII	High-temperature Physical Properties and Equation-of-state of Reactor Materials	NS-FS
02-120		Fast Reactor Safety Test Facility Study	NS-FS
02-122	VIII	TREAT Operations	NS-RD
02-126	VIII	Reactor System and Containment Structural Dynamic Response	NS-FS
02-131	I	EBR-II In-core Instrument Test Facility	PE-IC
02-133		NDT Measurement of Effective Cold Work in Cladding Tubes	RT-FM
02-134	VII	Fast Critical Experiments; Theoretical Support--Illinois	RT-PH
02-137	IV	Nonmetallic Impurity Interactions in Sodium-Metal Systems	RT-CC
02-138		Neutron-detector Channel Development	PE-IC
02-144		Reactor Analysis, Testing, and Methods Development	RE-CD
02-145	I	Metal Driver Fuel Development and Application	RE-FE
02-148		Operation with Failed Fuel	RE-CD
02-150	I	Hot Fuel Examination Facilities	PE-FH
02-151		Characterization of Irradiation Environment	RE-CD
02-156	IV	Sodium Impurity Analysis and Control	RT-CC
02-157	VI	LMFBR Fuel Materials Preparation--U/Pu Nitrates to Oxides	RT-FR
02-158	VI	LMFBR Fuel Fabrication--Analyses and Continuous Processing	RT-FR
02-159	VI	LMFBR Reprocessing--Plutonium Isolation	RT-FR
02-162		Thermophysical Properties of Reactor Fuels	RT-FR
02-164	VIII	Fuel-Coolant Interactions	NS-FS
02-165	VIII	Post-accident Heat Removal	NS-FS
02-166	IX	Thermal-plume Dispersion Studies	PA
02-173	VI	Molten Metal Decladding of LMFBR Fuels	RT-FR
02-175	V	Physical and Chemical Studies--Molten Fuel, Cladding, and Coolant	RT-FR
02-178		ZPR-6 and -9 Operations and Maintenance	RT-PH

189a No.	Reported This Month in Section	189a Title	RDT Branch
02-179	VII	Fast Critical Facilities; Experiments and Evaluations--Illinois	RT-PH
02-180		ZPPR Operations and Maintenance	RT-PH
02-181	VII	Fast Critical Facilities; Experiments and Evaluations--Idaho	RT-PH
02-184		Mass/Energy Balance of the Great Lakes	PA
02-185	IX	Lake Circulation Model Development	PA
02-194	I	Surveillance and Failure Evaluation of Experimental Fuel Irradiations	RT-FM
02-195		Scram-system Study	PE-LS
02-197		TREAT Improvement Studies	PM-EB
02-200		Conceptual Design Study of FFTF Vessel Head-cavity System	RE-CD
02-509	IV	Sodium Chemistry and Radioactive Contaminant Behavior	RT-CC
02-526		In-pile Stainless Steel Swelling and Mechanical Behavior	RT-FM
02-528	III	Plant Dynamics and Control Analysis	PE-IC
02-530		Operation of Data Acquisition System (DAS)	PE-IC

I. EXPERIMENTAL BREEDER REACTOR NO. II

A. Operations

1. Reactor Operations. G. E. Deegan (02-075; last reported: ANL-7776, pp. 41-42, Jan 1971)

The maintenance shutdown was completed, and the reactor has been operated for 505 MWd in Run 47B. The accumulated total of EBR-II operation now is 42,321 MWd.

During the shutdown, the drain tube of the intermediate heat exchanger (IHX) was cut with a pneumatic shear tool and removed from the secondary-sodium inlet line of the IHX. A final internal inspection of the IHX revealed no foreign objects and confirmed the integrity of the baffle section. Closure welding of the inlet elbow was then performed.

After the components of the No. 1 primary pump were cleaned and inspected, several minor changes and relocations were made in the pump. The pump was then reassembled, with a new lower-labyrinth seal, and reinstalled in the primary tank. A manual-rotation check of the pump showed that the shaft turned freely.

All systems were heated to 350°F, and the secondary system was filled. Operation of the secondary system at 50% flow produced no unusual noise in the IHX, and heatup of the systems to plant standby continued. At 580°F, the IHX was monitored over a full range of primary and secondary flows; no unusual noises were heard. The primary pumps operated satisfactorily, and a complete set of performance data and noise measurements was taken for each pump.

Fuel handling for Run 47B was conducted while the primary tank was being heated from 580 to 700°F. Difficulty with actuating the No. 8 control-rod jaws necessitated changing of the rod-drive assembly.

The reactor was started up on March 2, and a slow, deliberate approach to power was made to obtain proper operation, adjustment, and calibration of all systems. Full power was attained on March 4 at 0210. On the following day, power was reduced for rod drops at 0.05, 0.5, 50, 56, and 62.5 MWt. A small fission-gas release was observed on March 12. Operation continued until the occurrence of a second release that raised the ^{133}Xe activity to a level greater than five times normal background. At this time, an anticipatory reactor shutdown was made.

The seal trough of the large plug was cleaned. Scheduled replacement of three control-rod thimbles is in progress.

Fuel handling for Run 47B involved experimental subassemblies, as reported under Sect. I.A.4.a, and also included the following: The high-worth control rod and one surveillance subassembly of Mark-II driver fuel were relocated. One outer-blanket, materials-survey subassembly had completed its planned irradiation and was removed from the grid. The xenon-tag test subassembly was reinstalled in the grid to complete its irradiation. Two dummy structural subassemblies, installed before the cool-down, were removed, and the necessary reactivity adjustment was made before the startup for Run 47B.

2. Fuels and Examination Facility (FEF). M. J. Feldman (02-076)

a. Fuel Assembly. D. L. Mitchell (Last reported: ANL-7776, pp. 42-43, Jan 1971)

Fourteen Mark-IA subassemblies were assembled in the cold line during this reporting period. Of these subassemblies, six were made up of elements cast by the vendor and impact-bonded by ANL, and eight were made up of centrifugally bonded vendor-fabricated elements that had been heat-treated by ANL (see Sect. I.A.3.a). Vendor-fabricated elements that had been accepted by ANL verification inspection are being heat-treated to reclaim them.

Table I.1 summarizes the production activities for January 16 through March 15, 1971, and for fiscal year 1971.

TABLE I.1. Production Summary for FEF Cold Line

	1/16/71 through 3/15/71		Total for FY 1971
Subassemblies Fabricated with Mark-IA Fuel			
With Cold-line elements	0		2
With Vendor elements	14		80
Preirradiation Treatment of Vendor Mark-IA Fuel			
Heat treating of as-fabricated elements (22,614[a])			
Heat-treated, inspected, and accepted	3573		9533
Heat-treated, inspected, and rejected[b]	1398		3038
Total Elements Available for Subassembly Fabrication as of 3/15/71			
Cold-line fuel			
Mark IA		199	
Mark II		223	
Vendor fuel (Mark IA)			
Impact-bonded[c]		208	
Heat-treated		9371	

[a]These elements, cast and centrifugally bonded by the vendor, have been accepted by ANL verification inspection, but not yet approved for general use in the reactor. They are being heat-treated to reclaim them. (See Sect. I.A.3.a.)
[b]Void size in the sodium bond is the principal cause for rejection. Elements rejected for this reason may be reclaimed by impact-bonding. (See Sect. I.A.3.a.)
[c]Impact-bonding by ANL of 11,853 unbonded vendor fuel elements was completed in fiscal year 1970.

b. Fuel Handling and Transfer. N. R. Grant, W. L. Sales, and K. DeCoria (Last reported: ANL-7776, pp. 42-44, Jan 1971)

Table I.2 summarizes the fuel-handling operations performed.

TABLE I.2. Summary of FEF Fuel Handling

	1/16/71 through 3/15/71	Total for FY 1971
Subassembly Handling		
Subassemblies Received from Reactor		
Driver fuel (all types)	3	70
Experimental	1	31
Other (blanket)	0	27
Subassemblies Dismantled for Surveillance, Examination, or Shipment to Experimenter		
Driver fuel	0	37
Experimental	2	32
Other (blanket)	0	5
Driver-fuel Elements to Surveillance	0	1495
Number from subassemblies	0	28
Subassemblies Transferred to Reactor		
Driver fuel		
From air cell	0	6
From cold line[a]	6	68
Experimental	9	29
Fuel-alloy and Waste Shipments		
Cans to Burial Ground	2	15
Blanket Subassemblies to Burial Ground	0	17
Recoverable Fuel Alloy to ICPP		
Fuel elements[b]	1 (17.52 kg)	14 (244.63 kg)
Subassemblies[b]	3 (17.47 kg)	34 (173.50 kg)
Consolidation ingots[b]	1 (13.46 kg)	1 (13.46 kg)
Nonspecification material	0	0
Skull oxide and glass scrap	0	0

[a] Cold-line subassemblies, after fabrication and final tests, are transferred either to the reactor or to the special-materials vaults for interim storage until needed for use in the reactor.

[b] Figure outside parentheses is number of shipments made; figure inside is weight of alloy shipped.

c. Reactor Support. J. P. Bacca and N. R. Grant (Last reported: ANL-7776, p. 45, Jan 1971)

Three new control-rod thimbles were modified for future reactor operation. Measurements of irradiated thimbles had indicated that their overall length had increased up to 1/4 in. (See Progress Report for October 1970, ANL 7753, p. 99.) Since this could have (and may have) interfered with handling of subassemblies in the reactor (see ANL-7753, p. 96, and Progress Report for August 1970, ANL-7737, p. 58), the proposal was made to shorten future thimbles slightly. Accordingly, the hexagonal tubes of the three new thimbles were machined to remove 1/8 in. from their length. The thimbles were again inspected and are ready for use in the reactor.

3. Fuel and Hardware Procurement. M. J. Feldman (02-073)

a. Reclamation of Vendor Fuel. D. L. Mitchell (Last reported: ANL-7776, pp. 41-43, Jan 1971)

During this reporting period, 4971 more centrifugally bonded vendor elements were heat-treated to reclaim them. Examination of the 4971 heat-treated elements showed 3573 to be "accepts" and 1398 to be "rejects." The principal cause for rejection was void size in the sodium bond. The percentage of elements rejected for void size ranged from 16 to 46% for all fuel batches heat-treated in this reporting period. This is a higher rejection rate than the 8 to 38% previously reported. Rejection for void size was based on the definition in Revision 6 of Specification FCF-1 (Product Specification for the EBR-II Driver Fuel Elements). However, the elements rejected for void size may be acceptable on the basis of the approved Revision 7 of this specification, which allows acceptance of larger void sizes (to radial widths of 125 mils) than does Revision 6. The present sodium-bond testers can measure voids having a radial width up to about 80 mils. Components for a new sodium-bond tester, which will measure the larger voids acceptable under Revision 7, have been received and assembled. Testing of the new unit has been started. The elements rejected under Revision 6 will be reevaluated for void size with the new bond tester. Those still "rejects" will be impact-bonded in an effort to reclaim them.

4. Experimental Irradiation and Testing. R. Neidner (02-053)

a. Experimental Irradiations (Last reported: ANL-7758, pp. 37-39, Nov 1970)

Table I.3 shows the status of experimental irradiations in EBR-II on March 15, just after the end of Run 47B. Table I.4 lists all irradiated experimental-irradiation subassemblies now in the FEF for examination and reconstitution. Table I.5 lists the experimental-irradiation subassemblies transferred into the reactor after Run 47A. (No experimental-irradiation subassemblies were removed from the reactor after Run 47A.)

TABLE I.3. Status of Experimental Irradiations in EBR-II as of March 15, 1971

(Run 47B Completed)

Subassembly No. and (Position)	Date Loaded	Content and (Number of Capsules)		Experimenter	Accumulated Exposure, MWd	Estimated Goal Exposure, MWd	Burnup[a]
XX02 (5F3)	4/13/70	UO_2-25 wt % PuO_2	(36)	HEDL	8,423	11,500	3.2
XG03A (8D2)	9/14/70	UO_2-20 wt % PuO_2	(2)	GE	3,028	13,000	0.5+7.5[b]=8.0
XG04A (8A7)	9/15/70	UO_2-20 wt % PuO_2	(2)	GE	3,028	21,000	0.5+8.5[b]=9.0
X043A (6D3)	10/27/70	UO_2-25 wt % PuO_2	(37)	GE	1,478	3,100	0.6+6.2[b]=6.8
X056A (6B2)	10/27/70	UO_2-25 wt % PuO_2	(37)	GE	1,478	3,100	0.6+6.3[b]=6.9
X058 (7B6)	4/24/70	UO_2-25 wt % PuO_2	(37)	GE	17,609	21,800	6.2
X061 (7A1)	4/23/69	Structural	(7)	INC	18,379	18,450	3.7
X062 (7F3)	5/23/69	UO_2-25 wt % PuO_2	(37)	GE	15,706	19,000	6.4
X065E (7E5)	10/27/70	Structural	(25)	ANL	1,478	1,550	0.3+1.3[b]=1.6
X068A (6B4)	2/23/71	Mark IA	(61)	ANL	503	2,800	0.1+2.4[b]=2.5
X073 (7D3)	12/12/69	UO_2-25 wt % PuO_2	(37)	HEDL	12,279	35,000	2.7
X076 (7A2)	3/27/70	UO_2-25 wt % PuO_2	(19)	WARD	8,580	15,000	2.7
X078A (6B3)	2/24/71	Mark IA Mark IA	(1) (42)	ANL ANL	503	6,200	0.1+4.2[b]=4.3
X079 (4B2)	4/17/70	$(U_{0.85}$-$Pu_{0.15})C$	(19)	UNC	8,423	11,000	4.3
X080 (6E3)	9/11/70	UO_2-20 wt % PuO_2 Structural Structural	(12) (1) (4)	NUMEC/ANL GE GE	3,028	7,000	1.0+11.0[b]=12.0 0.8+8.2[b]=9.0 0.8+1.0[b]=1.8
X081 (7F6)	5/24/70	UO_2-25 wt % PuO_2	(9)	GE	7,079	19,000	2.1+6.7[b]=8.8
X082A (5A4)	2/23/71	Mark IA	(61)	ANL	503	3,000	0.1+2.8[b]=2.9
X083 (5E2)	9/15/70	Mark IA	(61)	ANL	3,028	13,900	0.8
X084 (5C2)	2/24/71	UO_2-20 wt % PuO_2 UO_2-25 wt % PuO_2	(1) (18)	ANL ANL	503	Failure	0.2+11.0[b]=11.2 0.2
X085 (4E2)	10/28/70	UO_2-25 wt % PuO_2	(19)	ANL	1,478	10,000	0.6
X086 (5D4)	8/ 7/70	$(U_{0.8}$-$Pu_{0.2})N$ $(U_{0.8}$-$Pu_{0.2})C$ $(U_{0.8}$-$Pu_{0.2})C$	(10) (5) (4)	BMI LASL WARD	4,378	7,000	2.1 2.1 1.9
X087A (6C2)	10/27/70	UO_2-25 wt % PuO_2	(61)	HEDL	1,478	19,000	0.3+1.1[b]=1.4
X088 (7C4)	5/24/70	UO_2-25 wt % PuO_2	(19)	WARD	7,079	14,500	1.7
X089 (2F1)	9/15/70	Structural	(7)	HEDL	3,028	7,800	1.2
X090 (7D5)	9/15/70	Structural Structural Structural Structural	(4) (1) (1) (1)	BMI INC ORNL HEDL	3,028	6,700	0.6 0.6 0.6 0.6
X091 (4B3)	9/11/70	Structural	(7)	HEDL	3,028	16,000	1.1
X092 (7B3)	9/15/70	Structural	(1)	LASL	3,028	2,700	0.6
X093 (6E4)	10/27/70	UO_2-25 wt % PuO_2	(61)	HEDL	1,478	16,000	0.5

TABLE I.3 (Contd.)

Subassembly No. and (Position)	Date Loaded	Content and (Number of Capsules)		Experimenter	Accumulated Exposure, MWd	Estimated Goal Exposure, MWd	Burnup[a]
X094 (7B4)	11/16/70	UO_2-15 wt % PuO_2	(7)	GGA	503	8,600	0.2
X095 (7A5)	9/18/70	Structural	(1)	NRL	3,028	11,000	0.6
X098 (4C2)	11/16/70	Structural	(19)	GE	503	8,000	0.2
X099 (7F5)	11/16/70	Boron Carbide	(6)	ORNL	503	20,000	0.1
X100 (2D1)	10/ 7/70	Structural	(7)	ORNL	2,277	10,000	0.9
X102 (7F1)	2/22/71	Structural Corrosion	(1)	ANL	503	10,000	0.1
X106 (6D5)	2/23/71	UO_2-20 wt % PuO_2	(7)	ANL	503	Failure	0.2+6.0[b]=6.2
X110 (7C5)	2/22/71	Structural	(7)	INC	503	7,500	0.1
X111 (8D5)	2/24/71	Fission Yields	(4)	INC	503	3,100	0.1
X117 (8B2)	2/24/71	UO_2-25 wt % PuO_2	(9)	GE	503	30,000	0.1+5.2[b]=5.3
X118 (8D7)	2/24/71	UO_2-25 wt % PuO_2	(10)	GE	503	30,000	0.1+5.2[b]=5.3

[a]Estimated accumulated center burnup on peak rod, based on unperturbed flux, but considering depletion effects (fuels, at. %; nonfuels, nvt x 10^{-22}).

[b]Previous exposure from another subassembly.

TABLE I.4. Experiments Awaiting Reconstitution at the FEF

Subassembly No.	Type	Experimenter	Content	Number of Capsules	Burnup[a]	Assigned to
X012A	A19	ANL	UO_2-20 wt% PuO_2	3	11.1	
X027	A19	GE	UO_2-25 wt% PuO_2	12	9.7	
X050	A19	ORNL	UO_2-20 wt% PuO_2	3	6.0	X119
X051	F37A	HEDL	UO_2-25 wt% PuO_2	37	3.2	X051A
X054	F37A	HEDL	UO_2-25 wt% PuO_2	37	5.7	X114; X116
X059	F37A	HEDL	UO_2-25 wt% PuO_2	37	4.8	X059A
X064	A19	GE	UO_2-25 wt% PuO_2	14	6.3	
X070	A19	WARD	$(U_{0.8}$-$Pu_{0.2})C$	1	3.7	X119
	A19	ANL	UO_2-20 wt% PuO_2	7	3.5	
X072	A19	ANL	UO_2-20 wt% PuO_2	18	3.8	X113
	A19	ANL	Structural	1	2.4	X113
X074	H37A	HEDL	UO_2-25 wt% PuO_2	37	3.4	X074A
X075	A19	UNC	$(U_{0.85}$-$Pu_{0.15})C$	9	2.7	

[a]Estimated accumulated center burnup on peak rod, based on unperturbed flux, but considering depletion effects (fuels, at. %; nonfuels, nvt x 10^{-22}).

TABLE I.5. Experimental Irradiation Subassemblies Transferred into Reactor after Run 47A

Subassembly No.	Transfer	To Position	Sponsor	Content	Burnup[a]
X068A	Loaded	6B4	EBR-II	Mark-IA (encap.)	2.4
X078A		6B3	EBR-II	Mark-IA	4.2
X082A		5A4	EBR-II	Mark-IA	2.8
X084		5F2	EBR-II	UO_2-20 wt % PuO_2	11.0
X094		7B4	GGA	UO_2-15 wt % PuO_2	0
X098		4C2	GE	Structural	0
X099		7F5	ORNL	B_4C	0
X102		7F1	EBR-II	Cr Corrosion	0
X106		6D5	EBR-II	UO_2-20 wt % PuO_2	6.0
X110		7C5	INC	Structural	0
X111		8D5	INC	Fission Yields	0
X117		8B2	GE	UO_2-25 wt % PuO_2	5.2
X118		8D7	GE	UO_2-25 wt % PuO_2	5.2

[a]Estimated accumulated center burnup on peak rod, based on unperturbed flux, but considering depletion effects (fuels, at. %; nonfuels, nvt x 10^{-22}).

b. Experimental Support. M. J Feldman, J. P. Bacca, N. R. Grant, R. V. Strain, R. D. Phipps, J. W. Rizzie, A. K. Chakraborty, D. B. Hagmann, C. M. Iverson, H. A. Taylor, and G. C. McClellan (Last reported: ANL-7776, pp. 28-30, Jan 1971)

Table I.6 summarizes the current status of examinations of experimental-irradiation subassemblies that are in the FEF. Also shown, as the last entry in the table, is the total number of FEF examinations of various types performed on the 32 experimental-irradiation subassemblies dismantled in fiscal year 1971 (through February 1971).

The following new subassemblies were made up with new capsules or elements in the FEF sent to the reactor. (Previously fabricated subassembly X102 was also transferred to the reactor.)

TABLE I.6. Status of Examinations of Experimental-irradiation Subassemblies in the FEF as of March 15, 1971

Subassembly No. and (Type)	Contents and (Experimenter)	Burnup[a]	Subassembly				Number of Capsules or Elements Examined													Number of Capsules or Elements...	
			Received	Subassembly Measured	Hex Can Measured	Dismantled	Examined Visually	Photographed	Diameter Measured with Optical Gauge	Diameter Measured with Profilometer	Length Measured	Bow Measured	Gamma-scanned	Weighed	Balance Point Measured	Neutron-radiographed	Bond Tested	Deencapsulated or Decanned	Sectioned	For Reconstitution	For Shipment to Experimenter
X040A (B37)[b]	Encapsulated mixed oxide (ANL;GE)	6.1					15	15	15	7	15	15	5	15	7					0	
X042B (B7)[c]	Encapsulated structural (HEDL)	3.5							7		7	7		7		7					
X051 (F37A)[b]	Unencapsulated mixed oxide (HEDL)	3.2	X[d]			X	37	37	37	33				37	5	37				33	
X054 (F37A)[b]	Unencapsulated mixed oxide (HEDL)	5.7	X[d]			X	20	37	2	37	37	37	5	22	22	37					
X059 (F37A)[b]	Unencapsulated mixed oxide (HEDL)	4.8	X[d]			X	37	37	37	7				37	5	37				33	
X068 (B61A)[e]	Encapsulated Mark-IA driver fuel (ANL)	2.4					58		9				5	61		15		9	2	0	
X069 (H37A)[b]	Unencapsulated mixed oxide (HEDL)	3.0	X[d]			X	37	37		24	37	37		37						0	
X072 (A19)[b]	Encapsulated mixed oxide (ANL)	3.8					19		19	19	19	19		19		19				14	
X074A (H37A)[c,f]	Unencapsulated mixed oxide (HEDL)	3.4				X	37	37		7	7	7				10				36	1
XX01[c]	Instrumented subassembly																				
	Encapsulated enriched UO_2 (HEDL)	0.9	X[g]			X	18	5								18					
	Encapsulated structural (HEDL)	1.3																			
Total Examinations for 32 Subassemblies Dismantled in FY 1971 (through February 1971)							238	-	416	250	436		20	371	18	345	0	10	-	-	107

[a] Peak burnup in at. % for fueled experiments; peak fluence in nvt x 10^{-22} for nonfueled experiments.

[b] Interim examinations completed; capsules or elements to be reconstituted into new subassembly(ies) for further irradiation.

[c] Interim examinations completed; capsules being stored pending decision to continue their irradiation or return them to experimenter.

[d] No problems were encountered when this multiple-hexagonal-wall subassembly was washed using the FEF standard washing procedure for experimental-irradiation subassemblies.

[e] Interim examinations to be continued.

[f] After being reconstituted (with fuel elements previously irradiated in subassembly X074 to a peak burnup of 3.4 at. %), this subassembly was dismantled because of handling problems in the FEF. The elements were reexamined and are being stored pending evaluation of their examination.

[g] Residual surface sodium on subassembly was reacted with moist argon only. Subassembly was heavily coated with sodium reaction products during disassembly and visual examination.

Subassembly No.	Subassembly Type	Content and (Number) of Capsules or Elements
X104 and X105	B7A	ANL gamma-heat-measuring capsules (3); dummy elements (4)
X110	B7A	INC unencapsulated structural elements (7)
X111	B7A	INC encapsulated fission-product-yield specimens (4); dummy elements (3)

Table I.7 lists the subassemblies that were reconstituted in the FEF and sent to the reactor during this reporting period.

TABLE I.7. Subassemblies Reconstituted in FEF

Subassembly No. and (Type)	Contents
X055A (A19A)	19 UNC encapsulated mixed-carbide fuel elements - two new and 17 previously irradiated to peak burnup of 4.8 at. % in subassembly X055
X069A (H37A)	37 WADCO mixed-oxide fuel elements - one new and 36 previously irradiated to peak burnup of 3 at. % in subassembly X069
X084 (E19E)	18 ANL unirradiated mixed-oxide fuel elements; one NUMEC mixed-oxide fuel element (D-5) previously irradiated to peak burnup of ~11 at. % as an encapsulated element in subassembly X012A
X106 (E7B)	Seven ANL mixed-oxide fuel elements previously irradiated to peak burnup of 6.1 at. % in subassembly X040A
X117 (A19)	Nine GE encapsulated mixed-oxide fuel elements previously irradiated to peak burnup of 5.2 at. % in subassembly X036; three dummy elements; seven irradiation positions closed with solid rods
X118 (A19)	10 GE encapsulated mixed-oxide fuel elements previously irradiated to peak burnup of 5.2 at. % in subassembly X036; two dummy elements; seven irradiation positions closed with solid rods

B. Fuels and Materials Studies

1. Coolant Chemistry. D. W. Cissel (02-051)

a. Monitoring of Sodium-Coolant Quality. W. H. Olson, C. C. Miles, T. P. Ramachandran, E. R. Ebersole, and G. O. Haroldsen (Last reported: ANL-7776, pp. 24-28, Jan 1971)

(1) Radionuclides in Sodium. Table I.8 lists results of analyses for ^{137}Cs and ^{131}I in primary sodium. Cesium activity increased to preshutdown levels as the primary sodium was heated up. The increase probably was caused by thermal-convection mixing.

TABLE I.8. ^{137}Cs and ^{131}I in Primary Sodium

Sample Date	Sample Size, g	Sample Flow, gpm	Flush Time, min	Sample Temp, °F	Bulk Sodium Temp, °F	^{137}Cs, 10^2 μCi/g	^{131}I, 10^5 μCi/g
2/11/71	14.2	0.5	15	310	350	0.5	n.d.[a]
2/18/71	13.4	0.65	15	480	580	1.2	n.d.
2/19/71	13.0	0.5	15	538	580	1.2	n.d.
2/22/71	13.3	0.4	15	550	600	1.0	n.d.
2/24/71	13.3	0.5	15	560	600	1.3	2.8
3/2/71[b]	12.2	0.4	30	655	700	1.2	1.2

[a] n.d. = none detected.
[b] Sampled from the FERD (fuel-element-rupture detector) loop.

A sample of sodium taken on 2/16/71 was analyzed for ^{210}Po. Alpha activity of ^{210}Po was 35 dis/min-g. Polonium is an activation product of bismuth.

(2) Trace Metals in Sodium. Table I.9 lists results of analyses for trace metals in sodium. Analyses were made on vacuum-distillation residues by atomic-absorption spectrophotometry.

TABLE I.9. Trace Metals in Sodium

Sample Date	Sample Size, g	Sample Flow, gpm	Flush Time, min	Sample Temp, °F	Bulk Sodium Temp, °F	Concentration, ppm														
						Ag	Al	Bi	Ca	Co	Cr	Cu	Fe	In	Mg	Mn	Mo	Ni	Pb	Sn
Primary Sodium																				
1/8/71	57	0.7	15	280	350	0.05	<0.6	0.9	<0.02	<0.02	<0.02	<0.02	0.28	<0.06	0.005	<0.005	<0.07	<0.04	2.9	24.6
2/16/71	59	0.75	15	350	400	0.05	<0.6	1.3	<0.02	<0.02	<0.02	<0.02	0.08	<0.06	<0.005	<0.005	<0.07	<0.04	7.1	22.8
Secondary Sodium																				
2/16/71	60	0.5	15	400	400	0.01	<0.6	<0.1	0.03	<0.02	0.58	<0.02	3.6	<0.06	0.005	0.031	<0.07	0.37	0.5	<0.5
2/22/71	1030	0.75	30	400	510	0.048	0.05	0.019	0.026	<0.002	0.004	0.007	0.11	<0.01	0.013	0.001	<0.01	0.005	-	-

(3) Oxygen in Sodium. Table I.10 lists results of analyses for oxygen in sodium. Samples of 15 g were taken in stainless steel vessels

and extrusion-aliquoted for analysis by the mercury-amalgamation method. Oxygen in both the primary and secondary sodium increased slightly during heatup of the systems after the extended maintenance shutdown. No plugging temperatures above 225°F were measured in the primary system. Plugging temperatures reached 400°F in the secondary system and were reduced to less than 225°F over a three-day period. Plugging temperature of the secondary sodium on 2/17/71, at the time the oxygen sample was taken, was in the range of 325-350°F.

TABLE I.10. Oxygen in Sodium

Sample Date	Sample Flow, gpm	Flush Time, min	Sample Temp, °F	Bulk Sodium Temp, °F	Number of Aliquots[a]	Average Concentration, ppm
			Primary Sodium			
2/16/71	0.75	15	350	400	3	2.2 ± 1.0
			Secondary Sodium			
2/17/71	0.8	30	480	500	3	3.7 ± 0.5

[a]Aliquot size ∿ 1 g.

(4) Carbon in Sodium. Table I.11 lists results of analyses for carbon in sodium. Samples of 15 g were taken in stainless steel vessels and extrusion-aliquoted for analysis by the oxyacidic-flux method.

TABLE I.11. Carbon in Sodium

Sample Date	Sample Flow, gpm	Flush Time, min	Sample Temp, °F	Bulk Sodium Temp, °F	Number of Aliquots[a]	Average Concentration, ppm
			Primary Sodium			
11/24/70	0.7	15	330	350	3	0.8 ± 0.06
2/16/71	0.75	15	350	400	4	1.6 ± 0.4
			Secondary Sodium			
2/17/71	0.8	30	480	500	3	1.0 ± 0.3
3/3/71	0.3	22	450	545	3	1.2 ± 0.2

[a]Aliquot size ∿ 1 g.

(5) Hydrogen in Sodium. Table I.12 lists results of analyses for hydrogen in sodium by the amalgam-reflux method. Analyses were performed by WADCO, Richland, Washington.

TABLE I.12. Hydrogen in Sodium

Sample Date	Sample Flow, gpm	Flush Time, min	Sample Temp, °F	Bulk Sodium Temp, °F	Hydrogen, ppm
			Primary Sodium		
12/23/70	0.7	15	305	350	< 0.06
2/18/71	0.75	15	480	580	0.22
			Secondary Sodium		
2/17/71	0.8	30	480	500	0.27

(6) Segregation of Impurities in Sodium. During the period of about three months while the primary sodium was stagnant (no pumping) at 350°F, there was evidence of several impurities segregating from the bulk sodium. Evidence of segregation of ^{137}Cs was reported in ANL-7776, p. 24, and is mentioned under Sect. B.1.a(1) above. Activity of ^{137}Cs decreased to 25-50% of the normal level over a 30-day period, then rapidly returned to normal as the sodium was heated, but before the main pumps were turned on.

Other impurities whose concentrations decreased during the shutdown are ^{125}Sb, ^{54}Mn, ^{3}H, bismuth, and lead. Activities of ^{125}Sb and ^{54}Mn dropped below detection limits. Tritium activity before and after heatup was 2.6×10^{-4} and 11.2×10^{-4} μCi/ml, respectively. The concentrations of bismuth and lead dropped to 0.9 and 2.9 ppm, respectively, compared with normal values of 2 and 10 ppm.

b. Radioactivity of EBR-II Primary-system Components.
C. R. F. Smith, T. N. Buchanan, A. F. Clark, R. N. Curran, R. E. Difelici, E. R. Ebersole, H. Hurst, M. T. Laug, W. J. Richardson, and R. Villareal (Not previously reported)

(1) Examination of Primary Pump. The No. 1 primary pump was removed from the primary tank for examination on December 27, about six weeks after EBR-II was shut down on November 14. Samples of deposits on various pump surfaces were taken for analyses on January 6, 1971. On the same day, an axial scan of radiation from the uncleaned pump was made with a Juno (beta-gamma) survey meter, and another scan was made with a GeLi gamma detector to identify radioisotopes. Data from these examinations are presented below.

Figure I.1 shows the results of the radiation survey of the uncleaned pump with the Juno survey meter. All measurements were made

in the "gamma-ray only" mode, on the 0 to 250-mR/hr range, and 1 ft from the pump surface. The maximum radiation reading (175 mR/hr) is at a point where the meter was 1 ft from the pump inlet and was flanked by the radioactive surfaces of two of the pump volutes.

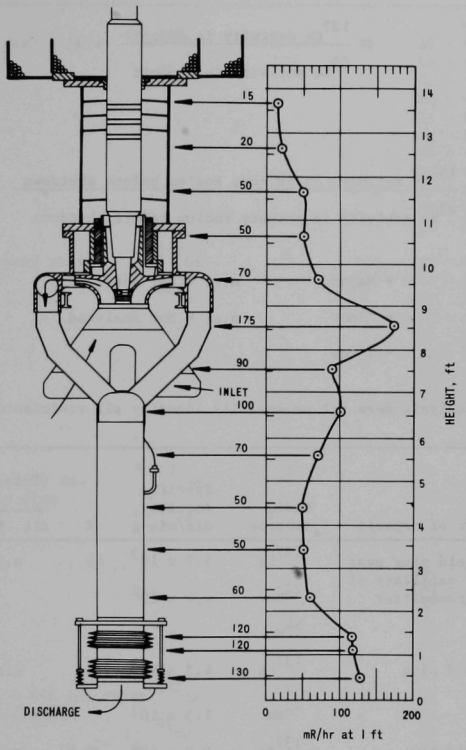

Fig. I.1. Results of Radiation Scan of EBR-II No. 1 Primary Pump. ANL Neg. No. 103-05810 Rev. 1.

In all, 28 samples from deposits found on various pump surfaces were analyzed. Table I.13 gives the results of these analyses. The locations from which the samples were taken are identified in Fig. I.2.

The radioisotopic analyses of ^{137}Cs and of ^{22}Na in Table I.13 are reported as the ratio

$$\frac{^{137}Cs \text{ activity in deposit}}{^{22}Na \text{ activity in deposit}} \div \frac{^{137}Cs \text{ activity in primary sodium before shutdown}}{^{22}Na \text{ activity in primary sodium before shutdown}}.$$

TABLE I.13. Analysis of Deposits on Assembly of No. 1 Primary Pump

Notes Pertaining to Table

Sample No. is identified in Fig. I.2.

$$R = \left\{ \frac{^{137}Cs \text{ activity in deposit}}{^{22}Na \text{ activity in deposit}} \div \frac{^{137}Cs \text{ activity in primary sodium before shutdown}}{^{22}Na \text{ activity in primary sodium before shutdown}} \right.$$

M = Major n.d. = Not detected

m = Minor n.a. = Not Analyzed

t = Trace

Radiometric analysis does not necessarily identify all radioisotopes present.

Sample No.	Location of Deposit	Radio-isotope	Specific Activity, dis/min-g	R	Results of Emission-Spectroscopic Analysis	
					Alc. Soln.	Insol. Res.
1	Top of shield plug near NaK-filled capillary of pressure transmitter	^{137}Cs	5.7×10^3	60	n.a.	n.a.
		^{22}Na	4.4×10^2			
		^{54}Mn	t			
2	Upper shield plug	^{137}Cs	4.3×10^3	15	n.a.	n.a.
		^{22}Na	1.3×10^3			
3	Upper shield plug	^{137}Cs	3.3×10^4	6.6	n.a.	n.a.
		^{22}Na	2.3×10^4			
4	Upper shield plug	^{137}Cs	5.7×10^3	52	n.a.	n.a.
		^{22}Na	5.1×10^2			
5	Upper shield plug	^{137}Cs	1.8×10^4	64	n.a.	n.a.
		^{22}Na	1.3×10^3			
		^{54}Mn	1.0×10^3			

TABLE I.13 (Contd.)

Sample No.	Location of Deposit	Radio-isotope	Specific Activity, dis/min-g	R	Results of Emission-Spectroscopic Analysis	
					Alc. Soln.	Insol. Res.
6	Pump shaft near shield-plug flange	^{137}Cs ^{22}Na	a	33	Al - M Ca - n.d. Cr - M Cu - m Fe - m Mg - n.a. Mn - t Mo - n.a. Na - M Ni - t Si - t	n.a.
7	Pump shaft near shield-plug flange	^{137}Cs ^{22}Na	a	51	Al - M Ca - n.d. Cr - M Cu - M Fe - m Mg - n.a. Mn - t Mo - n.a. Na - M Ni - t Si - t	m m M M M t t t m M t
8	Pump shaft, ∿ 10 in. above shield-plug flange	^{137}Cs ^{22}Na	a	3.1	Al - t Ca - n.d. Cr - M Cu - m Fe - t Mg - n.a. Mn - t Mo - n.a. Na - M Ni - m Si - t	m m M m m m m t m M t
9	Pump shaft, ∿ 4-6 in. above shield-plug flange	^{137}Cs ^{22}Na	a	2.4	Al - t Ca - n.d. Cr - t Cu - n.d. Fe - n.d. Mg - n.a. Mn - n.d. Mo - n.a. Na - M Ni - n.d. Si - t	m m M m m t m t M M t
10	Pump shaft, ∿ 4-6 in. above shield-plug flange	^{137}Cs ^{22}Na	a	8.8	Al - m Ca - n.d. Cr - M Cu - m Fe - t Mg - n.a. Mn - t	m m m M m m m

TABLE I.13 (Contd.)

Sample No.	Location of Deposit	Radio-isotope	Specific Activity, dis/min-g	R	Results of Emission-Spectroscopic Analysis	
					Alc. Soln.	Insol. Res.
10 (Contd.)					Mo - n.a.	t
					Na - M	m
					Ni - t	M
					Si - t	t
11	Pump shaft, ∿ 4-6 in. above shield-plug flange	^{137}Cs ^{22}Na	a	24	Al - m	m
					Ca - n.d.	m
					Cr - n.d.	M
					Cu - t	M
					Fe - n.d.	m
					Mg - n.a.	t
					Mn - n.d.	m
					Mo - n.a.	t
					Na - M	M
					Ni - n.d.	m
					Si - n.d.	t
12	Pump shaft, ∿ 4-6 in. above shield-plug flange	^{137}Cs ^{22}Na	a	0.88	Al - n.d.	m
					Ca - n.d.	m
					Cr - n.d.	M
					Cu - n.d.	m
					Fe - n.d.	m
					Mg - n.a.	t
					Mn - n.d.	m
					Mo - n.a.	t
					Na - M	M
					Ni - t	M
					Si - n.d.	t
13	Pump shaft, ∿ 6-8 in. above shield-plug flange	^{137}Cs ^{22}Na	a	1.4	Al - n.d.	m
					Ca - n.d.	m
					Cr - m	M
					Cu - t	m
					Fe - t	m
					Mg - n.a.	t
					Mn - t	t
					Mo - n.a.	t
					Na - M	t
					Ni - t	M
					Si - t	t
14	Pump shaft, on reduced diameter ∿ 2 ft above shield-plug flange		No detectable activity; insufficient sample			
15	Interior space above top baffle plate (∿ 2 in. below shield-plug flange)	^{137}Cs ^{22}Na	a	197	Al - M	m
					Ca - n.d.	m
					Cr - m	M
					Cu - m	M
					Fe - t	m
					Mg - n.a.	t
					Mn - t	m
					Mo - n.a.	m
					Na - M	M
					Ni - n.d.	M
					Si - t	t

TABLE I.13 (Contd.)

Sample No.	Location of Deposit	Radio-isotope	Specific Activity, dis/min-g	R	Results of Emission-Spectroscopic Analysis		
					Alc. Soln.	Insol. Res. No. 1	Insol. Res. No. 2[b]
16	Outside surface of baffle assembly (~ 0-6 in. below shield-plug flange)	^{137}Cs ^{22}Na	a	70	Al - n.d. Ca - n.d. Cr - n.d. Cu - t Fe - n.d. Mg - n.a. Mn - t Mo - n.a. Na - M Ni - n.d. Si - t	M m M m m m m t M M m	
17	Interior space above top baffle plate (180° rotation from Sample 15)	^{137}Cs ^{22}Na	a	115	Al - M Ca - n.d. Cr - m Cu - m Fe - t Mg - n.a. Mn - t Mo - n.a. Na - M Ni - n.d. Si - n.d.	m m M M m t m t M M t	M m M M m t m M M M t
18	Black sludge from alcohol cleaning of bolts holding pump to shield plug	n.a.	--	--	Al - m Ca - M Cr - M Cu - m Fe - m Mg - m Mn - m Mo - m Na - M Ni - M Si - m		
19	Deposit on bottom of shield plug and on bolts joining pump to shield plug	^{137}Cs ^{22}Na ^{54}Mn	8.9×10^6 n.d. 9.3×10^4	n.a.	n.a.	n.a.	
20	Same region as Sample 19	^{137}Cs ^{22}Na ^{54}Mn	2.6×10^6 6.7×10^4 2.7×10^4	180	n.a.	n.a.	
21	Black deposit (oxide?) from lower part of shield plug	^{137}Cs ^{22}Na ^{54}Mn	5.7×10^5 4.0×10^4 5.9×10^3	66	n.a.	n.a.	

TABLE I.13 (Contd.)

Sample No.	Location of Deposit	Radio-isotope	Specific Activity, dis/min-g	R	Results of Emission-Spectroscopic Analysis: Alc. Soln.	Insol. Res.
22	Na-like deposit from labyrinth seal flange	^{137}Cs	5.8×10^5	32	n.a.	n.a.
		^{22}Na	8.4×10^4			
		^{54}Mn	5.2×10^5			
23	Na-like deposit from pump shaft near bottom of shield plug	^{137}Cs	7.1×10^4	24	n.a.	n.a.
		^{22}Na	1.4×10^4			
		^{54}Mn	1.3×10^4			
24	Same region as Sample 22	^{137}Cs	5.3×10^4	11	n.a.	n.a.
		^{22}Na	2.2×10^4			
		^{54}Mn	1.2×10^4			
25	Na-like deposit from pump shaft about 2 ft below shield plug	^{137}Cs	6.1×10^4	31	n.a.	n.a.
		^{22}Na	9.0×10^3			
		^{54}Mn	2.5×10^3			
26	Dust from abrasive-cloth scrubbing of deposit on pump shaft about 2 ft below shield	^{137}Cs	4.5×10^5	36	n.a.	n.a.
		^{22}Na	5.8×10^4			
		^{54}Mn	3.0×10^5			
27	Na-like deposits from pump impeller	^{137}Cs	n.d.	n.a.	n.a.	n.a.
		^{22}Na	1.1×10^5			
		^{54}Mn	8.7×10^6			
		^{210}Po[c]	1.4×10^3			
28	Sludge obtained by soaking 24 baffle-assembly bolts in alcohol	^{137}Cs	2.8×10^5	26	n.a.	n.a.
		^{22}Na	5.0×10^4			
		^{54}Mn	2.3×10^5			

[a] The size and condition of these samples did not allow a careful measurement of the specific activity. The ratio R was estimated from the relative count rates for ^{137}Cs and ^{22}Na, which were measurable. In making the estimates, allowance was made for counting efficiencies.

[b] Insoluble residue No. 2, a copper-colored solid, is believed to be a piece of aluminum-bronze from the labyrinth seal.

[c] The source of ^{210}Po is ^{209}Bi. Bismuth entered the primary sodium on or before July 1965, probably from the seals of one or both rotating plugs. Polonium-210 is produced by the reaction $^{209}Bi(n,\gamma)^{210}Bi$. Bismuth-210 has a half-life of five days and β-decays to ^{210}Po.

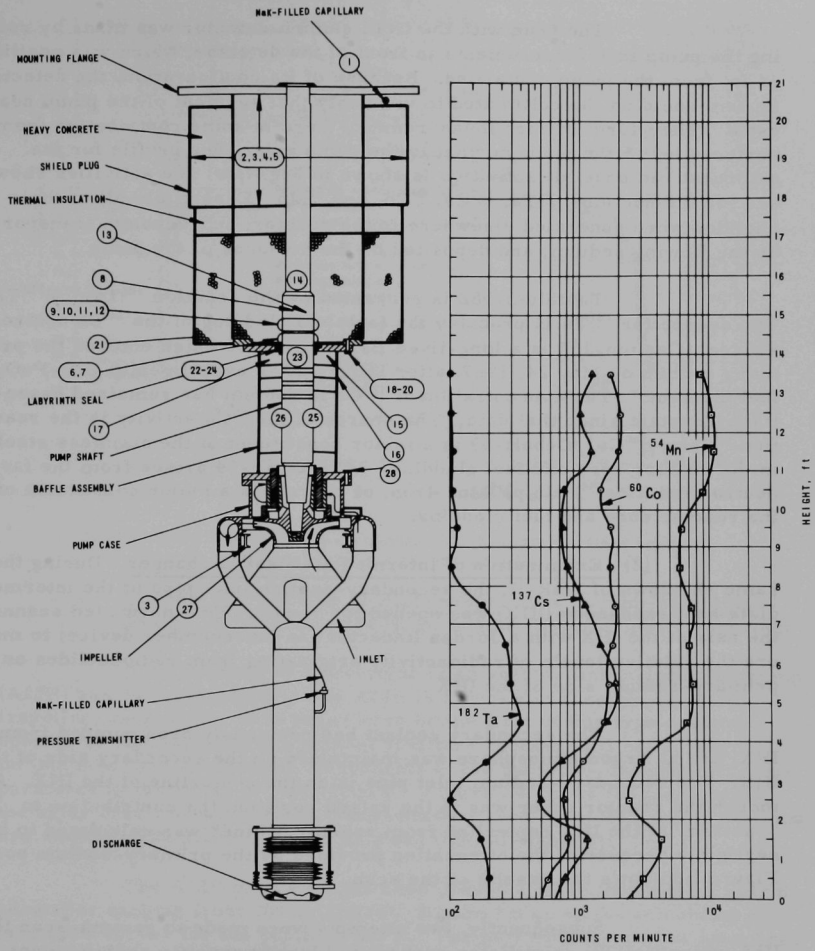

Fig. I.2. Left: Location of Deposits Sampled from Surfaces of Assembly of No. 1 Primary Pump. Right: Radioisotope Activities Measured with GeLi Detector 44 in. from Pump Centerline. ANL Neg. No. 103-05809 Rev. 1.

This ratio was developed to show the preferential separation of cesium from sodium. A more-extended discussion of this segregation phenomenon is presented at the end of Sect. I.B.1.a above.

The scan with the GeLi gamma detector was made by raising the pump in 1-ft increments in front of the detector, which was positioned 44 in. from the pump centerline. Because of its configuration, the detector system could not be collimated to view only that segment of the pump nearest it. Therefore, in each measurement, there is some contribution from surfaces below the plane normal to the pump axis. The profile for the strongest radionuclide activities is shown in Fig. I.2. The activities shown are for the nuclides ^{182}Ta, ^{137}Cs, ^{60}Co, and ^{54}Mn. Essentially all of these nuclides were generated elsewhere in the reactor, subsequently transported by the flowing sodium, and deposited on the surfaces of the pump.

Tantalum-182 is generated by the reaction $^{181}Ta(n,\gamma)^{182}Ta$. The source for ^{181}Ta is probably the tantalum cladding of the ^{124}Sb neutron source. Cesium-137 is a long-lived fission product which entered the primary sodium on May 24, 1967, after failure of an experimental UO_2-PuO_2 fuel element.* The concentration of ^{137}Cs in sodium has remained essentially constant since that date. The source of the ^{60}Co activity is the reaction $^{59}Co(n,\gamma)^{60}Co$. Cobalt-59 is a minor constituent of the stainless steel in the reactor core and fuel cladding. Manganese-54 arises from the fast-neutron reaction $^{54}Fe(n,p)^{54}Mn$. Iron, of course, is a major constituent of the reactor core and fuel cladding.

(2) Examination of Intermediate Heat Exchanger. During the same shutdown of EBR-II, the secondary-sodium inlet pipe of the intermediate heat exchanger (IHX) was opened for repair. This permitted scanning the axis of the IHX with a Jordan Radector (an ion-chamber device) to measure the relative levels of radioactivity originating from radionuclides on the primary-sodium side of the IHX.

The secondary coolant had previously been pumped from the IHX, and an argon atmosphere was maintained on the secondary side of the IHX. The secondary-sodium inlet pipe is on the centerline of the IHX. Although the reactor cover was in the raised position, the contribution to γ activity at the IHX centerline from reactor "shine" was calculated to be negligible because of the attenuation provided by the primary-sodium pool. Figure I.3 shows the results of the scan.

Subsequently, two attempts were made to gamma-scan the IHX, using NaI(Tl) scintillator probes, to identify specific radioisotopes. These attempts were unsuccessful because the gamma-ray energies were severely degraded by Compton scattering. Positive identification of characteristic energies was nearly impossible.

*R. R. Smith, D. W. Cissel, C. B. Doe, E. R. Ebersole, and F. S. Kirn, Locating and Identifying the Source of the May 24, 1967 Fission-product Release in EBR-II, ANL-7543 (Apr 1969).

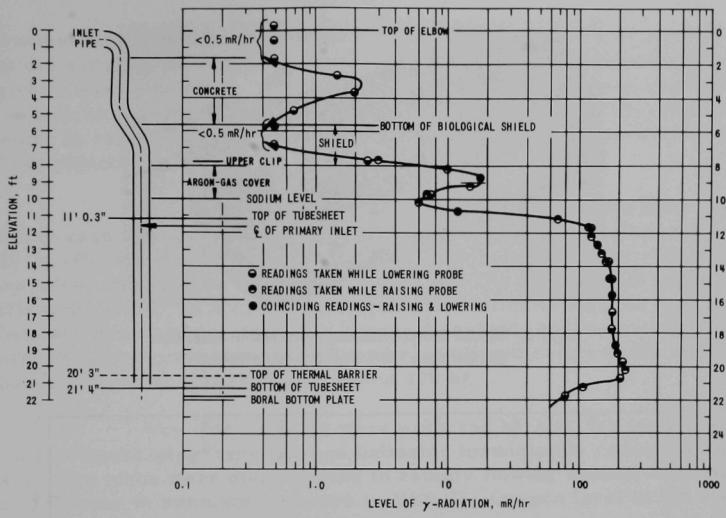

Fig. I.3. Results of Scan of EBR-II Intermediate Heat Exchanger with Jordan Radector (ion-chamber device). ANL Neg. No. 103-05811 Rev. 1.

c. Testing of Prototype of High-temperature Sodium-sampling Pump. W. H. Olson and H. E. Adkins (Not previously reported)

Initial testing of a prototype of an annular linear-induction pump (ALIP) has been completed. The ALIP is a two-pole Einstein-Szillard, traveling-wave pump. It is believed to be the first of this type designed to operate at high temperature without auxiliary coolant. All coils, magnetic laminations, and mechanical components of the pump are designed for temperatures in the range of 1600-2000°F. Figure I.4 shows the pump before the outer case was welded on. Coils, busbars, and laminated stator sections are visible. The pump is 13 in. long and 5 in. in diameter.

The ALIP prototype has been operated more than 500 hr at temperatures ranging from 700 to 1250°F. Figure I.5 gives the calculated performance curves for the pump at 700°F. The performance curves have been verified in the range of 0-7 gpm. Because of the high pressure losses in the small test loop, tests cannot be run above 7 gpm.

A second ALIP, which will be installed in the EBR-II primary-sodium sampling system, is being fabricated.

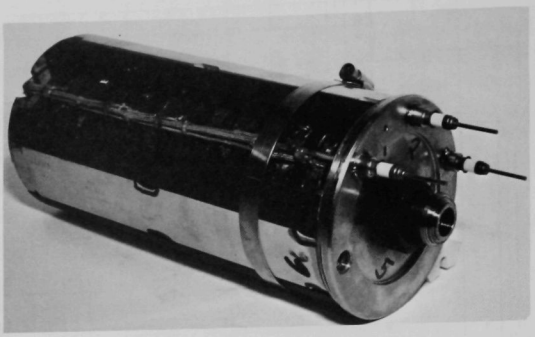

Fig. I.4. Annular Linear-induction Pump before Outer Case Was Installed. ANL Neg. No. 103-N5448.

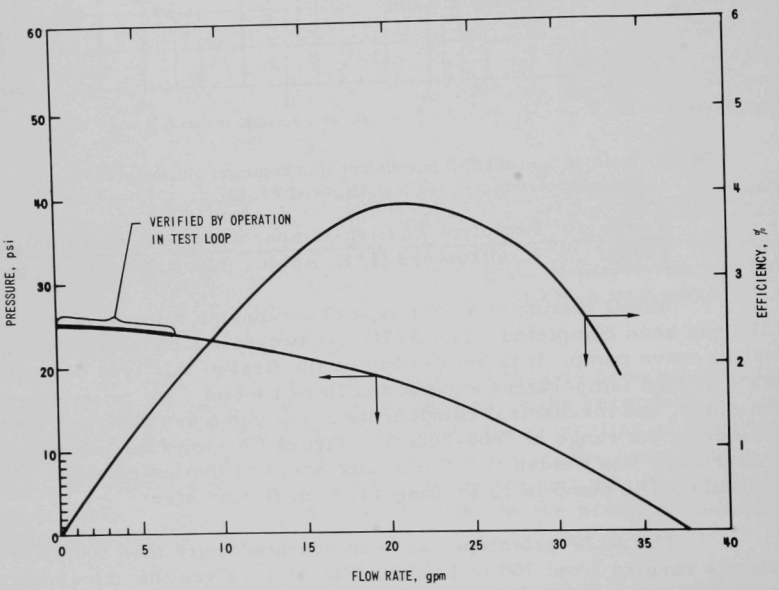

Fig. I.5. Calculated Performance, at 700°F, of Annular Linear-induction Pump for Sodium Sampling. ANL Neg. No. 103-05808 Rev. 1.

2. Materials-Coolant Compatibility. D. W. Cissel (02-063)

a. Evaluation and Surveillance of EBR-II Materials (Last reported: ANL-7776, pp. 31-32, Jan 1971)

(1) Evaluation of Delayed-release Capsules. A WADCO/EBR-II delayed-release experiment placed in EBR-II to establish the signal

characteristics of a fission-product release from a low-burnup fuel element did not give the expected signal after a much longer exposure than originally was anticipated. To determine the approximate time required for sodium to penetrate the deliberately made defect in the experiment capsule, an ex-reactor test was run with two similar capsules containing similar defects.

WADCO supplied the defected capsules for the test. The defect in each was a 0.005-in.-dia hole drilled through the wall of the 0.230-in.-OD stainless steel capsule tube. The hole was filled with a silver braze alloy, and the tube around the defect was first plated with copper and finally with nickel. In WADCO developmental testing of similar capsules in sodium at higher temperature, the copper dissolved, and the nickel plating peeled off, thereby exposing the silver braze alloy directly to the sodium. Sodium penetration occurred after about 100 hr.

The test capsules were prepared by ANL for testing by inserting a "spark-plug" type leakage indicator immediately under the known defect. The tubes were then exposed to rapidly flowing sodium on their outer surfaces to simulate exposure in EBR-II. Oxygen level in the sodium was maintained at ~1 ppm by a cold trap.

No leakage signal was received in a 1500-hr exposure consisting of 940 hr at a temperature of 740°F and a flow velocity of 12 fps plus 560 hr at 700°F and 6 fps. The capsules were removed and examined. The nickel plating was still in place on both capsules, and both passed a cursory helium leaktest with a Veeco detector. Small bumps were noted in the nickel plating over the location of the 0.005-in.-dia holes, so one capsule was sectioned. Sodium had penetrated the hole, but had formed a corrosion plug with residual oxygen in the capsule. No detectable amount of metallic sodium had entered the capsule, even though a 4-psi differential pressure favored its entry.

The nickel plating was pried back with a sharp knife. The copper underplating had been dissolved for only about 0.03 in. from the edge of the nickel overplate. When water was present, the prying-off of the nickel was accompanied by the release of tiny hydrogen bubbles as fresh copper plate was exposed. This suggests that lateral diffusion through a porous plating had allowed sodium to reach and react with the silver braze alloy in the hole.

The second capsule was not sectioned, but inspection of the interior of the defect revealed a telltale bump of corrosion product, which indicated that this capsule also had been penetrated.

The same sort of corrosion-product plug may be responsible for the lack of response in the reactor experiment. Small quantities of residual oxygen and moisture are possibly present in the experimental fuel element.

3. Metal Driver Fuel Development and Application. C. M. Walter (02-145)

a. Mark-IA Fuel. N. J. Olson (Last reported: ANL-7776, pp. 33-34, Jan 1971)

(1) Statistical Analysis of Performance of Mark-IA Fuel. A trend analysis of data from Subassembly X082, a Mark-E61 controlled-flow* subassembly, has been completed for the response parameter $\Delta D_{max}/D_0$ up to a maximum burnup of 2.8 at. %. This subassembly was made up of 61 elements that had initially been irradiated in other controlled-flow driver fuel subassemblies, so all had been irradiated under conditions simulating 62.5-MWt operation throughout their entire irradiation. The fuel in the elements came from four ANL-produced fuel batches (95II-98II) that had essentially the same composition except for aluminum, which varied from 52 to 116 ppm. The initial irradiations, all in Row-2 grid positions, were made to the burnups listed under Bu_1 in Table I.14. The irradiation in X082, in Row 5, was for an additional burnup of 1 at. %. The total accumulated burnups are listed under Bu_2 in Table I.14.

TABLE I.14. Diameter Change of ANL-produced Mark-IA Fuel Elements from Subassembly X082

	Initial Irradiation					Irradiation in X082					
Subassembly No.	Bu_1 Range, at. %	$\overline{Bu_1}$, at. %	$\Delta D_{max}/D_o$ Range, %	$\overline{\Delta D_{max}/D_o}$, %	Std. Dev. (σ),[a] %	Bu_2 Range, at. %	$\overline{Bu_2}$, at. %	$\Delta D_{max}/D_o$ Range, %	$\overline{\Delta D_{max}/D_o}$, %	Std. Dev. (σ),[a] %	Number of Elements Measured
C-2186S	1.17-1.23	1.19	0-0.21	0.10	0.06	2.18-2.28	2.23	0.46-0.77	0.64	0.07	20
C-2187S	1.42-1.50	1.46	0.04-0.30	0.16	0.08	2.43-2.54	2.50	0.67-1.07	0.89	0.13	18
C-2188S	1.67-1.76	1.72	0.20-0.53	0.34	0.09	2.67-2.81	2.75	0.89-1.62	1.24	0.18	21

[a] For $\Delta D_{max}/D_o$.

No preirradiation measurements of the elements were made, so D_0 had to be calculated from data-fitting techniques at the Bu_1 stage. The values shown for $\Delta D_{max}/D_0$ at Bu_1 and Bu_2 are based on those calculated values for D_0 and the postirradiation measurements of diameter. Of the 61 elements in X082, one was damaged and another was statistically eliminated from the analysis, leaving a total of 59 elements to be analyzed with respect to burnup, fuel volume swelling ($\Delta V/V_0$), and behavior of the element with respect to its position in the subassembly.

Figure I.6 shows the $\Delta D_{max}/D_0$ as a function of burnup. The maximum increases in diameter occurred near or at the center of all elements.

*In a controlled-flow subassembly, coolant flow is controlled to simulate temperatures corresponding to 62.5-MWt operation while operating at a lower power level.

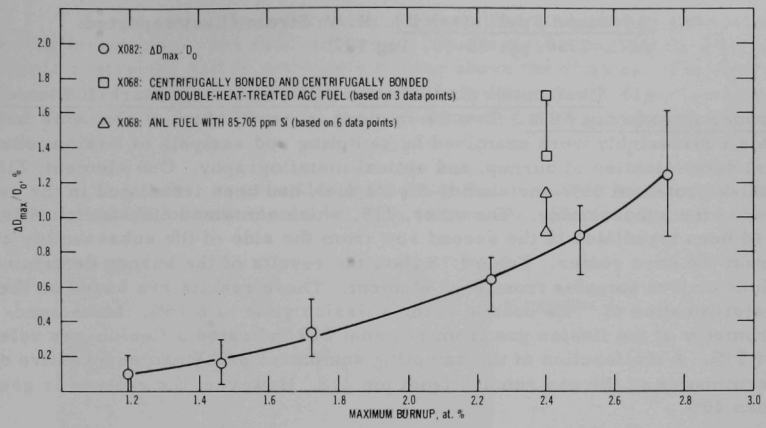

Fig. I.6. Comparison of Scatterbands for Experimental $\Delta D_{max}/D_0$ vs Burnup: Subassemblies X082 and X068

A linear-regression model was used to establish statistical trends for $\Delta D_{max}/D_0$ as a function of burnup. The model showed that burnup accounted for 53% of the variance of $\Delta D_{max}/D_0$ in the Bu_1 range and 70% of the variance in the Bu_2 range. This still leaves a significant portion of the variance unaccounted for.

Further study showed that the position of the element in the subassembly was important up to a burnup of about 1.6 at. %. Below this burnup level, values calculated using the WADCO swelling equation* were in reasonable agreement with the $\Delta D_{max}/D_0$ data. Elements in subassembly rows 2-4** tended to have larger diameter increases than those in Rows 5-6, but the variances in $\Delta D_{max}/D_0$ showed a relationship just the reverse; i.e., the largest variance was in Row 6, adjacent to the subassembly wall. The relationship of position to fuel volume swelling was similar at burnups less than 1.6 at. %; however, $\Delta D_{max}/D_0$ was not significantly dependent on fuel volume swelling. The element position within the subassembly accounted for 40% of the variance of $\Delta D_{max}/D_0$ and $\Delta V/V_0$ with a confidence level of 80% (determined with standard F test) for burnups less than 1.6 at. %.

Figure I.6 also shows $\Delta D_{max}/D_0$ scatterbands for elements in X068, a controlled-flow subassembly in which encapsulated elements were irradiated to a burnup of 2.4 at. % in reactor row 6. The reason for the difference between the results for X068 and X082 is being investigated.

*J. L. Straalsund and J. F. Bates, A Note on the Interdependency of Swelling, Void Diameter, and Void Number Density in Annealed AISI Type 304 Stainless Steel, WHAN-FR-15 (Oct 1970).

**Rows are numbered outward from the center of the subassembly.

b. Advanced Fuel (Mark II). R. V. Strain (Last reported: ANL-7737, pp. 88-93, Aug 1970)

(1) Destructive Examination of Encapsulated Mark-II Elements from Subassembly X071. Two 24-in.-long (overall) Mark-II elements from this subassembly were examined by sampling and analysis of fission, chemical determination of burnup, and optical metallography. One element, 218, which contained 93%-enriched U-5% Fs fuel, had been irradiated in the center of the subassembly. The other, 219, which contained 80%-enriched fuel, had been irradiated in the second row from the side of the subassembly away from the core center. Table I.15 lists the results of the burnup determinations on five samples from each element. These results are based on the determination of ^{139}La content using a fission yield of 6.15%. Mass spectrometry of the fission gas from Element 219 indicated a fission-gas release of 54%. A malfunction of the sampling equipment prevented quantitative determination of the gas release from pin 218. However, the release is greater than 40%.

TABLE I.15. Chemically Determined Burnups of Samples of Encapsulated Mark-II Elements from X071

Element 218		Element 219	
Sample Position,[a] in.	Burnup, at. %	Sample Position,[a] in.	Burnup, at. %
1	5.36	1	4.60
3½	6.44	3½	5.22
6½	6.56	6½	5.48
11	5.50	11	4.52
13½	4.62	13½	3.90

[a]Sample position given is the distance from the bottom of the fuel pin to the bottom of the sample. Samples were ¼ in. long.

Metallographic examination of samples from five axial positions of each element gave the following results:

(a) The fuel in both elements had continued to grow axially during irradiation. The fuel in Element 218 extended about 0.1 in. above the dimple restrainer and is extremely porous above the dimples. The fuel in Element 219 has grown approximately halfway through the ring restrainer in this element. In both elements, the fuel contained a large void just below the restrainer.

(b) Appreciable interaction had occurred between the fuel and the cladding of both elements. The interaction zone (see Fig. I.7) consists

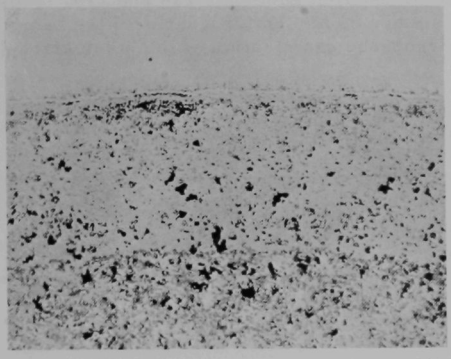

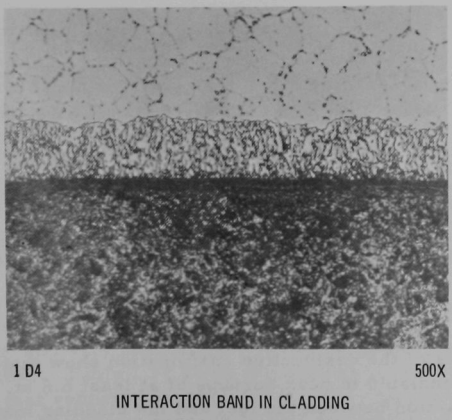

Fig. I.7. Interaction Bands at Fuel/Cladding Interface in Sample from the Midplane of Mark-II Element 218 at Burnup of 6.6 at. %

of (1) a band in the fuel that has a different appearance macroscopically, but much the same microstructure as the bulk of the fuel, and (2) a band in the cladding (Type 304L stainless steel) that has a much different microstructure than the cladding. Electron-microprobe examination of other encapsulated Mark-II elements from X071 shows that the band in the cladding has been depleted in nickel and that the band in the fuel has been enriched in nickel.

Table I.16 gives the depths of the interaction bands in samples taken at three axial positions from Elements 218 and 219. These data are based on measurements made on photomicrographs of the samples along with interpolation of the microprobe examination of the other Mark-II elements.

TABLE I.16. Depths of Interaction Bands in Samples of Encapsulated Mark-II Elements from X071

Element No.	Sample Position,[a] in.	Burnup, at. %	Depth of Nickel Depletion in Cladding,[b] in.	Depth of Nickel Penetration into Fuel,[b] in.
218	3-1/4	6.4	0.0012	0.0035
218	7	6.6	0.0011	0.0055
218	10-3/4	5.5	0.0010	0.0060
219	3-1/4	5.2	0.007 max[c]	0.002 max[c]
219	7	5.5	0.0012 max	0.003 max
219	10-3/4	4.5	0.0010 max	0.004 max

[a] Sample position given is the distance from the bottom of the fuel pin to the bottom of the sample. Samples were 1/4 in. long.

[b] Values are based on optical metallography of elements 218 and 219 and electron-microprobe examination of other Mark-II elements from the same subassembly.

[c] Depth of interaction bands varied significantly in element 219.

The results of the destructive examination show that the Mark-II element can be irradiated to peak burnups of at least 6.6 at. % without failing. The interaction between the fuel and the cladding may have a detrimental effect on the cladding and the ultimate life of the elements.

However, the maximum depth of the affected zone observed at a burnup of 6.6 at. % was 0.0012 in., a dimension equal to 10% of the nominal wall thickness and also to the maximum allowable defect in the as-received tubing.

4. Surveillance and Failure Evaluation of Experimental Fuel Irradiations. J. R. Honekamp (02-194)

a. Surveillance of Current Tests

(1) Evaluation of Reaction between Sodium and Mixed-oxide Fuel. S. Greenberg and W. E. Ruther (Last reported: ANL-7776, pp. 37-41, Jan 1971). As reported in ANL-7776, p. 40, a deposit was produced on the surface of deliberately defected sample 66B-4 from Element C15 when it was exposed to moist nitrogen and to moist air after it had been exposed in sodium. The deposit, presumably sodium hydroxide, has been examined for activity by gamma-ray spectrometry and alpha-energy techniques. The presence of fission products ^{95}Zr, ^{106}Ru, ^{137}Cs, and ^{144}Ce along with ^{239}Pu indicates that some fuel reached the exterior of the cladding during exposure to the moist gas. Metallographic examination of 66B-4 has been completed. The fuel had an unusual etched appearance, presumably caused by the moist environment.

During the exposure of 66B-4 (including the exposure to the moist gas), the length of the sample (as measured by micrometer) increased 6 mils. Metallographic examination showed that the fuel had expanded axially (at both ends) a total of 6.3 mils.

The behavior of 66B-4 after it was removed from the moist environment may be of interest to reactor operators and experimenters. After the hydroxide reaction product was removed from the exterior of the sample, the complete sample was cast in epoxy, using a clear plastic tube as a mold. The presence of alkaline reaction products inside the sample did not interfere with setting of the epoxy. Difficulties were introduced, however, in subsequent metallographic operations. Enough sodium had been removed by the moist environment, particularly in the region of the defect, so that it no longer acted as a "cement" holding the fuel together. However, enough sodium and/or reaction product remained to hamper impregnation by the epoxy. Three impregnations were necessary to produce a satisfactory longitudinal sample and prevent excessive loss of fuel material during grinding.

Sodium exposure of deliberately defected sample 66B-8, also from Element C15, was terminated after 86.9 days (45.2 days at 1200°F and 41.7 days at 700-1050°F). Metallographic examination is in progress. Table I.17 gives the results of exposure of 66B-8 for the period after that reported in ANL-7776. The "excess" sodium takeup is presumably due to sodium trapped in and around the end caps.

TABLE I.17. Results of Sodium Exposure at 1200°F on Sample 66B-8, Element C15

Elapsed Time,[a] days	Cumulative Diameter Change, mils[b]		Cumulative Length Increase, mils	Cumulative[c] Wt Gain, mg
	Plane of Defect	Normal to Defect		
66.6	--	9.7	--	--
68.3	7.2	10.1	24.2	206
73.3	9.1	10.1	24.6	265
86.9	8.4	10.3	25.1	244

[a] Includes 41.7 days at 700-1050°F.

[b] Distortion due to spacer wire reduces accuracy of these measurements.

[c] Weight gain is presumably due to sodium-logging. Calculated maximum sodium takeup, based on calculated smear density and assumed accessibility of all porosity, is 226 mg.

After 68.3 days of exposure, fine circumferential and axial cracks were observed generally in the cladding, but were most concentrated in the region of the end caps. The extent of cracking did not appear to increase during the last 18.6 days of exposure.

Metallographic examination of 66B-8 has shown that, as for Sample 59B-7* (the only other defected sample examined to date that had been exposed only to sodium), the central void and all other porosity is filled with sodium. The fuel has an etched appearance that is markedly different from that of the fuel of Samples 66B-4 and 59B-7, both of which had been exposed at 700°F. Considerable grain-boundary attack and loss of fuel grains seem to have occurred. There is evidence of attack at the fuel/cladding interface. This is not unexpected, because similar attack has been identified as cesium penetration by other investigators. The cause of the cladding cracking described above is not known. The cracks originate at the outside surface, and one, at least, which is normal to the defect, penetrates to a depth of about a third of the cladding thickness. Metallographic examination has not yet proceeded far enough to determine whether the large observed increase in length (25.1 mils) is due to fuel growth or is an experimental error.

A second deliberately defected sample (59B-11) from Element 007 has been exposed to sodium at 1200°F for 25.5 days. The purpose of this experiment is to determine directly the effect of temperature of exposure. Table I.18 gives the characteristics of the sample and the results of exposure to date. After 1.7 days at 1200°F, axial cracks, emanating

*This is the first sample taken from Element 007. It was identified simply as Sample 007 in ANL-7776, pp. 37-38, where the results of its examinations are reported.

from the ends of the milled defect, developed in the stainless steel cladding. After 5.2 days, the ends of these cracks were branched. There has been no apparent increase in size or number of cracks during the subsequent exposure.

TABLE I.18. Exposure of Sample 59B-11 from Element 007 to Sodium at 1200°F

Characteristics of Sample

Coprecipitated mixed oxide (20% Pu)

Oxygen/metal ratio - 1.98

Smear density - 76.5%

Pellet density - 79.4%

Burnup - 5.8 at. %

Length of defect in cladding - 0.59 in.

Depth of defect into fuel - 0.020 in.

Results of Exposure

Elapsed Time, days	Cumulative Diameter Change, mils		Cumulative Length Increase, mils	Cumulative Wt Gain, mg[a]
	Plane of Defect	Normal to Defect		
1.7	4.9	4.0	5.0	195
5.2	--	5.0	--	--
6.9	4.7	5.0	7.0	199
11.9	5.6	5.4	7.5	202
5.5	7.2	6.1	9.1	207

[a]Maximum sodium takeup, based on same assumption as for sample 66B-8, is 255 mg.

C. Engineering

1. Systems Engineering. B. C. Cerutti (02-068)

a. Surveillance, Evaluation, and Studies of Systems (Last reported: ANL-7776, pp. 32-33, Jan 1971)

(1) Maintenance of No. 1 Primary-sodium Pump (R. E. Seever). On two known occasions in the last year, the No. 1 primary-sodium centrifugal pump exhibited increased power requirements, which indicated that some binding may have occurred. During the recent maintenance shutdown of the reactor, the pump, which had been immersed continuously in hot sodium for more than seven years, was removed from the primary tank, disassembled, cleaned, inspected, reassembled, and reinstalled. Minor repairs and modifications were performed on the pump after it was cleaned. Highlights of the work were as follows:

(a) A considerable amount of sodium and sodium oxide was found both inside and outside the pump assembly. Because of the potential for a sodium fire, the baffle, shaft-impeller, and case-manifold subassemblies were cleaned on a sodium-cleanup pad outside the reactor building.

(b) The radioactivity and radioactive-contamination levels were high enough to require complete containment of the pump in a plastic envelope for disassembling. Air was supplied into the top of the envelope and exhausted from the bottom through an absolute filter. Entry into the envelope was controlled by Radiation Safety. Personnel working inside the envelope wore complete fire-retardant and anticontamination clothing as well as full-face shields supplied with air.

(c) Cleaning consisted of immersing in ethyl alcohol (except for the shield-plug subassembly), washing with water, wiping with water-dampened cloth, brushing, and soaking in decontamination solution. The sodium and sodium oxide were removed, and the radioactivity and radioactive-contamination levels were decreased. However, the levels remained high enough to require reassembling, as with disassembling, in a plastic envelope under the control of Radiation Safety.

(d) The void between the pump shaft and the lower 1 ft of the shield-plug liner was completely filled with sodium oxide. Rub marks were visible.

(e) The lower-labyrinth seal was badly corroded and had to be replaced. Sodium oxide had filled the void between the seal serrations and the shaft, destroying the serrations.

(f) The space above the first baffle plate and below the top flange of the upper-baffle subassembly was filled with sodium and sodium oxide. The void between the first and second baffle plates was about a fourth filled, but only a coating was present between the second and third baffle plates.

(g) Some very minor shaft damage had occurred in the area extending from about 6 in. above the 700°F sodium level in the primary tank to about 2 ft above that level.

(h) Oil from the lubricating grease in the lower bearing of the drive motor had leaked down the motor shaft into the central hole at the top end of the pump shaft, into which the motor shaft fits, and out the two keyway-relief holes there. This oil had run down the pump shaft to the sodium level.

(i) The welds on the 12-in. discharge pipe and its bottom bellows were examined with a three- and a ten-power magnifying glass. All welds appeared in excellent condition, including those joining the four 6-in. volute pipes to the discharge pipe.

(j) All bolts removed from the pump assembly showed stretching in the threaded portion that was not threaded into the tapped holes.

The pump rework done was minor. The existing cleanout holes for the upper baffle plates in the baffle-subassembly body were plugged with removable pipe plugs, and new holes were drilled just below the 700°F sodium level to direct the argon purge through the baffle and thereby reduce the buildup of sodium oxide. The keyway-relief holes in the pump shaft were plugged to prevent any oil that separated from the grease in the lower bearing of the drive motor from flowing out of the shaft bore and down the shaft. The grease system for the lower bearing of the motor was slightly changed to increase the reservoir capacity and provide grease containment. During reassembling of the pump, a new pressure transmitter, a new lower-labyrinth seal, and all new assembly bolts were used.

(2) Intermediate Heat Exchanger (A. F. Clark). It has been previously reported (ANL-7776, pp. 41-42) that the interior of the secondary-sodium inlet pipe of the IHX was inspected with a periscope and an argon-cooled remote TV system to find the source of the banging noise first encountered on November 14, 1970. The inspection concentrated on the 1-in.-dia drain tube and its supports. The upper J-shaped clip (about 8 ft below the inlet elbow) was found to be bent away from the tube. A clearance of 1/8 to 1/4 in. between the tube and clip was observed. The bottom clip (normally about 1 ft above the baffle assembly at the bottom of the IHX inlet pipe) was broken off close to the weld and was missing.

Further TV inspections while the baffle was being pulled on and the drain tube was being shaken did not identify any additional failed welds or broken parts. An unsuccessful attempt was made to locate the missing clip by close TV examination of the baffle assembly and by "raking" with a retrieval tool. Analysis indicates that the clip will not be carried further in the system by the sodium flow, and even if it were, no harm would result.

The status of the drain-tube clips verified earlier suspicions of the source of noise, and the remaining clip and the drain tube were removed. The upper clip was removed by using 10-ft-long twist tools designed to accommodate the special IHX geometry. Each tool was equipped with a lanyard to prevent loss of broken parts. The clip was simply twisted back and forth until it failed close to the weld point. The failure at the location of the upper clip looked similar to that at the location of the lower clip.

The upper end of the drain tube was cut with an arc welder by simply reaching through the access port. The bottom end of the tube was then cut by use of a "pinch-off" tool operated with high-pressure argon. The tool was essentially a heavy-duty, piston-driver assembly, designed to slide over the free end of the tube and shaped to fit the contour of the inlet pipe. This tool was worked downward by a series of light-pressure squeezes (using about 200 psi), which flattened but did not cut the tube, until the tool was within 7 in. of the baffle assembly. Application of the full 2000-psi argon pressure cut the tube, and the tube was then easily removed.

Marks on the tube, clip, and interior of the inlet pipe suggested that the tube had been vibrating within its supports for some time. The increased flow rate in the secondary system, which developed when reactor power was raised to 62.5 MWt, is believed to have increased the vibration amplitudes of the tube and accelerated the failure of the clips. With loosely held clips, the tube became free to vibrate even more violently and bang on the inside of the inlet pipe.

After final TV inspections, the 12-in. access patch was rewelded to the inlet-pipe elbow. The weld was inspected with satisfactory results, and the entire secondary system was returned to the normal operating mode. As the flow of sodium in the secondary system was increased, noise monitoring of the IHX revealed nothing other than normal background vibrations.

b. Plant Improvements. H. W. Buschman (Last reported: ANL-7742, p. 56, Sept 1970).

(1) Increased Capacity of Motor-driven Feedwater Pump. The capacity of the motor-driven feedwater pump (MDFP) has been increased

about 15% by installation of an automatic recirculation-control (ARC) valve. During initial operation of EBR-II at 62.5 MWt, the MDFP was found to be running wide open without an overflow margin. Since the pump was being operated with constant recirculation, there was a possibility of increasing the effective pump capacity by shutting off the recirculation flow when the main flow was above the minimum allowable flow. An ARC valve that accomplishes this recirculation control without flowmeters or instrumentation was procured and installed during the maintenance shutdown. Operational checkout of the pump and valve has verified that the MDFP now has adequate capacity, with some overflow margin, when the plant is operating at 62.5 MWt.

(2) Sampling of Secondary-system Cover Gas. A new gas sampler was installed for the secondary-system argon cover gas. It has a recirculation loop with a transport time of less than 30 sec. A small sample is withdrawn from this loop for analysis by a gas chromatograph. The sample is provided to the chromatograph much faster than with the old system (~1 min compared with >1 hr). Although the new sampler is operational, the newly installed sodium-vapor trap is not performing satisfactorily. Sufficient sodium aerosol and/or vapor passes through the trap to cause blockage in the downstream tubing. Methods for improving the efficiency of the trap are being investigated.

(3) Primary-tank Pressure-Vacuum Relief System. A pressure-vacuum relief system for the primary-system cover gas was installed and operationally tested. The system protects the primary tank from differential pressures caused by buildup of vacuum of pressure either inside or outside the primary tank. The limits of pressure relief, relative to reactor-building pressure, were measured by tests as +13.7 in. and -4.3 in. H_2O.

2. Instrumented Subassemblies. E. Hutter, A. Smaardyk, and J. Poloncsik (02-048)

a. Instrumented-subassembly Facility (Last reported: ANL-7679, pp. 37-39, Mar 1970)*

The instrumented-subassembly system has been operative in EBR-II since November 1969, when the first of two in-reactor tests of the system were begun. In the first test, the drive system and dummy (unfueled) subassembly were installed, and the subsystems were tested while the reactor was subcritical. In the second test (Subassembly XX01), which can be considered an extension of the first, fueled capsules were in the subassembly, and system performance was evaluated while the reactor operated at full power. The objectives of this test were to assess: (1) the full capability

*Reported under: a. Test One and Two and b. Test Three.

of the system during reactor operation and (2) the ability to continually monitor fuel temperatures, coolant flow, pressures, and other parameters within the subassembly. Subassembly XX01 was an ANL prototype that demonstrated the feasibility of a variety of instruments, including (1) various thermocouples to measure temperatures in the subassembly, (2) a magnetic flowmeter to measure coolant flow through the subassembly, and (3) fission-gas-pressure transducers to measure pressures in the fuel elements. The test with Subassembly XX01 was satisfactorily concluded in April 1970, and the subassembly was then removed from the reactor. The instrumented subassembly (XX02) for the third test contains fuel elements supplied by an experimenter. (See Progress Reports for September 1969, ANL-7618, p. 30, and February 1970, ANL-7669, pp. 53-56.) The instrumentation was similar to that in Subassembly XX01. This subassembly was installed in the reactor in April 1970 and is operating satisfactorily.

b. Instrumented-subassembly Test 4 (XX03) (Last reported: ANL-7776, pp. 22-23, Jan 1971)

This subassembly, being shipped to the reactor site, contains apparatus for measuring irradiation-induced creep of structural materials while they are being irradiated in the reactor. The subassembly includes two additional new features: a micropositioner for measuring length change of the specimens, and a heating element to control the temperature of the specimens.

c. Future Instrumented Subassemblies (Not previously reported)

Two additional tests are being designed: Subassemblies XX04 and XX05. Both will contain experiments of Hanford Engineering Development Laboratories (HEDL), who also sponsor the experiment in XX03.

Subassembly XX04 (HEDL P-17A) will contain 35 elements fueled with UO_2-PuO_2 pellets. The instrumentation will be similar to that in Subassemblies XX01 and XX02. Subassembly XX05 (HEDL Creep Mark II) will be similar to Subassembly XX03, but will contain some design refinements.

3. EBR-II In-core Instrument Test Facility. E. Hutter (02-131)

a. Design and Development of Facility (Last reported: ANL-7758, pp. 42-48, Nov 1970)

(1) Calculation of Reactivity Effects (O. S. Seim and C. J. Divona). During reactor operation, the coolant-flow control valve of the in-core instrument test facility (INCOT) may be adjusted to regulate

the flow rate (and hence the temperature) of the sodium in the INCOT. Since actuation of the valve, which is above the small rotating plug of the reactor, changes the temperature (and hence the density) of the sodium, calculations have been made to determine the reactivity effect caused by valve actuation.

From worth measurements made on a ZPR-3 mockup of EBR-II with a uranium blanket, the worth of sodium in Row 5, averaged over a distance extending from 14 in. above to 14 in. below the midplane of the reactor, is 40 Ih/kg. The volume of sodium in the middle 28 in. of INCOT is 241 cm^3. For an unrealistically extreme case, in which the 241 cm^3 of sodium at a uniform temperature of 1200°F is assumed instantly replaced by the same volume of sodium at 700°F, the corresponding change in reactivity would be 0.64 Ih. The average worth used, and hence the resulting reactivity, would be higher for the reactor with the steel reflector. Tending to offset this, however, is that no account was taken of the decrease in average worth in going from the ZPR-3 to the larger-volume current EBR-II configuration.

A minimum of about 200 sec would be required for the motor-operated valve to change the sodium flow rate in INCOT from 0.5 to 32 gpm (equivalent, respectively, to 1200 and 700°F outlet sodium temperature). The resulting rate of change of reactivity (~0.003 Ih/sec) is small compared with the maximum rate of change of reactivity due to control-rod motion (1-2 Ih/sec).

(2) INCOT Hydraulics (J. Pardini and R. Brubaker). When INCOT becomes operational, a test of the FFTF flow sensor in the facility is planned. Since 8 to 12 instrument leads will pass between the flowmeter and the connections in the INCOT terminal box, and since approximately 12 ft of the leads will be submerged in flowing sodium, studies have been made to ensure that the leads are adequately supported.

The relative pressure drop and vibration susceptibility of several potential support schemes were briefly studied. The studies indicated that a reasonable compromise between stiffness and pressure-loss requirements would result if the lead wires were fastened to a solid 1/2-in.-dia rod attached to the flowmeter at one end and the terminal box at the other. The feasibility of this method was investigated by testing a full-scale (30-ft-long) mockup assembly of a flowmeter and several lead wires in a water test facility constructed of Lucite pipe. The test, conducted to velocities exceeding those expected in the reactor, showed that the assembly was quite stable at all flows. No perceptible flow-induced vibration occurred, although a slight wandering of the assembly in the pipe took place at infrequent and apparently random intervals.

(3) Pressure Drop of Sodium in INCOT Thimble (O. S. Seim and J. Wendte). The pressure drop in the thimble assembly containing the Model 3 sensor assembly for testing the FFTF in-core flow sensor was calculated for a sodium flow rate of 38.8 gpm. The pressure drop over the entire thimble assembly (including the flow valve) was calculated to be 47.6 psi. This pressure drop includes the effect of 10 instrument leads (each 0.125 in. in diameter) extending from the outer surface of the flow sensor to the top of the assembly. Since the allowable pressure drop is 46.6 psi, the maximum flow rate through INCOT should be slightly less than 38.8 gpm.

The calculated pressure drop of 47.6 psi is divided as follows: from sodium inlet holes to flow-valve inlet (excluding screen), 3.5 psi; across screen, 3.0 psi; across flow valve (wide open), 11.3 psi; from flow-valve outlet to flowmeter guide, 23.6 psi; from flowmeter guide through sodium outlet hole, 6.2 psi.

(4) Design Considerations of INCOT Flow Valve (O. S. Seim and J. Wendte). The INCOT flow valve must be able to control the sodium flow rate over a range from 0.5 to about 38 gpm. Its sensitivity must be such that the sodium temperature (measured at the susceptor outlet) will drop only about 50°F per degree of valve rotation. An orifice size of 0.086 in. (No. 44 drill) will give a flow rate of 0.5 gpm when the valve is in the closed position (0°). The valve-opening contour was designed so that the drop in the sodium temperature (measured at the susceptor outlet) would be about 50°F per degree of valve rotation over the range from 0 to 9°. Over that range of valve rotation, the sodium flow rate would range from 0.5 to about 2.5 gpm. Above the flow rate of 2.5, the flow would be controlled by the remaining rotation (up to 102°) of the valve.

(5) Mockup Testing of INCOT Components (O. S. Seim and R. H. Olp). Mockup testing of various INCOT components has been successfully done in the full-scale mockup of the EBR-II small rotating shield plug in Building D-331. Included was a test of a mockup of the elevator drive assembly, designed to raise the entire thimble assembly (including the terminal box) clear of the reactor core during fuel handling. The drive assembly will be attached to and supported from the existing control-rod center support column (see Fig. I.8). With this design, the drive assembly, sliding yoke, lead screws, guide track, and guidance-and-support assembly are between the centerline of the control-rod opening and the outside surface of the center support column. Thus, the subassembly-and-extension-tube package can be installed and removed with minimum disassembly. Only the elevator assembly need be removed for insertion or withdrawal of the thimble assembly.

The principal parts of the drive assembly successfully tested are: (a) the drive motor and gear reducer, on top of the extension

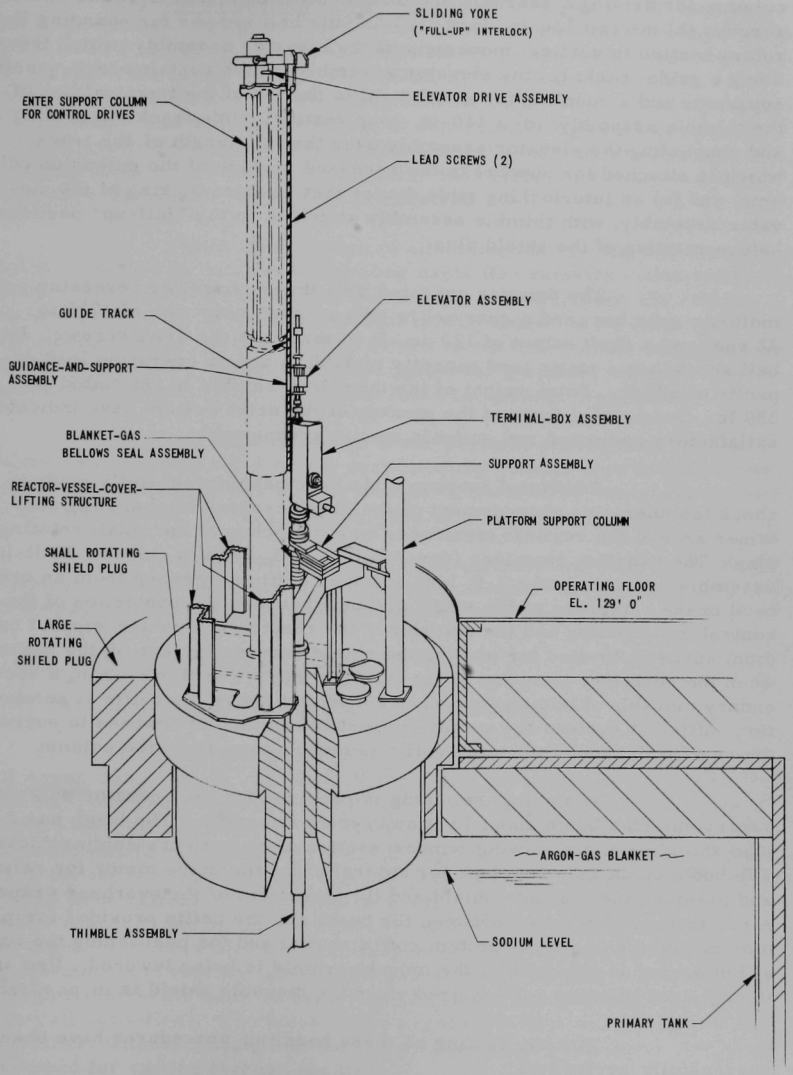

Fig. I.8. INCOT Elevating System

column, for driving a gear box and torque-limiting clutch to rotate two ball screws; (b) the two 120-in.-long, 1/2-in.-dia ball screws for changing the rotary motion to vertical movement of the elevator assembly, which travels along a guide track; (c) the elevator assembly, which contains load-sensing apparatus and a coupling for attachment to the top of the terminal box of the thimble assembly; (d) a 110-in.-long vertical guide track for guiding and supporting the elevator assembly over the full length of the track, which is attached for support to the recessed surface of the extension column; and (e) an interlocking slide device that ensures locking of the elevator assembly, with thimble assembly attached, in the "full-up" position before rotation of the shield plug.

The drive is operated by a three-phase, ac reversing gear motor, a gear box, and a gear set to give a speed reduction of 1725 to 32 rpm and a shaft output of 120-in.-lb of torque to the drive screws. Each ball screw has a static load capacity of 3150 lb and an operating load capacity of 600 lb. Total weight of the thimble assembly is estimated as 350 lb. Operational tests of the mockup of the drive system have indicated satisfactory operation and suitable spatial arrangement.

Additional mockup tests have been successfully made to check the operating arrangement of the thimble-assembly handling container around the vertical structures on the mockup of the small rotating plug. The handling container (described in ANL-7758, p. 45) is a 36-ft-long assembly consisting of a 7-ft-long shielded coffin suspended from an overhead crane. Because of the small distance between the centerline of the control-rod opening and the exterior of the control-rod center support column, space is limited for placing the shield around the rear of the coffin when the container is on top of the terminal box. For this reason, a secondary movable shielding section is suspended above the coffin at an elevation sufficient to clear the center support column and is lowered to surround the rear of the coffin when the coffin is moved away from the column.

Biological shielding is provided for the operator by a temporary shielded booth about 13 ft away from the coffin. The booth has 2-in. lead shielding and a viewing-window section of equivalent shielding thickness. The booth contains provisions for control of (a) the drive motor for raising and lowering the movable shield and (b) movement of the overhead crane. A mechanical connection between the booth and the coffin provides for manual closing and locking of the bottom coffin shutter and for positioning the coffin at the proper location while the movable shield is being lowered. Use of the shielded booth is not required after the movable shield is in position.

Mockup testing of these handling procedures have been successfully performed.

(6) Instrumentation and Control (W. Thompson, G. Giorgis, and R. Dickman). Design of the electrical control-and-interlocking network of the INCOT elevating system has been started. As with the instrumented-subassembly elevating system, the INCOT elevating system will be controlled from the EBR-II fuel-handling console. Almost identical circuitry will be used. The major differences in electrical design between the two systems are in the cabling arrangements and the location of electrical components such as junction boxes, force indicators, and relays. A new design for the junction boxes will be required.

Preliminary design of all wiring and cabling has been completed. The design includes a traveling cable that remains connected to the elevator assembly. Because of different space restrictions, the cabling scheme used on the instrumented subassembly could not be used. The scheme chosen for INCOT consists of two retractable cords, for power and control leads, and a spring-retracted pulley for guiding a shielded cable that carries the excitation and signal leads for a force transducer.

Preliminary design of the physical arrangement of the INCOT control components in the fuel-handling console also has been completed. These components will be located in the five-bay auxiliary cabinet next to the console. Detailed wiring diagrams are being prepared.

To test the operation of the controls and interlocks in the full-scale mockup, the temporary electrical control console originally used for testing the instrumented subassembly is being renovated.

4. Hot Fuel Examination Facilities (02-150)

a. Improvement of the FEF. M. J. Feldman

(1) Installation of Additional Wall Penetrations in the FEF Air and Argon Cells (M. D. Carnes). Fifteen new penetrations (14 and 16 in. in diameter) are being installed in the 5-ft-thick concrete shielding walls of the FEF air cell and argon cell. They will be used for future in-cell examination equipment or manipulators being planned. Five of the penetrations are in the walls of the air cell, and ten in the walls of the argon cell. The air-cell penetrations are for three new periscope locations, a precision gamma scanner, and an optical relay for use with an optical profilometer. The argon-cell penetrations are for eight new gas-sealed master-slave manipulators and two new gas-sealed periscopes. Drilling of the holes through the air-cell walls is being completed (with minimum interruption to in-cell activities). The holes in the argon-cell wall were drilled to the steel liner, without cutting into the liner. Plans and procedures are being developed for cutting through the liner.

(2) FEF Decontamination Facility (M. D. Carnes and K. H. Kinkade). A remotely operated decontamination facility has been installed in the basement of the FEF. Contaminated equipment (or apparatus) will be transferred through the air cell to the facility, where it will be decontaminated with steam or high-pressure water and various chemical agents. After being decontaminated to radiation levels permitting direct contact maintenance, the equipment will be transferred to a repair area. The facility is expected to be in routine operation soon.

(3) Filtration of Atmosphere of Argon Cell (M. D. Carnes and K. DeCoria). Two independent subsystems (north and south) cool and circulate the atmosphere of the argon cell. The equipment for the two subsystems is in the subcell area of the FEF. Because of radiation difficulties encountered in performing direct maintenance on the equipment, it was decided to remotely install in-cell subsystem filter units to filter all the circulating atmosphere. As reported in the Progress Report for June 1970, ANL-7705, pp. 111-112, the filtration system* for the north circulating subsystem was installed first. A similar system has now been installed for the south circulating system. Both circulating subsystems have been operating satisfactorily. All recirculating argon can now be filtered.

(4) Handling Subassemblies Containing Failed Fuel (D. M. Paige). A system is being developed for handling a subassembly containing a fuel failure in EBR-II that is too severe for safe handling with standard procedures. (See Progress Reports for March 1970, ANL-7679, pp. 34-36, and October 1970, ANL-7753, pp. 44-48.) Other equipment is being designed for transfer of the failed-fuel subassembly from the reactor to the FEF and for the in-cell disassembling and examination of the subassembly. The subassembly will be removed from the reactor in a sodium-filled container, which is sealed in a separate gas-tight container within a cask. The gas-tight container, holding the subassembly, will be removed from the cask through the air-cell floor port, raised into the air cell, and then transferred to the argon cell, where the subassembly will be examined and disassembled.

Before the subassembly is disassembled, it will be given nondestructive examinations in the argon cell. These will include gas-flow measurements, visual and photographic observations, neutron radiography, and dimensional measurements. Equipment for these examinations is in the conceptual stage, but some of it will only be modifications of existing FEF or commercially available items.

For the disassembling step, a commercially available milling machine with numerical control has been selected to cut the hexagonal can of the subassembly. It will be modified for use in an argon atmosphere.

*The filters are Dri-Pak 100 filter cartridges (glass-fiber media), fabricated by the American Filter Company, Inc.

The fuel elements from the subassembly will be examined in the air and argon cells, primarily with existing FEF equipment. The examinations will include visual and photographic observations; gamma scanning; neutron radiography; measurements of diameter, bow, length, and balance point; and gas sampling.

Besides those items directly associated with the failed-fuel subassembly, some additional equipment related to radiation protection will be provided because alpha contamination will be a possibility. This equipment will include alpha monitors and a breathing-air supply system.

(5) Installation of New In-cell Transfer Platen (K. H. Kinkade). All large items transferred between the air and argon cells are moved by a 78-in.-dia platen carried by a cart on tracks in a runway between the two cells. The platen, after being hydraulically lifted into position, also serves as the bottom cover of the large transfer lock in the argon cell. The existing platen, which had been in operation since 1962, was recently replaced. The new platen was installed because it had an additional feature: a well approximately 12 in. in diameter by 16 in. deep. This well will allow transfer of longer items (up to about $9\frac{1}{2}$ ft long), such as subassemblies, between the cells. The seal on the new platen was leak-tested after installation and found acceptable.

PUBLICATIONS

Yields of Fission Products for Several Fissionable Nuclides at Various Incident Neutron Energies

K. F. Flynn and L. E. Glendenin
ANL-7749 (Dec 1970)

Description of Software for the EBR-II Digital Data Acquisition System

R. W. Hyndman, J. M. Allen,* R. A. Call, E. W. Laird, M. R. Tuck, and K. D. Tucker
ANL/EBR-033 (Dec 1970)

A Prototype Analog Reactivity Meter for EBR-II

J. R. Karvinen, R. W. Hyndman, R. A. Call, and C. C. Price
ANL-7700 (Feb 1971)

Fine-Spectral Interface Effects of Resonance Scattering upon the Multigroup Cross Section Averaging

D. Meneghetti and K. E. Phillips
J. Nucl. Energy 24, 509-524 (1970)

Local Modification of Irradiation Conditions

L. B. Miller and R. E. Jarka
ANL/EBR-035 (Jan 1971)

Origin of Fission-product Releases in EBR-II, November 23, 1967, to May 6, 1968

R. R. Smith, E. R. Ebersole, R. M. Fryer, and P. B. Henault
ANL-7604 (Dec 1970)

*Division of Reactor Development and Technology, USAEC.

II. LMFBR DESIGN SUPPORT

A. Core Component Test Loop (CCTL).
R. A. Jaross (02-026)

The CCTL is operated, maintained, and modified to facilitate long-term tests of prototype FFTF fuel assemblies and in-core instrumentation in sodium under conditions established by the FFTF and LMFBR Programs. Technologies pertinent to sodium-loop operation (e.g., surveillance of sodium and cover-gas quality, and material compatibility, including the Type 304 loop structure) are developed and improved concurrently.

1. Operation of Loop to Test Second FFTF Subassembly. F. A. Smith
(Last reported: ANL-7783, pp. 30-31, Feb 1971)

As agreed with the FFTF Project staff, the CCTL was shut down on March 15 for interim examination and possible modification of the Mark-II fuel assembly.

At the time of shutdown, the CCTL had accumulated 6287 hr of flow-testing the Mark-II fuel assembly at 1100°F and ~525 gpm. During this period, the total downtime was 15.8 hr, yielding an overall facility operating factor of greater than 99%. This reflects the fact that no significant malfunction of either the fuel assembly or the CCTL occurred throughout the flowtest. Based on the flow rate of 525 gpm, it is estimated that 26.6 million cubic feet of sodium passed through the fuel assembly.

After shutdown of the CCTL, the in-core instrument package associated with the fuel assembly was removed first and cleaned. On March 23, the fuel assembly was removed from the test vessel, and is presently being cleaned of a trace film of residual sodium on the surfaces. Examination of the fuel assembly will be conducted by the FFTF Project staff at Hanford. Upon completion of the examination, the fuel assembly will be returned for resumption of the flowtest to complete the goal of 9000 hr.

PUBLICATIONS

Vibration of a Class of Nonconservative Systems with Time-Dependent Boundary Conditions
S. S. Chen
Shock Vib. Bull. 41 (Part 7), 141-150 (Dec 1970)

Turbulent Mixing and the Thermal Deflection of Fuel Pins--a Procedure with Application to the LMFBR
T. Ginsberg
Nucl. Eng. Design 14, 191 (1970)

III. INSTRUMENTATION AND CONTROL

A. Instrumentation Development for Instrumented Subassembly. T. P. Mulcahey (02-024)

Instruments for in-core measurement of flow, fuel and coolant temperatures, and fuel-pin pressure are being developed consistent with requirements defined by the EBR-II Instrumented Subassembly test program. Development encompasses instrument design, performance analysis, fabrication, and tests leading to specifications and quality-assurance procedures for procurement from commercial vendors.

1. Fuel-pin Thermocouples. A. E. Knox

a. In-pile Tests in EBR-II Instrumented Subassembly (Last reported: ANL-7705, p. 39, June 1970)

Procedures for postirradiation examination of Fuel Center Thermocouples (FCTC) 1, 2, 7, and 17 have been prepared. These thermocouples were irradiated in the Test XX01 EBR-II Instrumented Subassembly (ISA).

FCTC 2 and 7 will be examined in conjunction with examinations by the Materials Science Division at Argonne. FCTC 1 and 17 will be examined at the EBR-II site. FCTC 1 will only be examined metallographically. Examinations of FCTC 2, 7, and 17 will include loop and insulation resistance measurements and metallographic analysis. Equipment for the in-cell electrical examinations has been fabricated.

A report on the design and construction of fuel center thermocouples for the Test XX01 ISA was initiated.

B. FFTF Instrumentation Development. R. A. Jaross (02-025)

Prototypes of permanent-magnet, eddy,current, and magnetometer probe-type flowsensors are being designed, fabricated, and flowtested to establish detailed specifications and design for the FFTF permanent-magnet probe-type flowsensor, and to provide technical guidance to ensure competence in commercial fabrication of probe-type flowsensors. Supporting tests are conducted to determine long-term thermal effects on permanent-magnet materials of interest, and to study the effects of simulated fission-gas release on flowsensor response.

Flowtests and certain supporting tests are conducted in existing facilities (CCTL or CAMEL); new specialized facilities are designed and constructed, as required.

1. Permanent-magnet Probe-type Flowsensors. F. Verber (Last reported: ANL-7783, pp. 21-22, Feb 1971)

Design of a 20-furnace system for long-term temperature-stability testing of Alnico VIII magnets for Type A-4¼ flowsensors is in progress. In operation, measurements of magnetic field strength at temperature will be made, using built-in search coils and an integrating fluxmeter to determine stability or aging of the magnets. These measurements will indicate the combined structural, irreversible, and reversible temperature effects as they will occur in dynamic sodium systems. A prototype electric furnace has been built and is undergoing testing.

Work has continued to adapt the permanent-magnet flowsensor to the dry-thimble concept with spring-loaded electrodes. (See Progress Report for December 1970, ANL-7765, Fig. I.C.2, p. 25.) A contact-resistance test in an air-atmosphere furnace is in progress, using a test assembly consisting of two coiled pieces of 0.060-in.-dia Inconel welding rod inserted into a 1-in.-OD Type 304 stainless steel tube.

Measurements at temperatures from 1000 to 1350°F show that the contact resistance has not exceeded 1.5 Ω.

2. Eddy-current Probe-type Flowsensors. J. Brewer (Last reported: ANL-7783, pp. 22-24, Feb 1971)

On the date of CCTL shutdown (March 15, 1971), Eddy-current Probe No. 12 had completed 1117 hr of operation in sodium at 1100°F and ~525 gpm, or an average sodium velocity of 16.4 ft/sec in the annulus around the probe. The probe was removed from the CCTL on March 16, 1971.

In ANL-7783, it was stated that although the sodium velocity was held constant at 16.4 ft/sec, the flowsensor signal output increased during the first two days of operation, and thereafter remained stable. Therefore, before removal of Probe No. 12 from the CCTL, a series of tests was performed to aid in determining the cause of the increase in signal output.

The results of these tests, when compared to data taken during the first day of CCTL testing, indicate that the balance was corrected by: (1) decreasing the CCTL flow rate to 2 ft/sec, (2) adjusting the balance controls (phase and amplitude) to lower the signal output to the correct level (see Fig. I.C.1, ANL-7783, p. 22), (3) increasing the flow to 16.4 ft/sec, (4) comparing the signal output with the original value, and (5) trimming the balance controls as necessary.

The success of this correction proves that the actual flow sensitivity of the probe did not change during the first two days of CCTL testing; rather

the balance did and never changed thereafter. Figure III.1 shows the data taken on March 15 with the original balance setting (Curve A) and with the corrected balance setting (Curve B).

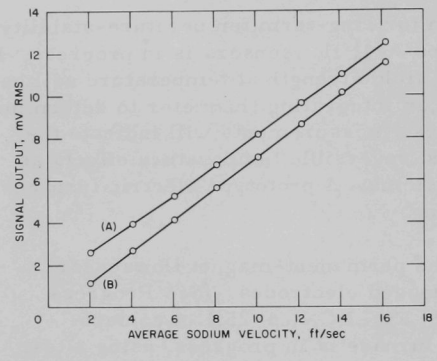

Fig. III.1. Comparison of Eddy-current Probe No. 12 Output Signals in the CCTL at 1055°F: (A) with Original Balance Setting, and (B) with Corrected Balance Setting. Drive Current: 500 mA at 1000 Hz.

Further static tests will be performed on Probe No. 12 to determine the cause of the initial shift in balance.

3. Magnetometer Probe-type Flowsensors. D. E. Wiegand (Last reported: ANL-7783, pp. 24-25, Feb 1971)

A partial shipment of lock-in amplifier equipment was received and used in dry tests of Magnetometer Flowsensor No. 2 (MFS-2). As expected, marked improvements in flowsensor performance were achieved. In particular, the bothersome residual signal has been eliminated, and linear response through zero signal was obtained without operating in an offset mode. (See Progress Report for November 1970, ANL-7758, pp. 30-32.) This has reflected a large increase in fluxgate sensitivity. For example, a change in ambient field of 50 gammas (0.5 mG) gave a large deflection of the instrument meter. Further increases in sensitivity were prevented by limitations in the method used to balance the ambient field, and the high magnetic-noise level in the laboratory.

Demonstration of this sensitivity attests that the problem of saturation of the fluxgate core end regions by the field magnets is not serious. Possible paralysis of the sensor had been envisioned, since the fluxgate is located in the neutral region between the magnets, but the field is zero only at the core center.

4. Thermal Stability Tests on Permanent Magnets. G. A. Forster (Last reported: ANL-7776, pp. 15-16, Jan 1971)

Table III.1 lists the average percentage change in magnetic field strength of Alnico V and VIII magnet samples after 3200 hr in the individually heated, multisection, high-temperature oven. The values are based on the average of five samples for the specific temperature and L/D ratio shown. The measurements were made at room temperature.

In general, there is an average increase in field strength in the range 900-1100°F. This "recovery effect" has been noted previously and is probably a function of the temperature used in the stabilization procedure.

No leveling off is apparent, especially at the highest temperatures; here, rapid decreases continue. The maximum operating temperatures would appear to lie between 1000 and 1100°F for the Alnico V magnets, and between 1100 and 1200°F for the Alnico VIII magnets.

TABLE III.1. Thermal Stability of Alnico V and VIII Magnets at 700-1200°F

Temp, °F	L/D Ratio	Avg Change in Magnetic Field Strength, %				
		818 hr	1500 hr	1900 hr	2600 hr	3200 hr
		Alnico V				
700	1	- 3.2	- 3.8	- 5.0	- 5.2	- 5.0
	2	- 1.1	- 1.1	- 1.1	- 1.1	- 0.5
	4	+ 0.5	+ 0.5	+ 0.3	+ 0.2	+ 1.7
800	1	- 1.3	- 1.0	- 1.3	- 1.9	- 0.7
	2	- 0.1	+ 0.6	- 0.1	+ 0.3	+ 1.0
	4	0.0	+ 0.3	- 0.3	- 0.9	+ 1.8
900	1	+ 2.8	+ 3.7	+ 2.9	+ 4.2	+ 4.1
	2	+ 1.8	+ 2.2	+ 2.1	+ 2.9	+ 3.1
	4	+ 3.2	+ 3.7	+ 3.5	+ 4.4	+ 4.2
1000	1	+13.6	+14.0	+13.2	+13.9	+14.0
	2	+ 6.1	+ 7.2	+ 6.1	+ 6.9	+ 7.4
	4	+ 7.5	+ 7.6	+ 7.6	+ 5.9	+ 7.1
1100	1	+ 3.2	- 4.9	-13.6	-16.2	-21.8
	2	+ 0.5	- 2.1	- 4.9	- 7.6	-11.7
	4	+ 3.5	+ 1.8	- 6.2	- 4.8	- 5.4
		Alnico VIII				
900	1	+ 6.1	+ 7.1	+ 6.5	+ 7.6	+ 8.2
	2	+ 5.1	+ 5.9	+ 5.2	+ 6.7	+ 7.5
	4	+ 4.4	+ 4.6	+ 4.1	+ 4.2	+ 5.2
1000	1	+14.6	+16.5	+16.9	+20.2	+21.9
	2	+ 8.5	+10.9	+10.2	+12.8	+14.5
	4	+ 7.7	+ 9.1	+ 8.2	+10.2	+11.8
1100	1	+17.0	+16.8	+15.1	+14.3	+13.5
	2	+11.7	+12.2	+ 7.9	+ 9.5	+ 8.7
	4	+ 7.8	+ 7.2	+ 3.9	+ 4.7	+ 4.2
1200	1	- 7.0	-24.5	-33.6	-44.5	-53.3
	2	-10.8	-28.8	-33.0	-43.0	-48.3
	4	- 6.4	-16.4	-25.4	-31.3	-36.3

To more accurately predict the performance of a single sample exposed to these temperatures, knowledge of the statistical spread of data is necessary. Table III.2 presents an analysis of the data for the latest measurements; it includes the standard deviation (sigma), maximum and minimum change, and maximum deviation from the average change. Also

included are instrumentation and operator errors; an estimate of these is available from the reference magnet readings taken at the same time. For example, if the reference magnets are assumed 100% stable, an analysis of the data yields a standard deviation of 0.9%. Therefore, much of the scatter in data for the lower temperatures could be caused by measurement errors. At the higher temperatures (1100°F for Alnico V and 1200°F for Alnico VIII), where there is rapid decay of magnetic strength, the standard deviation is definitely greater than measurement errors.

TABLE III.2. Data Spread for Alnico V and VIII Magnets after 3200 hr at 700-1200°F

Temp, °F	L/D Ratio	% Change				
		Avg	Sigma	Max	Min	Max Dev from Avg
			Alnico V			
700	1	- 5.0	1.1	- 6.7	- 3.4	1.7
	2	- 0.5	1.4	- 4.2	+ 0.3	3.7
	4	+ 1.7	0.7	+ 3.1	- 0.9	1.4
800	1	- 0.7	0.4	- 1.3	0.0	0.7
	2	+ 1.0	1.1	+ 2.6	- 1.1	2.1
	4	+ 1.8	1.2	+ 3.0	+ 0.8	2.8
900	1	+ 4.0	1.3	+ 6.8	+ 3.1	2.8
	2	+ 3.1	0.8	+ 4.4	+ 1.6	1.5
	4	+ 4.2	0.6	+ 5.3	+ 3.1	1.1
1000	1	+14.0	0.9	+15.9	+12.5	1.9
	2	+ 7.4	0.7	+ 8.2	+ 6.4	1.0
	4	+ 7.1	1.3	+ 9.6	+ 5.6	2.5
1100	1	-21.8	9.1	-34.7	-12.7	12.9
	2	-11.7	9.7	-27.8	- 3.0	16.1
	4	- 5.4	2.4	- 8.5	- 1.5	3.9
			Alnico VIII			
900	1	+ 8.2	1.5	+11.6	+ 6.4	3.4
	2	+ 7.5	0.8	+ 9.1	+ 6.2	1.6
	4	+ 5.2	1.5	+ 6.9	+ 1.6	3.6
1000	1	+21.9	4.3	+30.8	+17.2	8.9
	2	+14.5	1.2	+17.3	+13.1	2.8
	4	+11.8	1.0	+13.0	+ 9.6	2.2
1100	1	+13.5	1.1	+15.7	+12.3	2.2
	2	+ 8.7	2.6	+11.3	+ 3.6	5.1
	4	+ 4.2	0.9	+ 5.3	+ 3.0	1.2
1200	1	-53.3	6.4	-61.5	-42.9	10.4
	2	-48.3	3.3	-52.9	-43.9	4.6
	4	-36.3	2.7	-40.5	-33.0	4.2

C. Advanced Technology Instrument Development. T. P. Mulcahey (02-096)

1. Boiling Detector. T. T. Anderson

a. Acoustic Method

(1) Irradiation and Resistance Tests on Piezoelectric and Insulator Materials. T. T. Anderson (Last reported: ANL-7776, p. 81, Jan 1971). Irradiations of lithium niobate by 2-MeV Van de Graaff electrons and by ^{60}Co gamma rays (using ANL Chemistry Division facilities) have shown that lithium niobate has radiation stability comparable to close-packed oxides such as sapphire. However, exposure to neutrons is expected to result in a segregation of gas within the lithium niobate crystal structure from the nuclear reaction

$$^{6}Li + {}^{1}n \rightarrow {}^{4}He + {}^{3}H.$$

Irradiation to destruction in a nuclear reactor would be lengthy; on the other hand, results from a study on gas segregation may be indicative of what might occur. Therefore, it was proposed that the experience and techniques developed by Primak and Luthra* for studying radiation blistering from gas injection be applied to compare the behavior of lithium niobate to previously studied materials, and from this make an estimate of possible effects of gas buildup from the $^{6}Li(n,\alpha)T$ reaction. Polished disks of lithium niobate and sapphire were bombarded with 140-keV H^+, D^+, and He^+ ions produced by the Chemistry Division Cockcroft-Walton accelerator.

Blisters and exfoliated areas formed on the lithium niobate and the sapphire in a manner similar to that reported by Primak and Luthra for magnesium oxide, sapphire, and spinel. In their studies, specimens with 10% of the gas load normally required to cause blistering developed exfoliated areas after heating to 900°C. Therefore, for engineering purposes, a 10% factor was used to estimate that an accumulated gas load of less than 6×10^{20} atoms/cc in lithium niobate may prevent blistering at elevated temperatures. For example, since this amount of gas corresponds to fissioning of 20% of ^{6}Li in natural lithium, the equivalent gas load might be reduced a factor of 4 or 5 by depletion of ^{6}Li relative to the more abundant ^{7}Li isotope.

Further studies on radiation effects are in progress. The feasibility of using the ANL Cyclotron for accelerated radiation-damage testing of lithium niobate is being evaluated.

*W. L. Primak and J. Luthra, Radiation Blistering: Interferometric and Microscopic Observations of Oxides, Silicon, and Metals, J. Appl. Phys. 37(6), 2287-2294 (1966).

(2) Development of High-temperature Detector. A. P. Gavin (Last reported: ANL-7783, p. 76, Feb 1971). Five sensors have been constructed, using 36° Y-cut lithium niobate crystals, platinum foil electrodes, stainless steel housings, and 3-ft lengths of aluminum-oxide insulated, 1/8-in.-OD stainless steel-clad coaxial cable with a stainless steel conductor. Three of these sensors, each backfilled with oxygen at 150 mm Hg, were cycled to 1200°F in a furnace test facility.

Each sensor showed good reproducibility of both resistance and output signal. The measured resistance approximated that calculated for the crystals, using available data for resistivity of lithium niobate. However, the output signal, measured with a voltage amplifier, decreased rapidly as the resistance decreased with increasing temperature. It is anticipated that a new charge amplifier, designed for use with low-resistance units, will alleviate this problem.

A procedure has been developed for sealing the 1/8-in.-OD vent tube employed on all sensors being evaluated. After the characteristics of the five units are established, tests will be initiated on units sealed with an internal atmosphere of oxygen at 150 mm Hg abs at room temperature.

(3) Tests of High-temperature Detectors in Water, Furnace, and Sodium. A. P. Gavin (Last reported: ANL-7783, p. 76, Feb 1971). A programmable control system has been obtained for the furnace calibration facility. In operation, the system will permit unattended cycling of high-temperature detectors from room temperature to 1200°F in 8 hr, and then back to room temperature over an equal time span. During the 16-hr cycle, an automatic plot is made of the sensor response and of the reference accelerometer output as a function of furnace temperature. The automatic features of this system will facilitate evaluations for longer continuous periods at reproducible cycling conditions.

(4) Development of Acoustic Waveguides. T. T. Anderson (Not previously reported). A real-time spectrum analyzer and a digital cross-correlator have been employed in conjunction with accelerometers mounted on the Core Component Test Loop (CCTL) to determine if transmission of acoustic-range vibration signals along loop structures could be detected by these methods. There was no apparent cross-correlation for accelerometers located at the top and bottom of the test vessel during loop operation. Slight correlations were observed for vibration signals from adjacent locations on the sodium pump housing. These observations indicate that interference may be occurring as a result of multiple acoustic paths and reflections. Further studies with the correlator will be deferred until the unit is modified to minimize the possibility of input overload.

Spectra obtained with the real-time analyzer were comparable to those obtained with a sweep-frequency analyzer; however, the amplitude range of the spectrum averager was insufficient for quantitative studies. The analyzer, which was rented for the stu

Preparations are being made to evaluate acoustic waveguides which would simulate FFTF instrument guide tubes and the acoustic transmission path to an accelerometer mounted in the Test XX03 EBR-II Instrumented Subassembly. One 20-ft-long tubular waveguide has been fabricated; a solid waveguide is in fabrication. A catwalk has been constructed around a large (5.5-ft-dia x 11-ft-deep) water-filled vessel to facilitate handling long waveguides that extend down into the water.

2. Flow Monitor. T. T. Anderson

a. Two-thermocouple Method. A. E. Knox

(1) Temperature Variations of Coolant Sodium at Outlet of the EBR-II Instrumented Subassembly (Last reported: ANL-7705, pp. 154-155, June 1970). The results of spectrum analyses of thermocouple output from the Test XX01 Instrumented Subassembly (ISA) have been prepared for limited distribution.* A procedure outlining the data to be obtained from the Test XX02 ISA has been prepared.

D. Plant Dynamics and Control Analysis.
W. C. Lipinski, RAS (02-528)

1. Simulation of Simplified Plant Model on Hybrid Computer (Last reported: ANL-7783, p. 30, Feb 1971)

Simulations of various plant controllers are being added to the hybrid-computer simulation of a complete LMFBR plant. These control simulations are to be used in the analysis of proposed methods of trim control about a fixed load demand.

PUBLICATIONS

High-Temperature Acoustic Sensors for Boiling Detection
A. P. Gavin and T. T. Anderson
IEEE Trans. Nucl. Sci. NS-18(1) (Part I), 340-344 (Feb 1971)

Studies of Fission-gas Disengagement and Transport Phenomena for FFTF Fuel-failure Detection
E. S. Sowa, F. Verber, and G. T. Goldfuss
ANL-7774 (Jan 1971)

*A. E. Knox and C. W. Michels, Coolant Temperature Variations in the EBR-II XX01 Subassembly, ANL/ETD-71-02 (Jan 25, 1971).

IV. SODIUM TECHNOLOGY

A. Monitoring and Sampling Systems Development and Reactor Proof-test (02-021)

Argonne has been given the responsibility of implementing a national meter program for developing, testing, and establishing commercial availability of meters for use in the sodium systems of FFTF and LMFBR's. The meters to be developed and characterized in this program are monitors for oxygen, carbon, and hydrogen and a leak detector for steam generators. Meter modules that provide flow and temperature control are being developed for FFTF. These modules will be tested at EBR-II.

1. Oxygen Meter. J. T. Holmes, J. M. McKee, and V. M. Kolba (Last reported: ANL-7765, pp. 29-30, Dec 1970)

A program has been established that is expected to result in the commercial availability of improved electrochemical oxygen meters by July 1971. ANL is coordinating efforts to produce improved solid-electrolyte tubes (isostatically pressed thoria-7.5 wt % yttria) at WADCO and Zircoa (Zirconium Company of America) and to evaluate the material by performance tests in sodium at Westinghouse and Brookhaven National Laboratory (BNL). The work is showing encouraging results: Two cells with electrolyte tubes produced at WADCO have been operated for more than 1000 hr at 370-485°C.

A pumped-sodium apparatus has been constructed to proof-test up to four oxygen meters, and operation of the apparatus has begun.

Apparatus is being designed to provide for an extended characterization of the performance of 10 standard oxygen meters. These will be installed in a pumped-sodium system in series with a specimen-equilibration module, which will be used to calibrate the oxygen meters by the vanadium-wire equilibration method,* and with a cold trap to control the oxygen content of the sodium. Initial calibrations at 430°C and at oxygen levels from <1 to 15 ppm will be repeated after three months of continuous operation. Testing will continue for at least a year under conditions determined by results of the three-month tests.

Preparations have continued for a test at EBR-II to determine the effect of radiation on the oxygen meter. The meter to be tested was supplied by Westinghouse and has an electrolyte tube produced at WADCO by isostatic pressing. A unit that includes the meter, a heater, thermocouples, and the auxiliary piping for installation has been assembled and the unit has been shipped to EBR-II.

*Sodium Technology Quarterly Report: January, February, March 1970, ANL/ST-2, pp. 2-4 (July 1970).

2. Hydrogen Meter. J. T. Holmes and D. R. Vissers (Last reported: ANL-7765, p. 30, Dec 1970)

Development work is being continued on an equilibrium-type hydrogen-activity meter having a direct pressure readout of the equilibrium hydrogen pressure above the sodium.* A capacitance manometer has been evaluated for possible use as a pressure gauge for the meter. A Varian Millitorr ionization gauge was also tested previously for this application (see ANL-7765). The tests of the capacitance manometer have shown that when the device is carefully operated, the hydrogen contents derived from the measured pressures agree well with results of gas-chromatographic analyses. However, the capacitance manometer is sensitive to vibration and temperature fluctuations, a disadvantage that may prevent its use as a component of the hydrogen meter, except in laboratory applications.

The response of the hydrogen-activity meter to changes in hydrogen concentration was tested at a lower temperature (372°C) than had been previously used in meter operation (~500°C). This information is needed because it may be necessary to operate the hydrogen meter at the lower temperature in the oxygen-hydrogen meter modules. In the recent tests, the capacitance manometer was used as the pressure-sensing device. The time required for the meter to respond to a step change in the hydrogen level of the sodium was 40-60 min at 372°C as compared with 10-20 min at 500°C. The response time at 372°C should be adequate for reactor applications.

Low-level gamma-radiation studies with ^{60}Co indicated that neither the capacitance manometer nor the Varian Millitorr pressure-sensing device is affected by an exposure of ~15 min to low-level gamma radiation (surface dosage rate, ~200 R/hr). Tests at higher radiation levels are planned.

Nickel bellows-shaped membranes are currently being evaluated for applications in which the membranes will be subjected to high pressures. Tests of membranes produced by an electrodeposition process showed that the membranes developed small blisters during hydrogen annealing. Moreover, tests in sodium indicated that these membranes do not diffuse hydrogen adequately. Electrodeposited membranes will not, therefore, be considered further. Bellows-shaped membranes formed both from tube and sheet nickel are being obtained for evaluation.

3. Carbon Meter. J. T. Holmes and C. Luner (Last reported: ANL-7765, p. 31, Dec 1970)

The meter being given primary consideration for the carbon-meter module is a modification of the United Nuclear Corporation (UNC) diffusion meter. Studies are being carried out at various operating conditions to

*Sodium Technology Quarterly Report: July, August, September 1970, ANL/ST-4, pp. 12-13 (Dec 1970).

optimize the response of the carbon meter at low carbon levels. These studies will also provide a comparison of the response of the UNC carbon probe (stainless steel housing) with that of the ANL-modified probe, which has a molybdenum liner in the high-temperature housing and in which all hot surfaces in contact with collected carbon-bearing gases are copper plated.

The effects of sodium flow, probe temperature, water content of decarburizing gas, and gamma radiation on the carbon flux through the membrane are being investigated. A threefold increase in the sodium flow (0.02 to 0.06 gpm) produced a small (10-15%) increase in the flux of the ANL version of the meter; similar flow effects had been noted earlier with the UNC meter. An increase in temperature produced a small increase in the carbon flux of both meters. An increase in the water content of the decarburizing gas increased the carbon flux of both meters significantly.

The gamma radiation to which the carbon probe will be exposed during reactor operation is not expected to affect the structural components markedly. However, radiation-induced reactions of the gases in the probe (CO and H_2O) could affect the carbon flux. To test this possibility, the operating UNC probe was exposed to low-level gamma radiation from a ^{60}Co source (20-min exposure at a surface dose rate of 89 R/hr). This radiation level had no effect on the carbon flux. Exposures at higher radiation levels are planned.

4. Meter Modules for FFTF. J. T. Holmes, V. M. Kolba, and J. M. McKee (Last reported: ANL-7765, pp. 29-30, Dec 1970)

The objective of this work is to design, proof-test, and establish commercial availability for on-line meter modules to be installed at FFTF. These modules include flow and temperature controls as well as the meters for monitoring impurities.

a. Oxygen-Hydrogen Meter Module

A detailed design* has been completed for an on-line monitoring module containing two oxygen meters and one hydrogen meter and the associated hardware and electronics. Comments from EBR-II and FFTF on the conceptual design have been incorporated in the detailed design. Procurement of materials, equipment, and electronic components has been initiated. Two modules will be built. The first module to be completed will be tested on a pumped loop at ANL-Illinois to establish the performance of the instrumentation for control of temperature and flow. The second module will be installed and proof-tested at EBR-II.

*Electrical design work is being done by M. A. Slawecki, Chemical Engineering Division; mechanical and structural design work, by E. C. Filewicz, EBR-II Project.

b. Carbon-meter and Specimen-equilibration Module

A detailed design* has been completed for an on-line carbon-meter module. By substitution of a specimen holder for the carbon-meter probe, this unit can also serve for equilibrating metal specimens to be used in calibration of the oxygen and carbon meters. Fabrication of two modules has been started. One module will be tested at ANL-Illinois; the other will be installed and proof-tested at EBR-II.

5. Detection of Leaks in Steam Generators. (J. T. Holmes, D. R. Vissers, and C. C. McPheeters (Last reported: ANL-7765, p. 31, Dec 1970)

The work in this program involves the evaluation of requirements for a leak detector for LMFBR steam generators and the development and proof-testing of a detection system to meet these needs. A diffusion-type hydrogen monitor is being developed at ANL. This monitor appears to have a capability of detecting a 4% change in the hydrogen level at a concentration of 0.1 ppm hydrogen in sodium. This is well above the sensitivity required for detecting water inleakage that would lead to rapid perforation of adjacent tubes in a large generator (10^6 lb sodium/hr).

The ion-current stability of a special ion pump has been evaluated to determine its potential as the detector component of the hydrogen-meter leak detector. The pump is specially designed to pump hydrogen and should therefore possess a longer pumping life than a standard pump. The results of the studies with the special ion pump (pumping speed, 20 liters/sec) indicated a stability of $\pm 0.53\%$, as compared with $\pm 0.06\%$ for the D-I ion pump (pumping speed, 11 liters/sec) presently being used. The larger deviation for the special pump is thought to result from its larger size. Special hydrogen pumps having pumping speeds of 11 liters/sec are now available, and these will be similarly tested for stability.

ANL has agreed to supply a hydrogen-meter leak detector to the Liquid Metal Engineering Center (LMEC) by April 1, 1971; the leak detector will be used on the Sodium Components Test Installation (SCTI) at LMEC. The detector design has been approved by LMEC, and the unit is being fabricated. The leak-detector alarm system has been designed and ordered. Orders have been placed for all of the instrumentation, and the project appears to be on schedule.

*Ibid., see previous page.

B. Sodium Impurity Analysis and Control (02-156)

1. Establishment and Operation of a Sampling and Analytical Standards Program. R. J. Meyer, F. A. Cafasso, M. H. Barsky, H. S. Edwards, S. B. Skladzien, M. D. Adams, and M. F. Roche (Last reported: ANL-7765, p. 63, Dec 1970)

Argonne has the responsibility of certifying sampling and analytical methods for use throughout the sodium-technology program. The short-range goal is a set of interim standard methods, selected from existing technology, which will be uniformly applied at all sites participating in the program. To this end, an Analytical Standards Laboratory has been established, whose function is to manage the analytical standards program, as well as to participate in it.

With the aid of an advisory group representing both reactor and nonreactor laboratories, ANL has established a set of interim sampling and analytical methods. Procedural details of these methods have been incorporated into a manual titled Interim Methods for the Analysis of Sodium and Cover Gas, to be published as ANL/ST-6. Prepublication copies of the manual have been distributed to all laboratories participating in the analytical standards program.

Samples of EBR-II primary and secondary sodium to be used in a sample interchange program among the reactor laboratories were taken by EBR-II personnel, and these have been sent to each participant. Analyses will be performed for hydrogen, carbon, oxygen, and trace metals. Plans have been made for future interchange programs, which will also include the nonreactor laboratories.

ANL has been given the responsibility for generating purity specifications for sodium systems. The RDT standard for sodium purchase specifications (RDT M13-IT) is being revised. A meeting was held recently with representatives from E. I. duPont de Nemours, a major supplier of sodium, to obtain information on sodium production. This information will be useful in producing the new purity specifications. Meetings are also planned with Ethyl Corp. and U. S. Industrial Chemicals Co.

Preparations are being made to perform a set of experiments to determine the effect of line length on the trace-impurity content of sodium samples. In these experiments, a sudden increase in impurity content will be produced at one end of a 100-ft-long section of tubing in a bypass loop. The magnitude of the change in concentration at both ends of the bypass loop will be measured, as will the time required for detecting the change. Initial experiments will be with oxygen as an added impurity. Modification of an existing loop is complete.

A preliminary design of an overflow sampler for use in the remote sampling facility at FFTF is complete. Fabrication will begin after FFTF comments on the design and the operational procedure are received.

A standard procedure for the analysis of particulates in sodium is needed. A primary concern is the recovery of the particulate matter from sodium in an unchanged form. Separations from sodium involving distillation, dissolution in mercury, and dissolution in liquid ammonia are being investigated. The suitability of a commercially available filter assembly for collecting particulates is also being examined.

2. Characterization of Impurity Meters and Meter Response to Impurity Species. J. T. Holmes and C. C. McPheeters (Last reported: ANL-7765, p. 64, Dec 1970)

The primary goal of this work is to determine the effect of impurity species on the response of oxygen and hydrogen meters. The relationship between the meter readings and the total dissolved impurity concentrations will be determined as a function of oxygen-to-hydrogen ratios with only dissolved oxygen and hydrogen present and also with other oxygen- and hydrogen-bearing species present. Experimental work will be carried on in a pumped-sodium apparatus (Apparatus for Monitoring and Purifying Sodium, AMPS) that will provide stable but adjustable impurity levels in the sodium fed to the test section.

Current work is directed primarily toward the design of AMPS, which is scheduled for completion by November 1, 1971. Work on the conceptual design* has been completed and preliminary specifications for fabrication of vessels have been prepared. The piping and equipment layout is essentially complete, a stress analysis has been performed, and detailed design is being started.

C. Nonmetallic Impurity Interactions in Sodium-Metal Systems (02-137)

1. Development of Equilibration Methods for Determining the Activity of Nonmetallic Impurities in Sodium. T. F. Kassner and D. L. Smith (Last reported: ANL-7705, pp. 51-52, June 1970)

The purpose of this work is to develop methods for accurately measuring the activity of nonmetallic elements (e.g., O, C, N, and H) in sodium at the low concentrations of interest for LMFBR applications.

A procedure for determining the oxygen activity in liquid sodium by the vanadium-wire equilibration method has been developed** and the

*Design work is being done by personnel of the Engineering and Technology Division.

**D. L. Smith, An Equilibration Method for Measuring Low Oxygen Activities in Liquid Sodium, to be published in Nucl. Appl. Technol. (May 1971).

necessary distribution-coefficient data obtained.* The present effort in this area is directed toward (1) standardization and characterization of the method and (2) comparison of the results with other methods of oxygen analysis. Additional 4-hr exposures of vanadium wire to liquid sodium of known oxygen concentrations at 750°C have been made to establish the precision of the method.

Results of vanadium-wire equilibrations were compared with results obtained from four UNC electrochemical oxygen meters used consecutively on a pumped-sodium system. Three important characteristics of cell operation were noted: (1) The curves of emf versus oxygen concentration for the four cells did not have the same slope or intercept. These differences may be due to variations in structure or impurities in the cell electrolyte. (2) The slopes were considerably greater than that of the calculated curve, thereby resulting in higher than theoretical voltages at high oxygen concentrations in sodium. (3) Linear plots of the cell emf versus the logarithm of the oxygen concentration in sodium were obtained for all the cells. Of particular interest was the linearity observed in one of the cells over three orders of magnitude in the oxygen concentration.

The sodium temperature in an LMFBR will vary from the cold-trap temperature to the maximum sodium temperature in the core. Moreover, electrochemical oxygen meters will be operated at temperatures between 300 and 500°C, and their outputs must be correlated with results of vanadium-wire equilibrations, which will be conducted at 750°C. It is, therefore, important to determine whether the oxygen content of sodium, and thus the cell emf, is affected by contact of the sodium with materials of construction at the high temperatures. Accordingly, measurements of cell emf were made while the maximum temperature of the loop was varied between 450 and 750°C. In this range of maximum loop temperatures, no effect on cell emf was noted for oxygen concentrations in sodium between 0.34 and 30 ppm.

A UNC oxygen meter operating at 402°C has been calibrated using the standard vanadium-wire equilibration method over the range 0.8 to 11 ppm oxygen in sodium. All points were within 1 mV of the curve.

The equilibration method is being extended to the measurement of carbon activities in sodium. The properties of a suitable detector metal are the same as those specified previously for an oxygen detector, i.e., (1) a low solubility in liquid sodium, (2) a significant range of carbon solid solution in the metal, (3) relatively high diffusion rates for carbon in the solid, and (4) experimentally measurable distribution coefficients for carbon which are greater than unity. Both iron and vanadium appear to be acceptable detector metals for carbon, and work is in progress to establish the

*D. L. Smith, Investigation of the Thermodynamics of V-O Solid Solutions by Distribution Coefficient Measurements in the V-O-Na System, Met. Trans. 2, 579-583 (Feb 1971).

required distribution-coefficient data for carbon between these metals and liquid sodium. Further work will be required, however, to establish optimum exposure times and temperatures and the effects of other nonmetallic elements on the distribution coefficients and the carbon activity.

D. Sodium Chemistry and Radioactive Contaminant Behavior (02-509)

1. Studies of the Sodium-Oxygen-Hydrogen System. F. A. Cafasso and K. M. Myles (Last reported: ANL-7765, p. 83, Dec 1970)

Investigation of the nature and behavior of oxygen- and hydrogen-bearing species in liquid sodium is continuing. The effort at present is directed toward elucidation of the phase relations that exist between Na, Na_2O, NaOH, and NaH at room temperature. When complete, this information will provide a foundation for determining which one of two potential phase diagrams of the Na-Na_2O-NaH-NaOH systems (see Progress Report for September 1970, ANL-7742, pp. 125-126) is more correct, i.e., which of the two diagrams should be used to guide further work in this area.

The experimental technique involves welding, in nickel capsules, mixtures of Na, Na_2O, NaOH, and NaH, subjecting the mixtures to various heat treatments, cooling gradually to room temperature, and examining the products with a diffractometer. In recent experiments, various mixtures of Na-Na_2O-NaH, Na-NaOH, and Na_2O-NaOH-NaH were heated to 500-600°C and slowly cooled to room temperature in an attempt to achieve room-temperature equilibrium. Thus far, caking and consequent separation of the reaction products has inhibited further reactions from occurring as the samples were cooled. Efforts are currently being directed toward circumventing this difficulty by modifying the experimental procedure.

In other experiments, capsules at 500°C were quenched rapidly in an attempt to retain the high-temperature phases at room temperature. These preliminary experiments have indicated that NaOH is an equilibrium phase at 500°C.

2. Studies of Carbon Transport in Sodium-Steel Systems. T. F. Kassner, K. Natesan, and C. A. Youngdahl (Last reported: ANL-7765, pp. 85-86, Dec 1970)

The objectives of this work are an understanding of the thermodynamics and kinetics of carburization-decarburization processes involving austenitic and ferritic steels and a correlation of the compositional and microstructural changes with the mechanical-property behavior of these materials.

Previous equilibration experiments to determine the distribution of carbon between sodium and iron and iron-base alloys at 650 and 750°C have

indicated that the carbon concentrations in sodium were in the sub-ppm range. In a recent experiment, foil specimens (2 mils thick) of Types 304 and 316 stainless steel, Fe-18 wt % Cr-8 wt % Ni, Fe-8 wt % Ni, and iron were exposed to flowing sodium at 650 and 750°C. Iron and vanadium wires were also included at each of the temperatures. To increase the carbon concentration in sodium to a more readily measurable range, a carburized iron source was located downstream from the specimen.

Combustion analyses of the equilibrated foil specimens indicated a substantial increase in the carbon concentrations; for example, the carbon concentration in Types 304 and 316 stainless steel increased from 0.045 and 0.074 wt % to 0.64 and 1.13 wt %, respectively, at 750°C. The iron, Fe-8 wt % Ni, and Fe-18 wt % Cr-8 wt % Ni foils also showed significant increases in carbon concentration. The iron and vanadium wires and the sodium samples are being analyzed for carbon. This experiment will yield additional information on the carbon activity in sodium and on the distribution of carbon between sodium and the austenitic alloys.

Three austenitic stainless steels (Types 304, 316, and 347) were equilibrated with Fe-8 wt % Ni alloys at 600, 700, and 800°C in Vycor capsules at different carbon activities. The carbon activities corresponding to the carbon concentrations in the steels will be reported when the carbon-activity studies in the Fe-8 wt % Ni alloys are completed. The experiments described above will provide a means for extending the results for the distribution of carbon between sodium and the stainless steels over a much wider range of carbon activities than can be achieved experimentally in loop systems over a reasonable time period.

3. Development of Radioactive Monitoring Methods

a. Monitoring of Fission-product Iodine. W. E. Miller and N. R. Chellew (Last reported: ANL-7765, p. 86, Dec 1970)

Fission-product cesium, rubidium, iodine, and tellurium should be easily leached from oxide fuel by coolant sodium contacting the oxide fuel at cladding defects. The concentration level of certain isotopes of these fission products in the coolant should provide the means for characterizing a failure and indicating the magnitude of the cladding defect. Therefore, monitoring methods for measuring concentration levels of these isotopes are being investigated. At present, a monitoring concept for measuring the ^{135}I content of reactor sodium is of primary interest. In this concept, the concentration of ^{135}I is determined by (1) sparging a sample of sodium with inert gas to remove the xenon present, (2) allowing the xenon daughters of iodine to build up for a predetermined time, (3) restripping the xenon from the sodium so that ^{135m}Xe can be gamma-counted, and (4) calculating the amount of parent ^{135}I from the count rate of the daughter.

The method of application of this monitoring concept is dependent on the kinetics of the transfer of xenon from sodium to the carrier gas. Accordingly, mass transfer in gas-sodium contactors is under investigation. Because of the short half-life (15.6 min) of ^{135m}Xe, the isotope of interest for reactor application, 5.3-day ^{133}Xe will be used in laboratory experiments to obtain the requisite data.

An experimental apparatus is being built that will permit testing of gas-sodium contactors of various designs. The first contactor to be tested is one in which helium is bubbled through sodium to strip out the xenon. Apparatus design, except for the sparger, has been completed, and the components are being built or procured.

b. Sampling and Analytical Procedures for Fission Products in Cover Gas. R. J. Meyer and M. H. Barsky (Last reported: ANL-7742, p. 129, Sept 1970)

High-temperature gas chromatography is being investigated as a means of separating fission-product gases and vapors from sodium vapor and aerosol so that the types and levels of radioactive fission products in cover gas can be determined. This information will be useful in the detection and characterization of fuel failures.

The method presently under investigation involves the following steps: (1) separation of metal vapor and aerosol from the noble fission-product gases and the permanent gases on a high-temperature column, (2) further separation of the gases (e.g., ^{23}Ne and ^{41}Ar from krypton and xenon isotopes) on a room-temperature column, and (3) further separation of the vapors (e.g., sodium from rubidium and cesium isotopes) on a high-temperature column.

Construction of a gas-chromatographic system to demonstrate vapor-gas separations has been completed. Experimental work to establish the conditions necessary for the separations is in progress.

V. FUELS AND MATERIALS DEVELOPMENT

A. Fuels and Fuel Elements

1. Fuel Properties

a. High-temperature Properties of Ceramic Fuels (02-094)

(1) Deformation of Polycrystalline Uranium Monocarbide. J. L. Routbort and M. D. Odie (Not previously reported). The design, construction, installation, and proof testing of an apparatus to be used for high-temperature deformation studies on advanced fuels have been completed. The apparatus is built around a Model TT-DM-L (10,000 kg) Instron testing machine. Cylindrical specimens 6 mm in diameter and 12 mm long are deformed under compression using a tungsten compression cage. A Brew furnace is used to obtain temperatures of 2000°C (in a vacuum of 10^{-6} Torr or in an inert atmosphere) with a ±1°C control. A temperature gradient of ±0.5% exists for a 12-mm-long specimen. The temperature is measured by a Pt-6% Rh, Pt-30% Rh thermocouple that is in contact with the center of the sample. Stainless steel bellows complete the vacuum (or atmosphere) seals. The elastic strains in the load system and tooling were calibrated with excellent reproducibility.

Two types of preliminary tests have been performed on a hyperstoichiometric, 100% dense polycrystal of uranium monocarbide. Figure V.1 shows the flow stress σ_f as a function of temperature from 870 to 1200°C. In all tests, σ_f was calculated from the load at which the load-versus-deflection curve became nonlinear. Table V.1 presents the results of two methods of strain measurement. As long as the sample dimensions remain uniform, both methods agree, and accurate strain measurements can be made without using an extensometer. The sample exhibited barreling after ~4.0% deformation and also exhibited considerable plasticity even at 870°C.

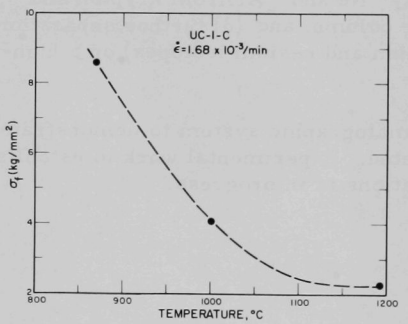

Fig. V.1. Flow Stress σ_f as Function of Temperature at $\dot{\epsilon}$ = 1.68 x 10^{-2}/min. Neg. No. MSD-54046.

Results of stress-relaxation tests are shown in Fig. V.3. The change in load ΔL with time is logarithmic, which is consistent with stress-relaxation theory. The parameters measured from three tests are tabulated in Table V.2. When the results are extrapolated to higher temperatures and hence lower stresses, they coincide approximately with those

reported by Chang,* who measured the stress relaxation in stoichiometric uranium monocarbide from 1500-1900°C.

TABLE V.1. Strain Measurements

Temperature, °C	ΔL/L Measured, %	ε(Calculated from Instron Crossroad), %	Comments
1200	1.18	1.08	-
1000	1.40	1.05	Sample cracked[a] and nonuniform
870	1.40	1.10	Barrelling

[a]The sample cracked along a transverse grain boundary. Grain-boundary separation is clearly evident in Fig. V.2.

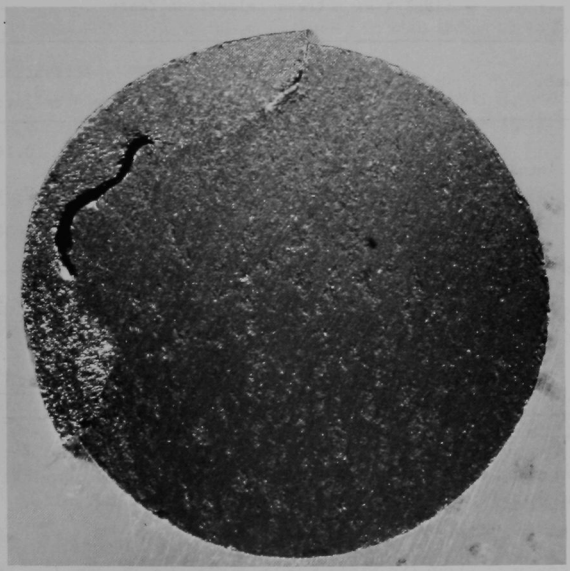

Fig. V.2. Uranium Monocarbide Sample after 4% Deformation in Compression Showing Offset due to Grain-boundary Separation. Mag. 18X. Neg. No. MSD-54026.

*R. Chang, J. Appl. Phys. 33, 858 (1962).

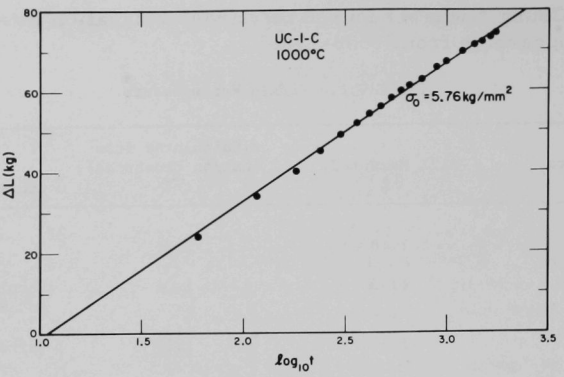

Fig. V.3. Stress Relaxation at 1000°C, ΔL vs $\log_{10} \tau$.
Neg. No. MSD-54045.

TABLE V.2. Stress-relaxation Tests

Temperature, °C	σ_o, kg/mm^2	Slope s, kg/cm^2	Activation Volume, v = cm^3/atom x 10^{20}
870	10.5	224	0.166
870	11.5	251	0.148
1000	5.76	110	0.378

b. Physical and Chemical Studies--Molten Fuel, Cladding, and Coolant. A. D. Tevebaugh and M. G. Chasanov, CEN (02-175)

(1) Reactor Materials--Fuel Phase Studies at High Temperatures: Investigation of the Distribution of Fission Products Among Molten Fuel and Reactor Phases. M. G. Chasanov (Last reported: ANL-7765, pp. 82-83, Dec 1970). Experiments are being carried out to determine the distribution of major heat-producing fission products among the various phases that would result from a meltdown of an LMFBR core.

A series of experiments has been completed in an arc-melting furnace to show the distribution of Zr, La, Y, Pr, Ce, Mo, Ru, and Nb between molten iron and UO_2. A comprehensive report will be issued on these experiments when all the analytical results are available. The general procedure for these experiments, together with the results showing that zirconium was distributed to the UO_2 phase, was described in the Progress Report for September 1970, ANL-7742, pp. 123-125. The

following additional results have been obtained: Lanthanum is also distributed to the oxide phase. Molybdenum is distributed to the iron phase. Ruthenium, when it is initially present as metal, remains in the iron phase. Ruthenium and niobium, when they are initially present as oxides in the oxide phase, are partially reduced to metal and distribute to the iron phase. The kinetic aspects of the distribution of ruthenium and niobium have been studied by carrying out experiments for various equilibration times. Analytical work is being done on the products of these experiments.

2. Irradiation Behavior of Fuel

a. Behavior of Reactor Materials (02-086)

(1) Fuel-element Behavior: Theory, Modeling, and Analysis. V. Z. Jankus and R. W. Weeks (Last reported: ANL-7776, p. 63, Jan 1971). Several modifications have been incorporated into the LIFE-I Code:

(a) More recent expressions for phenomenological swelling of solution-treated (NØH = -1) and 20% cold-worked (NØH = -2) Type 316 stainless steel have been included in the code, as suggested by R. D. Leggett et al.*

(b) LIFE-I now requires the fuel to stick to the cladding after thorough contact has been established at high temperature.

(c) The output of LIFE-I has been augmented, mainly by requiring the code to print the hoop stress and various strains pertaining to the cladding at every converged time step.

(d) The increment of creep strain at every elementary time interval consists of thermal and neutron-enhanced creep. Each component of the incremental creep strains is now accumulated and printed in the program output. The separation is performed not only for the cladding but also for each zone of the fuel.

(e) Computation of thermal expansion and irradition swelling of the capsule (if present) has been incorporated into LIFE-I. Only options of phenomenological swelling (NØH $\leq$ 0) are allowed for the capsule.

(f) Theoretical calculation of cladding swelling (NØH $>$ 0) has been found to be strongly dependent on the time interval used to reach full power, when it is less than 1 hr. Although this rapid rate does not occur in normal practice, it has been used in the calibration of the subroutine HKNS. A fictitious rapid full-power burst at the beginning of an irradiation

*R. D. Leggett et al., Correlation of Predictions and Observations in Mixed Oxide Fuels, ANS Trans. 13(2), 574-576 (Nov 1970).

history is suggested* if a relevant theoretical calculation of cladding swelling is desired, pending a revision of the subroutine.

3. Fuel-element Performance

a. Oxide Fuel Studies (02-005)

(1) Fuel-swelling Studies. L. C. Michels, J. D. B. Lambert, L. A. Neimark, and G. M. Dragel (Last reported: ANL-7783, pp. 66-67, Feb 1971). Full radial examination by fracture-replica electron microscopy of a transverse section from mixed-oxide fuel element 012 has been completed. The average radial extents and calculated fuel-operating temperature ranges** for the different fuel structural regions are: unrestructured, 0.126-0.117 in. and 745-885°C; equiaxed grain growth, 0.117-0.096 in. and 885-1285°C; transition from equiaxed grain growth to columnar growth, 0.096-0.086 in. and 1285-1485°C; and columnar grain growth, 0.086-0.041 in. and 1485-1780°C.

The observations and conclusions derived from this investigation of the different fuel structural regions are as follows:

(a) Unrestructured Region. The room-temperature fracture mode was intergranular. The specimen was fractured at room temperature to produce fresh fracture surfaces for examination. The grain edges (grain-boundary intersections) were smooth-rounded or smooth-grooved as contrasted with the sharp grain edges seen in low-temperature intergranular fractures of unirradiated mixed-oxide specimens.† This observation indicates the presence of interlinked grain-edge openings that could collect fission gas which would subsequently be released through cracks formed during reactor cycling.

No fission-gas bubbles were observed. Bubbles smaller than 1000 Å (0.1 μ) are not resolved by this technique.

(b) Equiaxed Grain-growth Region. The room-temperature fracture mode was mixed intergranular and transgranular fracture for about the outer half of the region, and was mostly transgranular fracture for the remainder. Evidence of grain-edge openings was found in the outer half of the region, but not in the remainder. The mechanism suggested for fission-gas release for the undisturbed region could also be operative for at least the outer half of the equiaxed grain-growth region.

Fission-gas bubbles were first observed ~0.016 in. from the fuel surface. The observed bubbles were situated on grain

*S. D. Harkness, Argonne National Laboratory, private communication (1971).

**Calculated using a recent version of the LIFE-I Code.

†J. T. A. Roberts, Argonne National Laboratory, private communication (1971).

boundaries, were relatively few in number, and ranged from ~0.1 to ~0.3 μ in diameter. A few fission-gas bubbles were observed ~0.026 in. from the fuel surface. Again they were on grain boundaries and ranged from ~0.1 to ~0.5 μ in diameter. No bubble interlinkage was observed.

(c) Transition Region and Columnar Grain-growth Region. The room-temperature fracture mode was mixed intergranular and transgranular fracture.

Large numbers of fission-gas bubbles were observed starting about the middle of the transition region and continuing throughout both regions, mostly on grain boundaries and along grain edges. Two different cases were found. In the first, extensively interlinked and elongated gas bubbles were observed on some boundaries, in addition to a distribution of smaller, rounded bubbles. Elongation of interlinked bubbles was seen only in the columnar grain-growth region. In the second case, little interlinkage was observed on other boundaries, although many bubbles were present. This difference did not appear to be related to observed differences in the orientations of the boundaries relative to the direction of the temperature gradient. However, the difference may be related to the formation and migration of subgrain and grain boundaries and the attendant fission-gas bubble sweeping previously observed in the columnar and transition regions of mixed-oxide fuel irradiated in EBR-II. (See Progress Report for February 1970, ANL-7669, pp. 112-113.)

(2) Fuel-element Performance. L. A. Neimark, W. F. Murphy, and J. D. B. Lambert

(a) Group O-3, Void Deployment (Last reported: ANL-7776, p. 72, Jan 1971). Five mixed-oxide fuel elements from Group O-3 are being examined in the hot cells at ANL, Illinois. These elements are part of a group of 18 encapsulated fuel elements that were irradiated in EBR-II to 3.5 at. % peak burnup. The peak linear power ratings were 12-14 kW/ft. Irradiation of the other 13 elements is continuing to the next burnup level of 7.5 at. %.

Three of the elements being examined (SOPC-1, SOPC-3, and SOPC-5) contain pellet fuel; SOV-15 contains vibratorily compacted Dynapak powder, and SOVG-17 contains vibratorily compacted Sol-gel microspheres. The five elements are clad in 0.290-in.-OD, 15-mil-wall Type 304 stainless steel, except for SOV-15, which has a 20-mil cladding. SOPC-5 had a large initial diametral gap of 15 mils, compared with 4 mils for SOPC-1 and SOPC-3.

Nondestructive examination of the encapsulated fuel elements has been reported previously. (See Progress Reports for November 1970, ANL-7758, pp. 71-72, and January 1971, ANL-7776, p. 72.)

The plenums of the capsules were punctured, and the gases were collected. The gases were all nonradioactive, indicating that fission gases had not leaked from the elements. The sodium bond was melted, and the capsules were disassembled without difficulty.

The results of nondestructive measurements on the fuel elements are given in Table V.3. The data are reasonably consistent, except for the relatively large increase in the weight of SOPC-1. Visual examination of this element revealed nothing that would account for the apparent weight gain. The weight losses of the other four elements are equivalent to a volume of stainless steel of about 0.002 cm^3. The volume changes due to length increase range from 0.010 to 0.021 cm^3. The net volume changes due to diametral increases range from 0.021 to 0.059 cm^3, and are equivalent to calculated diameter increases ranging from 0.6 to 1.7 mils. Measured average diametral increases over the fuel and over the plenum, respectively, were: SOPC-1, 0.7 mil, 0.4 mil; SOPC-3, 0.6 mil, 0.2 mil; SOPC-5, 0.6 mil, 0.2 mil; and SOVG-17, 0.5 mil, 0.2 mil. Diameter profiles of SOV-15 have not yet been made. The diameter profiles of the four elements showed larger diameter increases over the lower half of the fuel column, with no evidence of a peak diameter increase near the reactor midplane. The diametral profile of SOPC-3 differed from the profiles of the other three elements by having an irregular degree of ovality of as much as 4-5 mils over the length of the fuel column.

TABLE V.3. Results of Nondestructive Measurements

Element	Weight Change		Volume Change		Length Change		Balance Point,[a] in.	
	mg	%	cm^3	%	mils	%	Initial	Change
SOPC-1	+245	-	+0.035	+0.11	+13	+0.04	11.14	+0.05
SOPC-3	-20	-0.012	+0.042	+0.13	+19	+0.06	11.15	+0.10
SOPC-5	-12	-0.007	+0.053	+0.16	+11	+0.04	11.22	+0.03
SOV-15	-19	-0.011	+0.067	+0.20	+ 9	+0.03	11.63	+0.06
SOVG-17	-15	-0.009	+0.061	+0.18	+17	+0.05	11.12	+0.13

[a]Measured from the bottom of the fuel element.

Although major fission-product agglomeration was not noted in the axial gamma profiles, minor indications of peaks for ^{137}Cs, and sometimes ^{103}Ru, were seen.

The four elements for which nondestructive examination has been completed have been punctured and the gases collected. The following quantities of gas at standard temperature and pressure were obtained (including the original fill gas): SOPC-1, 58.7 cm^3; SOPC-3, 55.4 cm^3; SOPC-5, 46.2 cm^3; and SOVG-17, 49.6 cm^3. Samples of these gases have been submitted for mass-spectrographic

Fuel element SOPC-5 has been sectioned, and two as-polished radial sections have been given a preliminary examination. The usual central-void, columnar-grain, equiaxed-grain, and "as-fabricated" regions were evident. Small metallic-appearing particles of fission products were evident, but no large agglomerations were seen. Of particular interest were the closure of the initially large 15-mil-diametral gap and the absence of any evidence of fuel melting. Detailed examination of the five elements continues.

(b) Examination of NUMEC Groups B and C Elements (Last reported: ANL-7776, pp. 72-75, Jan 1971). Table V.4 summarizes the postirradiation examination results for the four NUMEC high-burnup fuel elements now undergoing destructive examination in the Alpha-Gamma Hot Cell. The fabrication variables and irradiation conditions were previously reported (see ANL-7776, p. 73).

TABLE V.4. NUMEC Mixed-oxide Fuel Elements

Analysis	Fuel Element B-2	C-1	C-11	C-15
Peak % ΔD/D capsule	1.57	1.76	1.50	1.28
Peak % ΔD/D[a] element	2.53	4.01	3.26	3.11
Element %[b] eccentricity	0.29	1.43	1.51	1.36
% ΔL/L on[c] fuel column	1.8	{2.3 / N A}	{2.4 / 2.5}	{2.3 / 2.4}
Volume Xe+Kr (NTP, cc)	138.7	163.5	153.9	107.6
% Fission-gas[d] release	89.8	95.7	90.8	68.0

[a] Effect of wire-wrap distortion averaged.

[b] (Maximum OD-minimum OD)/mean OD as percent.

[c] Measured from neutron radiographs {Interim X012 / Final X012A}.

[d] Based on 0.246 gas atoms per fission and mean calculated burnups.

Elements C-11 and C-15 were previously reported (see ANL-7776, pp. 72-75) to contain fission-product ingots in their central void. The central void of C-11 also contained a dendritic structure that had a slightly darker gray color over the fuel matrix. A section from C-11, shown in Fig. V.4, has been analyzed with the shielded microprobe, and the results are summarized below.*

*E. M. Butler and D. R. O'Boyle, Argonne National Laboratory, private communication (1970).

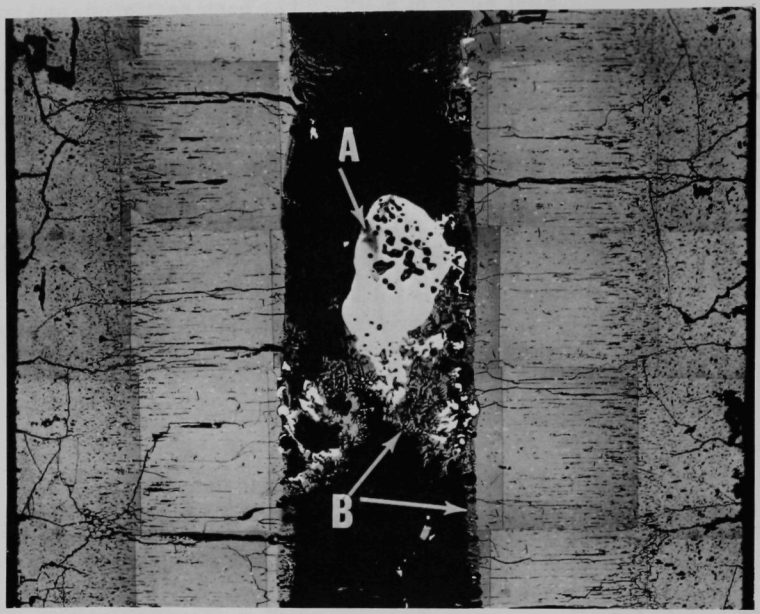

Fig. V.4. Fission-product Ingot (A) and Dendritic Structure (B) in Central Void of NUMEC Element C-11. Mag. 24X. Neg. No. MSD-160259.

The large metallic ingot contained a high concentration of molybdenum, ruthenium, and technetium.

In the dendritic structure, seven distinct phases were observed: (1) mixed-oxide fuel with Pu/U ≃ 0.35; (2) mixed-oxide fuel with Pu/U ≃ 0.17, which also contains barium and cerium; (3) an optically dark gray phase that contains molybdenum, barium, and cerium with ≃1.5 wt % uranium and no detectable plutonium; (4) an optically red phase containing molybdenum, barium, and cerium, but with a higher molybdenum concentration compared to Phase 3 and no detectable uranium or plutonium; (5) cesium in cracks throughout the fuel from the central void to the fuel-cladding interface; (6) an optically bright metallic phase containing molybdenum, ruthenium, and technetium; and (7) an optically bright phase of essentially pure molybdenum.

Probe traces from the fuel surface to the central void indicated an increase in the plutonium content of the fuel near the central void; work is being continued to obtain accurate values for the Pu/U ratio as a function of radius.

A significant feature of both Groups B and C elements was the appearance in the fuel-cladding gap of thin layers of bright material parallel to the internal surface of the cladding. Generally, these thin layers were surrounded by a gray phase. Figure V.5 shows the typical appearance of one of these layers. Microprobe analysis indicated that these layers contained >80% molybdenum, whereas the gray phase consisted of a mixture of cesium, molybdenum, tellurium, and oxygen. Penetration of the cladding by cesium was no more than 0.002 in. and generally did not occur preferentially along the grain boundaries of the steel.

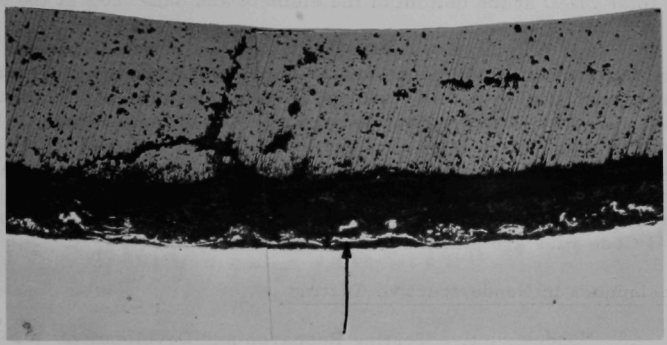

Fig. V.5. Thin Layers of Bright Material in Fuel-cladding Gap of NUMEC Element C-11, Analyzed >80% Molybdenum. Mag. 165X. Neg. No. MSD-160260.

For purposes of analysis, the respective 0 and 90° orientation profilometry results from Elements C-1, C-11, C-15, and B-2, and their capsules were averaged. It was then assumed that the temperature difference between the capsule wall and the fuel cladding at any axial position on the elements can be ignored in terms of the effect it will have on the steel swelling at a given fluence. Spot checks using the latest PNL-WARD swelling equation* indicate that, in the temperature and total fluence regimes involved, this approximation will yield only small inaccuracies. The capsule $\Delta D/D$ profiles have been subtracted from the element $\Delta D/D$ profiles to yield $\Delta D/D$ profiles on the elements solely due to fuel-cladding interaction, fuel swelling, and cladding creep. (From here on, the term "fuel swelling" will be used to denote these three components.)

The following features of the profiles were then apparent:

(1) In all four elements, "fuel swelling" contributed more to total cladding strain over the lower, cooler half of the elements

*R. D. Leggett, Plutonium Fuels for LMFBR--An Extrapolation, WHAN-SA-51 (Oct 5-9, 1970).

than over the upper, hotter half. (With the exception of C-1, the diametral fuel-cladding gap was considerably smaller over the lower halves of the elements than over the upper halves.)

(2) In Elements C-1, C-11, and C-15, "fuel swelling" contributed ~65% of the total $\Delta D/D$ at the bottom of the elements and ~50% at the top.

(3) In Element B-2, "fuel swelling" contributed ~50% of the total $\Delta D/D$ at the bottom of the element and only ~20% at the top.

There were three differences between Element B-2 and the three Group C elements. Element B-2 operated in a different subassembly with slightly lower cladding temperatures; the mean burnup of B-2 was lower (~8.7 at. %) than for the three Group C elements (~9.7 at. %); and the cladding thickness on B-2 was 0.030 in. compared with 0.015 in. on C-1, C-11, and C-15. The lower "fuel-swelling" contribution to overall cladding strain in B-2 compared with the values for the Group C elements is tentatively attributed to the combined effect of these three factors. LIFE-I Code runs are planned to confirm this hypothesis.

4. Techniques of Nondestructive Testing

a. Nondestructive Testing Research and Development (02-092)

(1) Development of High-temperature Ultrasonic Transducers. K. J. Reimann (Last reported: ANL-7776, p. 76, Jan 1971). Difficulties were encountered in the attempt to calibrate the high-temperature transducer prototypes with a capacitive transducer. It proved to be impossible to achieve a sound field of uniform intensity over a wide frequency range (1 kHz to 10 MHz) or to eliminate the direct feedthrough of the transmitter voltage into the receiver. A reciprocal self-calibration method, which hopefully will eliminate these shortcomings, is currently under investigation.

The high level of activity of acoustic-emission monitoring of fatigue specimens during the heating and cooling cycle was traced to the fast heating rate of the transducer. This activity is manifested by voltage spike pulses, which reverse polarity when changing from heating to cooling. The effect could be greatly reduced by using a slow heating rate or a pressure-contact transducer instead of a brazed transducer.

The monitoring of acoustic emission in cyclic fatigue of stainless steel specimens resulted in the determination of the optimum bandpass between 20 and 150 kHz under the existing background noise of the test arrangement. To determine the correlation between the number of emission pulses and the major surface cracks, the test was interrupted after

the first few emission pulses occurred, and the specimen was examined microscopically. Although the correlation was good, surface microcracks did not record on the recorder trace.

Experiments are under way to increase the sensitivity of the method and to find ways of determining if cracks initially develop only on the surface of the specimen or in its interior.

B. Core Materials Applications

1. Core Design Technology

a. Empirical Assessment of Swelling and Creep Correlations. P. R. Huebotter and T. R. Bump, Program Coordination (Last reported: ANL-7783, pp. 61-64, Feb 1971)

Contemporary LMFBR core design requires reliable expressions for fast-neutron-induced swelling and radiation-enhanced creep of stainless steel, as well as an understanding of integral swelling-creep effects on core structural components. Existing correlations involve considerable uncertainty and are based on controlled experiments to a fluence that is a small fraction of FTR and LMFBR Demonstration Plant targets.

Core components removed from EBR-II, at fluences now approaching these targets, exhibit deformations that are attributable to a combination of swelling and creep. These deformations are being analyzed to ascertain the reliability of existing swelling and creep correlations and to gain further insight into the response of stainless steel, in typical core structural applications, to the LMFBR environment. The EBR-II Project provides the neutron fluxes, temperatures, and nondestructive measurements employed in the analyses. Destructive measurements are obtained from EBR-II and other projects within ANL and from other participating United States laboratories.

(1) Wrapper Tube on Experimental Assembly XA08 (T. R. Bump). Additional zero-restraint, wrapper-tube-bow displacements were calculated with the GROW code, using a more recent WADCO correlation for swelling of solution-treated steel.* The maximum calculated displacement is somewhat less than that obtained with the earlier BNWL-WARD correlation, 0.112 in. versus 0.138 in. However, both calculated displacements are substantially larger than the measured value (0.053 ± 0.014 in.) and the calculated value obtained with the ANL correlation (0.065 in.). Additional density measurements are being made by the EBR-II Project to establish the density-distribution map for the tube. The calculation of

*H. R. Brager et al., Irradiation Produced Defects in Austenitic Stainless Steel, WHAN-FR-16, 11 (Dec 1970).

displacements, using the density values, should indicate whether the measured displacements were influenced by creep.

Figure V.6 shows the results of additional AXICRP calculations made in an effort to reproduce the moat observed around the wrapper-tube spacer pads. A centrally loaded, circular, flat-plate (disk) representation and a solution-treated steel creep correlation* were employed. The conditions for Curve A are: (a) The disk edge is prevented from rotating (by application of a suitable pressure distribution) but is free to move radially; (b) 4600 psi are added to the edge pressures; (c) a 25-lb pad load is maintained; and (d) the elapsed time is 9580 hr. (Effective full-load exposure time of the pads was about 10,300 hr.) The added pressures were intended to simulate compressive stresses produced by swelling. These stresses could have been as high as 200,000 psi at the end of exposure, if the wrapper-tube corners had been fixed and no creep occurred, but of course neither condition was maintained. In addition, the compressive stresses exist circumferentially only, in a wrapper tube free to bow, so that the edge pressures on the simple disk representation should properly simulate average rather than maximum compressive stresses. No sign of moat formation is apparent in Curve A, which suggested that the effects of higher pad load merited further study.

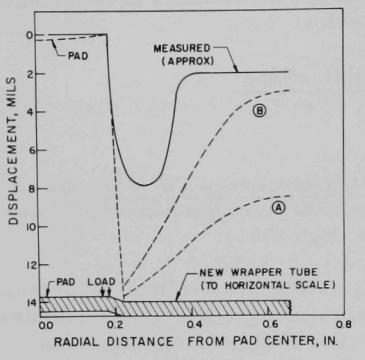

Fig. V.6. Permanent Displacement vs Radial Distance from Spacer-pad Center for EBR-II Assembly XA08 Wrapper Tube. Neg. No. MSD-54241.

The conditions for Curve B are similar to those for Curve A, except that the pad load is 50 lb, and the elapsed time is 10,700 hr. Although Curve B still does not come close to duplicating the measured curve, at least some degree of similarity is seen. Few additional calculations of this type are planned until AXICRP has been modified to account for the local swelling effects that have been observed (see Progress Report for November 1970, ANL-7758, pp. 5-6) and that might influence moat formation.

According to recent BOW-V calculations,** the pad loads should be less than 25 lb, rather than more. However, there is evidence that the creep equation used predicts excessive creep (see below). Therefore, the possibility exists that pad loads in the reactor are higher than calculated.

*E. R. Gilbert and L. D. Blackburn, Irradiation-induced Creep in Austenitic Stainless Steel, WHAN-FR-30, 1 (Oct 1970).

**D. Mohr, Argonne National Laboratory (EBR-II Project), private communication (Mar 1971).

(2) Fuel-element Claddings in Experimental Assembly X040A (T. R. Bump). Additional cladding-bow displacements were calculated for Elements B-5 and B-16, using the CRASIB code, the more recent WADCO swelling correlation, and the LIFE-I (NOH = 0 option) creep correlation.* The latter correlation includes thermal as well as flux creep. The maximum calculated bow was 1.08 in., which is even larger than the 0.98-in. value reported previously. It is not now believed that the assumption of a large degree of restraint during operation is responsible for the calculated values being so much larger than the 0.10 to 0.18-in. measured values. The WADCO fuel-element-bundle compression test results** indicate that it takes about 0.17 psi to compress a bundle 1 mil, and the maximum calculated pressure the restrained elements exert is at most 3 psi.

The explanation for the discrepancy may be radiation hardening of the steel. To permit study of this effect, the SCIM code, which accounts for age hardening,† is being incorporated into CRASIB.

*V. Z. Jankus and R. W. Weeks, LIFE-I, a FORTRAN-IV Computer Code for the Prediction of Fast-reactor Fuel-element Behavior, ANL-7736, 49 (Nov 1970).

**R. B. Baker and D. E. Blahnik, CCTL Mark I and Mark II Prototype FFTF Subassembly Compression Test Development Work, WHAN-FR-18, 6.5 (Aug 1970).

†S. D. Harkness, J. A. Tesk, and C-Y Li, An Analysis of Fast Neutron Effects on Void Formation and Creep in Metals, Nucl. Appl. Tech. 9, 24-30 (July 1970).

PUBLICATIONS

Dielectric Loss in Fluoride Crystals
E. Barsis* and A. Taylor
Phys. Rev. B3(4), 1506-1507 (Feb 1971)

Deformation of UO_2 at High Temperatures
R. F. Canon, J. T. A. Roberts, and R. J. Beals
J. Am. Ceram. Soc. 54(2), 105-112 (Feb 1971)

Crystal Structures of URhGe, HoNiGe, and Related Compounds
A. E. Dwight
Program Book, Am. Cryst. Assoc. Winter Mtg., Tulane University, New Orleans, Mar 1-5, 1970, No. D2, p. 31 Abstract

Crystal Structures of PuFeAl, PuRhGa, Pu_2AlGa_3, and Related Compounds
A. E. Dwight
Program Book, Am. Cryst. Assoc. Summer Mtg., Carleton University, Ottawa, Canada, Aug 16-22, 1970, No. I2, p. 59 Abstract

Crystal Structures of Some Uranium Intermetallic Compounds
A. E. Dwight
Program Book, Am. Cryst. Assoc. Winter Mtg., University of South Carolina, Columbia, Jan 31-Feb 4, 1971, No. F12, p. 40 Abstract

*Sandia Corp.

VI. FUEL CYCLE

A. Molten Metal Decladding of LMFBR Fuels. D. S. Webster (02-173)

A head-end liquid-metal process for preparing spent stainless steel-clad oxide fuel for subsequent reprocessing steps is under study. Stainless steel cladding is first dissolved in liquid zinc having an overlying salt layer, the resulting zinc-steel solution is separated from the unreacted $(U,Pu)O_2$ fuel, and the fuel oxide is reduced to metal and dissolved in the reduction solvent. (This process may also be applicable for the removal of Zircaloy cladding.)

1. Engineering Developments. R. D. Pierce (Last reported: ANL-7783, pp. 82-83, Feb 1971)

a. Reduction of UO_2 Pellets

Three additional oxide reduction runs (Mg-Zn-R10 to -R12) have been completed in which UO_2, a stand-in for $(U,Pu)O_2$, was reduced to metal by contacting it with salt-metal systems. The purpose of two of these runs (Mg-Zn-R10 and -R12) was to determine the practical limit of CaO loading of the salt (i.e., the maximum loading at which good separation of the salt phase from the metal phase is attained and the reduction rate of UO_2 pellets is adequate). The advantage of a high CaO loading would be to decrease the volume of waste salt that must be stored.

In run Mg-Zn-R10, the salt-metal system was $CaCl_2$-20 mol % CaF_2/Zn-29 at. % Mg-6 at. % Ca, and in run Mg-Zn-R12, $CaCl_2$-20 mol % CaF_2/Mg-17 at. % Zn-9 at. % Ca was used. Samples of the metal were taken during each run, as well as samples of the metal and salt phases at the end of a run. All samples are being analyzed for uranium. Samples of the Mg-17 at. % Zn-9 at. % Ca alloy (in which uranium is nearly insoluble) were taken at intervals and are being analyzed for calcium to determine the rate of UO_2 reduction.

In other work, the minimum CaF_2 concentration in the feed salt that is associated with good separation of the salt phase from the metal phase at the end of a reduction is being determined. Reducing the fluoride concentration in the salt used in the reduction step is desirable since some salt may adhere to the uranium and plutonium metal products which are subsequently dissolved in nitric acid and fed to aqueous extraction steps; fluoride ion in acid solution is highly corrosive to the stainless steel equipment used in aqueous processes. (Chloride salt remaining would be removed during the vacuum evaporation step, which is proposed to concentrate the plutonium alloy prior to acid dissolution.)

In run Mg-Zn-R11, UO_2 pellets were contacted with a metal-salt system containing no CaF_2--specifically, Zn-29 at. % Mg-6 at. % Ca/$CaCl_2$.

Separation of the salt phase from the metal phase was poor. Melt samples taken at intervals during the run and salt and metal samples taken after the run are being analyzed for uranium.

Analytical results have been obtained for two earlier runs (see ANL-7783) made with $CaCl_2$-20 mol % CaF_2 and either Zn-29 at. % Mg-6.6 at. % Ca or Mg-17 at. % Zn-4 at. % Ca. Analyses of the streams for the run with a zinc-rich alloy gave an overall uranium material balance of 100 ± 0.5% and indicated that 99% of the uranium had been reduced to metal, confirming that the reduction system used is practical. Analysis of the magnesium-rich alloy at the end of the run showed that 91% of the uranium charged was in solution. The overall material balance was poor but the reduction is believed to have been >99% complete.

Approximately three additional oxide reduction experiments will be made with a salt containing less than 20 mol % CaF_2 to determine the minimum CaF_2 concentration at which salt-metal phase separation is good.

2. Process Demonstration Experiments. R. D. Pierce (Last reported: ANL-7765, p. 80, Dec 1970)

a. Irradiated-fuel Experiments

Two additional experiments to test the apparatus and procedures that will be used to demonstrate the decladding and reduction of irradiated fuel have been completed outside the shielded facility, using nonirradiated stainless steel tubes containing UO_2 pellets and simulated fission gases. In the first of two decladding-reduction experiments, the UO_2 pellets could not be removed from the basket during the reduction step. The base of the basket was changed from a conical shape to a cylindrical shape, and in the second run, the oxide pellets were completely removed from the basket into the reduction alloy.

Results for the first run also indicated that the volume of the Molecular Sieve traps which will be used for collecting the fission gases was too small. Larger traps were installed that appeared to perform satisfactorily during the second run.

This apparatus is being installed in the shielded facility for work with irradiated fuel. Two irradiated fuel pins are en route to our laboratory.

B. LMFBR Reprocessing--Plutonium Isolation. D. S Webster A. A. Jonke, G. J. Bernstein (02-159)

1. Centrifugal Contactors for Plutonium Handling (Last reported: ANL-7783, pp. 80-81, Feb 1971)

Performance testing continues for a stainless steel centrifugal contactor having critically favorable dimensions

high-plutonium LMFBR fuel. The size of the mixing chamber baffles was increased, and the earlier reported flow surging (see ANL-7783) was essentially eliminated in runs with dilute nitric acid and Ultrasene (refined kerosene). This modification had the effect of reducing the pumping capacity through the mixing chamber and resulted in more uniform flows.

Preliminary runs were made to measure maximum total flow through the contactor under conditions giving desired phase separation (less than 1% entrainment of either phase in the other phase). With 0.03M HNO_3 as the aqueous phase and Ultrasene as the organic phase, throughputs were determined at rotor speeds of 2500 to 3500 rpm. Throughputs were ~12, ~14, and ~18 gpm at aqueous-to-organic (A/O) flow rates of 1:3, 1:2, and 1:1 and a rotor speed of 3500 rpm. In a run at a rotor speed of 2000 rpm with 0.5M HNO_3 aqueous phase and an organic phase consisting of 15 vol % tributyl phosphate (TBP) in Ultrasene at an A/O flow ratio of 1:1, phase separation was not as readily achieved and throughput was 4 gpm. Some flow surging was evident in the run with TBP, indicating that further evaluation of the pumping characteristics of the unit is needed.

C. LMFBR Fuel Materials Preparation--U/Pu Nitrates to Oxides. A. A. Jonke and N. M. Levitz (02-157; last reported: ANL-7783, pp. 83-84, Feb 1971)

A fluid-bed denitration process is under development for converting U/Pu nitrates in nitric acid solutions to mixed oxides suitable for the fabrication of fuel shapes.

1. Crystallization Temperatures for $UO_2(NO_3)_2$-$Pu(NO_3)_4$ Solutions

In current laboratory work, measurements were continued of the crystallization temperatures of dilute nitric acid solutions containing uranium and plutonium in concentrations totaling 1 to 2M. Information on solubility limits is pertinent to the selection of the range of feed solution compositions for the fluid-bed denitration process. The crystallization temperatures for 10 solutions have been determined (see Table VI.1); each value represents an average of two or three measurements. In these solutions, approximately 30% of the plutonium was present as the hexavalent (plutonyl) ion.

The effect of a given change in nitric acid concentration appears to diminish as the acid concentration increases. For example, an increase in acid concentration from 2 to 3.4M gave an increase of 12°C in the crystallization temperature for a solution containing 1.28M U and 0.34M Pu. A similar increase in acid concentration from 3.4 to 4.8M increased the crystallization temperature by only 5.6°C. Also, replacement of some uranium with plutonium lessened the sensitivity of crystallization temperature to nitric acid concentration.

TABLE VI.1. Crystallization Temperatures of U-Pu-HNO_3 Solutions

Solution Composition, M			U/Pu Ratio	Measured Crystallization Temp., °C
U	Pu	HNO_3		
1.6	0.2	2.0	8.0	13.2
1.6	0.3	2.0	5.3	15.9
1.6	0.4	2.0	4.0	18.0
1.28	0.34	2.0	3.8	3.2
1.28	0.34	3.4	3.8	15.3
1.28	0.34	4.8	3.8	20.8
1.40	0.0	3.4	---	17.2[a]
1.12	0.28	3.4	4.0	10.2
1.12	0.28	4.8	4.0	17.6
0.98	0.42	3.4	2.3	5.3
0.70	0.70	3.4	1.0	1.5

[a]Extrapolated from literature data on UNH solubility.

The effect on crystallization temperature of replacing some of the uranium with plutonium (at a fixed nitric acid concentration and a fixed total heavy-metal concentration) was studied. The data (see Table VI.1) indicate that increased substitution lowers the crystallization temperature.

The uranium-plutonium-HNO_3 system conforms to general phase-rule behavior. That is, the replacement of a portion of a solute with another solute (in this case, plutonium nitrate) without changing the total solute molarity or the nitric acid concentration resulted in a lowering of the crystallization temperature. It is believed that the material that has initially precipitated in the uranium-rich systems tested to date is uranyl nitrate hexahydrate (UNH). Additional tests will be made with high-plutonium solutions to help locate the invariant point (where precipitated uranyl nitrate and plutonium nitrate are in equilibrium with the liquid). This datum is important to this application for criticality safety reasons, i.e., to avoid conditions under which plutonium nitrate could precipitate.

The solution composition tentatively planned for our fluid-bed experiments is 1.44M uranyl nitrate, 0.36M plutonium nitrate, and 2.0M nitric acid. This highly concentrated feed should give a high process throughput. The temperature of crystallization for such a solution should be approximately 13°C. Normally, solutions will be at ambient temperature during operations.

These measurements will be repeated with similar uranyl nitrate-plutonium nitrate-nitric acid solutions in which all the plutonium is quadrivalent.

D. LMFBR Fuel Fabrication--Analyses and Continuous Processing. A. A. Jonke and M. J. Steindler (02-158)

Analytical methods for reactor fuel are being developed to measure rapidly, precisely, and accurately preirradiation properties that are strongly related to fuel performance in fast reactors.

1. Pu/U Ratio in Fuels (Last reported: ANL-7776, pp. 91-93, Jan 1971)

X-ray fluorescence is being studied as an in-line method for determining Pu/U ratio in PuO_2-UO_2 fuel materials, with UO_2-ThO_2 being used as a stand-in for PuO_2-UO_2. X-ray fluorescence analysis is a sensitive nondestructive method in which exciting radiation impinges on a sample and causes the emission of radiation that is characteristic of the elements present.

Emission lines of impurity elements that might possibly interfere with the use of X-ray fluorescence analysis of U-Pu oxides were identified, and the line intensities of impurities at the expected or specified concentrations in fuel material were compared with the line intensities of plutonium and uranium at their expected concentrations.

In the group of impurity elements having L spectra in a region of possible interference, protactinium, neptunium, and americium merit comment. They would not be present in the plutonium used in the fabrication of FFTF fuel, but might be present in subsequent LMFBR fuels. However, these elements will probably not be present at high enough concentrations to have to be considered as possible interferences.

Within the series of elements having K spectra in a region of possible interference, strontium is the only possible interference if present at a concentration greater than 100 ppm. Because FFTF specifications provide a maximum calcium concentration of 250 ppm, and because strontium might be incorporated with calcium as a result of their chemical similarity, the presence of greater than 100 ppm strontium in the fuel material seems unlikely.

PUBLICATIONS

The EBR-II Skull Reclamation Process. Part V. Design and Development of Plant-scale Equipment

G. J. Bernstein, D. E. Grosvenor, J. F. Lenc, W. E. Miller, I. O. Winsch, J. Wolkoff, and R. C. Paul

ANL-7772 (Jan 1971)

Chemical Engineering Division Fuel Cycle Technology Quarterly Report, October, November, December 1970

D. S. Webster, A. A. Jonke, G. J. Bernstein, N. M. Levitz, R. D. Pierce, M. J. Steindler, and R. C. Vogel

ANL-7767 (Jan 1971)

VII. REACTOR PHYSICS

A. ZPR Fast Critical Experiments

1. Fast Critical Facilities; Experiments and Evaluations--Illinois (02-179)

a. Clean Critical Experiments. R. A. Lewis (Last reported: ANL-7783, pp. 13-14, Feb 1971)

(1) Radial Reactivity Worth Distributions in ZPR-6 Assembly 7. The reactivity worths of sodium, plutonium (98.9% ^{239}Pu), depleted uranium, Type 304 stainless steel, and tantalum were measured at several points along a radius located at the axial midplane of ZPR-6 Assembly 7. Samples approximately 2.0 in. long and 0.87 in. in diameter (either solid cylinders or annular in shape) were oscillated between fixed points on the radius and a point external to the core. The reactivity change was measured with a calibrated autorod which held the power constant.

Figure VII.1 is a vertical section through the core showing the arrangement of the sample, sample holder, sample tube, sample tube support tray, assembly matrix, and plate drawers. The direction of the view is horizontally along the radius. The ZPR plates are positioned in the same plane as that of Fig. VII.1. All the structural pieces shown in Fig. VII.1 are Type 304 stainless steel.

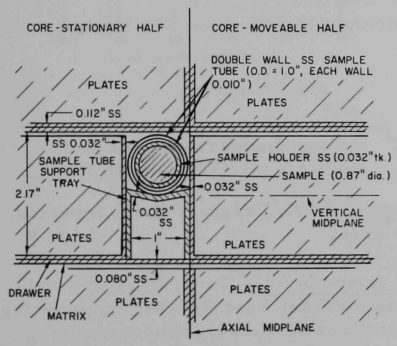

Fig. VII.1. Vertical Section of ZPR-6 Assembly 7, Showing Arrangement of the Sample and Radial Sample-changer Tube in Assembly

Radial-worth curves for plutonium and sodium are shown in Figs. VII.2 and VII.3, and the sample weights are indicated on each figure. The sodium values have relatively large experimental uncertainties, due mostly to the small signal available from the small mass of sodium in the sample. The measurement uncertainties indicated in Figs. VII.2 and VII.3 include only the random errors associated with the scatter in the measured data. The solid curves in Figs. VII.2 and VII.3 do not represent a fit to the data, but are included only as an aid in visualizing the radial shapes.

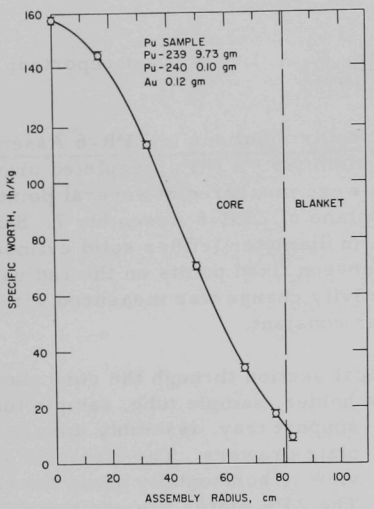

Fig. VII.2

Spatial Distribution of the Reactivity Worth of Plutonium Measured Radially at the Axial Midplane (Z = 0) of ZPR-6 Assembly 7

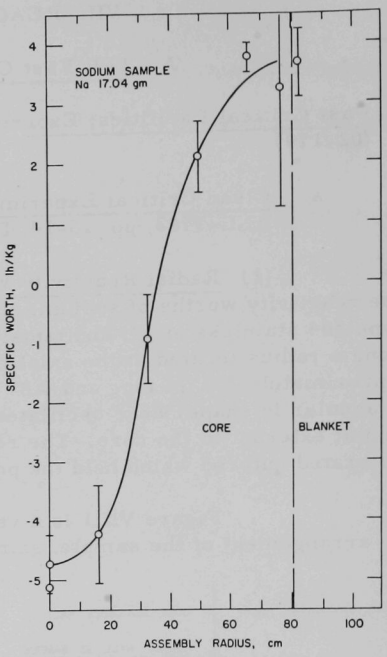

Fig. VII.3

Spatial Distribution of the Reactivity Worth of Sodium Measured Radially at the Axial Midplane (Z = 0) of ZPR-6 Assembly 7

b. Mockup Critical Experiments. J. W. Daughtry (Last reported: ANL-7783, pp. 14-19, Feb 1971)

(1) Description of ZPR-9 Assembly 27 (J. W. Daughtry and C. D. Swanson). ZPR-9 Assembly 27 is the Fast Test Reactor Engineering Mockup Critical (FTR-EMC). The objectives of the experiments to be performed with the EMC are to verify the neutronics characteristics of the FTR preliminary design and to provide data for fixing final design parameters, such as fuel enrichments and boron loading in control and safety rods, and for assessing power distributions, fixed-shim methods, test-loop loading effects, safety characteristics, and end-of-life conditions.

The FTR is the main component of the Fast Flux Test Facility (FFTF) being built primarily for fast-reactor fuel testing. The FTR is to be a plutonium-fueled, sodium-cooled, fast reactor with a core volume of 1034 liters (cold) designed to operate at 400 MW. It is to be made up of hexagonal subassemblies equal in cross-sectional area to

approximately 4.1 ZPR-9 matrix tubes. This, in itself, constitutes a limitation to the degree of accuracy of the mockup.

Within the constraints imposed by the ZPR-9 matrix and drawers and the available material inventory, the EMC will approximate, as closely as possible, the current design of the FTR. In particular, the EMC will be similar to the FTR in fissile mass and in the atom densities and volumes of each region and in the locations of the test loops and control, safety, and shim rods. The length of the ZPR-9 matrix limits the extent of the axial mockup to approximately 47 in. from the midplane of the reactor. Both the size of the matrix and the limited inventory of stainless steel prevent the mockup of the complete radial shield.

The EMC experiments constitute Phase C of the FFTF Critical Experiments Program. They are related to the experiments previously performed in Phases A and B of the same program. However, while the Phase A and B experiments were used to study idealized models of the FTR in clean experiments, the EMC experiments will be performed in assemblies which will reproduce as closely as possible the actual configuration anticipated for the FTR.

The FTR itself will have a variety of configurations during its operating life, such as the beginning-of-life, end-of-first cycle, beginning-of-equilibrium cycle, and end-of-equilibrium cycle.

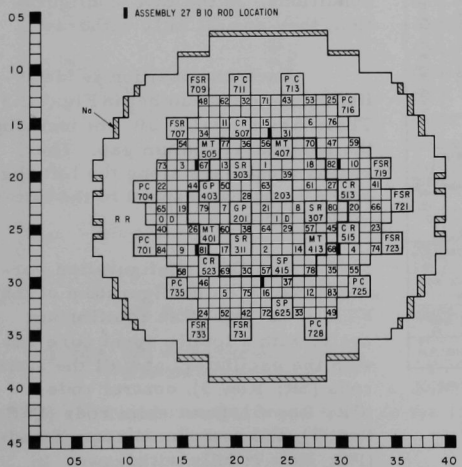

Fig. VII.4. FTR-EMC Initial End-of-Cycle Configuration (EOC-1) with Depletion Pattern

The initial configuration of the engineering mockup was intended to approximate the end-of-cycle (EOC) conditions of the FTR.

The part of the EMC that represents the top half of the FTR was loaded into the movable half of the ZPR-9 matrix. Figure VII.4 represents the front face of the stationary half of ZPR-9 when the reactor is loaded with the EOC configuration. This corresponds to a cutaway view at the midplane of the FTR looking vertically down. The various regions of the assembly are identified by letters: ID (inner driver), OD (outer driver), RR (radial reflector), MT (material test), GP (general-purpose loop), SP (special-purpose loop), SR (safety rod), OSC (oscillator), CR (control rod),

PC (peripheral control rod), and FSR (fixed shim rod). No radial shield is represented, but segments of a 1.0-in.-thick sodium ring surround the reflector; the ring will be completed and surrounded by a radial shield if and when suitable materials become available.

Each hexagonal subassembly of the FTR is identified by a number which gives the row (or ring) in which that subassembly is located plus the location in that row. In this numbering scheme, the central assembly is designated 101. In the first row surrounding the central subassembly, Row 2, there are six subassemblies numbered from 201 to 206. In Row 3 there are 12 subassemblies, 301 through 312, and so on. In Fig. VII.4, individual four-matrix-tube arrays are identified by letters, defined above, and subassembly number.

Also shown in Fig. VII.4 are the locations of the six ZPR-9 ^{10}B rods. The front face of the movable half is the mirror image of that shown in Fig. VII.4.

Every region identified in Fig. VII.4 is divided axially in subregions of various sizes and compositions described in Fig. VII.5. The regions representing the control, safety, and shim rods and the oscillator are shown for both the fully inserted and the fully withdrawn conditions. In the EOC configuration, they are all fully withdrawn.

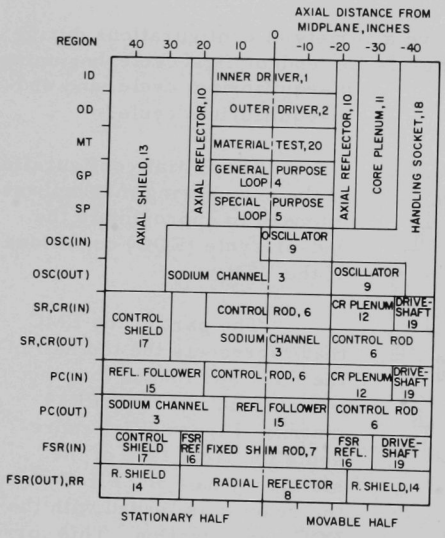

Fig. VII.5. Regions in the Core Loading for the FTR-EMC on ZPR-9

Each composition is identified by name and number in Fig. VII.5. There are a total of 20, not including the peripheral sodium gap. The region identifiers along the left edge of the chart correspond to the letters in Fig. VII.4.

The EOC configuration corresponds to the configuration of the FTR at the end of an equilibrium cycle, with a totally spent core and with the oscillator, and all the safety rods (SR: Row 3), control rods (CR: Row 5), fixed shim rods (FSR: Row 7), and peripheral control rods (PC: Row 7) fully withdrawn. In addition, to simulate burnup, some fuel in the driver regions was replaced with depleted uranium. Before the fuel-loading operation for the approach to critical, one 1/4-in. column of depleted uranium was loaded into a

potential 1/4-in. Pu-U-Mo fuel column location in 84 matrix tubes in the driver regions. The location of depleted-uranium columns was in the left fuel position in the Type A drawer patterns. The 84 depleted driver matrix tubes are indicated with numerals in Fig. VII.4.

(2) Approach to Critical--EOC-1 (A. B. Long, J. W. Daughtry, C. D. Swanson, R. B. Pond, K. E. Plumlee, and G. K. Rusch). During the approach to critical in the initial EMC end-of-cycle configuration (EOC-1), subcritical count-rate data were accumulated from four fission chambers, two BF_3 counters, and two other sets of ZPR-9 operating ion chambers.

Eight sequential loadings were required to bring the reactor to a critical configuration. The first five loadings consisted of replacing void cans with Pu-U alloy plates. Each loading was done in a uniform manner throughout the inner and outer cores. The sixth loading consisted of replacing the remaining void cans with fuel as well as replacing a column of ^{238}U with fuel in depletion tubes No. 84-61 (see Fig. VII.4). Loadings seven and eight continued the substitution of fuel for ^{238}U in depletion tubes No. 60-50 and 49-47, respectively. The final reactor configuration is shown in Fig. VII.4.

The total plutonium mass divided by the recorded count rate is plotted against the total plutonium mass for counters, FC1, FC2, and BF1 in Fig. VII.6. The results are normalized to one at the first loading. Counter FC1 was plotted because it was representative of the detector at the edge of the reflector, FC2 because it was the only detector near the center of the core, and BF1 because it was representative of the detectors on the top of the matrix.

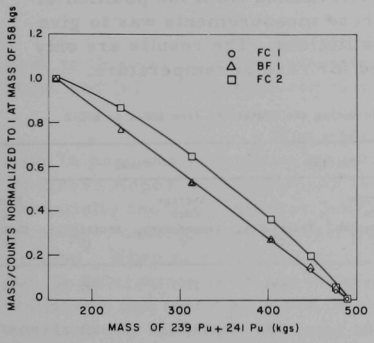

Fig. VII.6. Data for the Approach to Critical in the EOC-1 Configuration

(3) Transition from Initial EOC to EOC-2 (A. B. Long, J. W. Daughtry, C. D. Swanson, and G. K. Rusch). As a result of changes in the FTR reference core maps, it was necessary to make several changes in the EMC end-of-cycle (EOC) configuration. The initial EOC configuration is shown in Fig. VII.4. The following changes were made in the transition to the present EOC-2 configuration shown in Fig. VII.7:

(a) The depletion pattern was revised by shifting depletion numbers 8, 14, 26, and 44 one matrix position directly to the left and shifting depletion number 33 one matrix position directly to the right.

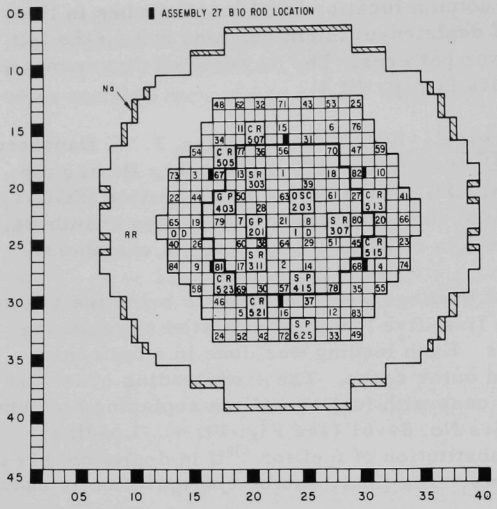

Fig. VII.7. FTR-EMC Revised End-of-Cycle (EOC-2) Configuration with Depletion Pattern

(b) MT-505 and the outer driver composition in matrix positions 30-20, 30-21, 31-20, and 31-21 were removed and replaced with withdrawn control-rod assemblies.

(c) All eight withdrawn peripheral control rods (PC), were removed and replaced with radial reflector assemblies.

(d) MT-401, -407, and -413 were removed and replaced with the inner driver.

During the transition, the worths of a number of these substitutions were measured. The results are presented in Table VII.1. Subcritical reactivities were measured by the rod drop-inverse kinetics technique and excess reactivities were determined from the position of calibrated control rods. The intent of these measurements was to give approximate worths for the various substitutions. The results are only approximate and have not been corrected for reactor temperature.

TABLE VII.1. Reactivity Worths of Changes Made during the Transition from EOC-1 to EOC-2

Description of Change	Initial		Final		Worth of Change, Ih
	Average Core Temperature, °C	Reactivity, Ih	Average Core Temperature, °C	Reactivity, Ih	
1. Remove MT-505 and replace with withdrawn CR-505	27.5	+97	25.5	86	-11
2. Remove outer driver and replace with withdrawn CR-521	25.5	+86	24.6	-591	-677
3. Remove withdrawn PC-711, 716, 701, 725 and replace with reflector	24.6	-591	26.9	-472	+118
4. Remove MT-401 and replace with ID	29.0	-1322	26.8	-671	+651
5. Remove MT-413 and replace with ID	24.5	-562	22.7	+136	+698

(4) FTR-3 Subcritical Reactivity Measurements. R. B. Pond and J. W. Daughtry

(a) Introduction. During November 1970, experiments were conducted to compare and evaluate methods for measuring subcritical

reactivity being considered for the FTR. The experiments were done in ZPR-9 Assembly 26. The general types of measurements were (1) noise analysis, (2) asymmetric source, (3) rod insertion, and (4) source multiplication.

1. Noise Analysis. Three noise-analysis techniques were attempted: (a) Cross-power spectral density by ORNL; (b) polarity spectral coherence by WADCO; (c) polarity correlation in the time domain by ANL.

The data obtained by ORNL and WADCO will be reported by those organizations. The ANL noise measurements were unsuccessful due to instrumentation problems.

2. Asymmetric Source. A ^{252}Cf source (410 ± 20 μg) was used for these measurements. It was stored in a container of borax and paraffin outside the ZPR-9 matrix when not in use. The increase in the count rates and ion-chamber currents due to the californium source were negligible when the source was in the storage container. The source could be transferred remotely from the storage container to the edge of the core. When fully inserted in the reactor, the source was in the stationary-half radial reflector $26 \pm 1/8$ in. from the center of the core, radially, and 4 in. axially from the midplane of the core.

3. Rod Insertion. This method includes two techniques used in this series of experiments: (a) the rod-drop inverse-kinetics technique and (b) the constant-rod technique.

The rod-drop inverse-kinetics technique has been used in previous subcriticality measurements in the FTR-3 program. (See Progress Report for September 1970, ANL-7742, pp. 9-13.) It was used in essentially the same manner during these experiments. In the constant-rod technique, control rods are calibrated accurately with the reactor near critical. When new subcritical configurations are built, the subcriticality can be determined from the count rates recorded with the calibrated rods withdrawn and inserted based on the worth of the calibrated rods. The constant-rod technique assumes that the worth of the rods is the same in the subcritical configuration as it was near critical. It also assumes that inserting the rods does not change the efficiency of the detector used to record count rates. When these assumptions are not valid, calculated corrections can be made to improve the accuracy of the measurement. The results obtained by the constant-rod technique will be given in a later report.

4. Source Multiplication. In this method, count rates or ion-chamber current readings are recorded for each configuration. When some other method is used as a calibration, this method can be used to estimate subcriticality beyond the range of any of the other techniques. This technique suffers from problems of changes in detector efficiency and changes in source strength when plutonium is added or removed.

(b) Description of Initial Configuration for Subcritical Reactivity Measurements. The FTR-3 reference configuration was described in previous Progress Reports (December 1969, ANL-7655, pp. 10-13; January 1970, ANL-7661, pp. 15-16; February 1970, ANL-7669, pp. 27-29). The initial configuration for the subcriticality measurements was significantly different from the reference configuration. Figure VII.8 shows the matrix loading pattern for loading 125, which was the initial configuration for the subcriticality measurements. All 16 peripheral B_4C control zones were removed and replaced with radial reflector composition. The zones marked by letters in Fig. VII.8 are the locations of simulated FTR open and closed loops in FTR-3. Sufficient fuel was removed from the core in these zones to obtain the desired excess reactivity for the beginning of the shutdown-margin measurements. The drawers labeled A in the inner-core region contained closed-loop Type A drawers. The rest of the drawers in the inner core loops, labeled B, contained closed-loop Type B drawers. The zones labeled C contained safety-rod channel composition, and the zones labeled D contained open-loop composition. (These compositions are described in the Progress Reports for September 1970, ANL-7742, p. 9, and October 1970, ANL-7753, p. 15.)

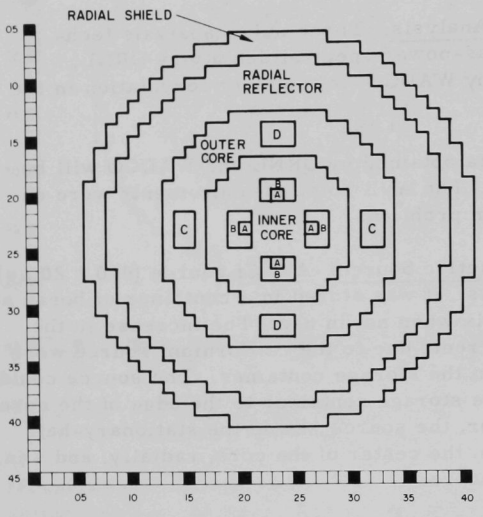

Fig. VII.8. Initial Configuration for Subcritical Reactivity Measurements in FTR-3

Neutron detectors were installed in the assembly at various locations for these experiments. Except as noted, all detectors were inserted into drawers in the radial reflector region so that one end of the detector was at the end of the drawer at the midplane of the assembly. The installation of the detectors required the removal of reflector composition from the drawers. Space in the drawers not occupied by the detectors, leads, etc., was filled with nickel and sodium cans in approximately equal volumes.

The excess reactivity of the initial configuration for the subcriticality measurements as described above was determined to be 136.3 ± 4.0 Ih at 30°C. Several of the ZPR-9 ^{10}B and fuel-bearing control and safety rods were recalibrated in this configuration.

(c) Loading Changes Made during Subcritical Reactivity Measurements. From the initial configuration described above, loading changes were made which provided subcritical configurations in which measurements were made using the methods discussed earlier to determine the subcriticality, within the capability of the method. The changes are cumulative. Figure VII.9 represents the stationary half of ZPR-9 during this experiment. The movable half is the mirror image, except for the source transfer tube.

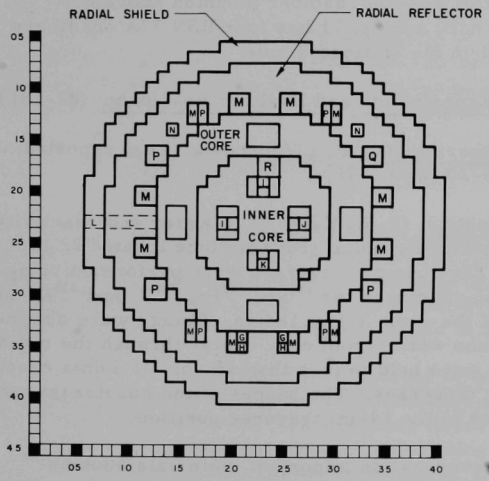

Fig. VII.9

FTR-3 Matrix Loading Diagram, Showing Locations of Zones Reloaded during Subcritical Reactivity Experiment

(d) Results Obtained by the Rod Drop-Inverse Kinetics Technique. System improvements provided the capability to store data from two sets of ion chambers simultaneously. The first channel of data was obtained from a single ^{10}B ion chamber located in matrix position M23-23 in the axial reflector region. The end of the detector nearest the core was approximately 6.4 in. from the core or 24.4 in. from the midplane of the assembly. The second channel was obtained from a bank of four ion chambers mounted above the stationary half of the matrix near the midplane of the assembly. An examination of the data shows small differences in the results, depending on the locations of the rods dropped and the locations of the detectors (i.e., differences between the two channels). To obtain additional subcritical states without making additional time-consuming loading changes, selected ZPR-9 ^{10}B rods were inserted.

Temperature corrections were based on a measured value of -3.39 Ih/°C for the temperature coefficient of reactivity. The method of estimating the uncertainty in the experimental results is described in the Progress Report for September 1970, ANL-7742, pp. 11-12.

(e) Source Multiplication Data. At each configuration during these measurements, ion-chamber current readings and detector count rates were recorded from the ^{10}B ion chamber and the four ANL fission counters. In addition, ion-chamber current readings were recorded from three detector channels located just above the ZPR-9 matrix near the midplane of the assembly. These were reactor channel 3 and experimental channels Sp. 10 and Sp. 11. The ion current for Sp. 10 came from three compensated ion chambers mounted above movable half columns 35-42. Reactor channel 3 uses one RSN 77A ion chamber mounted above columns 18-20 in the stationary half, and Sp. 11 has four RSN 77A chambers mounted above columns 33-41 in the stationary half.

2. Fast Critical Facilities; Experiments and Evaluations--Idaho (02-181)

a. Clean Critical Experiments. P. I. Amundson (Last reported: ANL-7783, pp. 19-20, Feb 1971)

(1) ZPPR Assembly 2 (R. E. Kaiser). Counter and reactivity traverses have been completed in the radial traverse tube located 22 in. from the reactor interface. The counter traverses were performed using 2.173-in. active-length fission chambers for ^{239}Pu, ^{240}Pu, ^{238}U, and ^{235}U, and also for a $^{10}B(n,\alpha)$ detector of the same active length. Counts were obtained every 2.173 in. (one matrix tube width) from core center through the radial reflector. Statistical errors were held to less than 1% for all points except those at the outer ends of the traverses. The shapes of the counter traverses were similar to those obtained in the 14-in. traverse position.

Reactivity traverses for important materials such as sodium, ^{238}U, ^{239}Pu, tantalum, and ^{10}B were performed as were central, or axial centerline, worths of stainless steel and its components, Fe_2O_3, carbon, and a ^{252}Cf neutron source. The reactivity measurements were performed by inverse-kinetics techniques, which included a correction for third-order reactor drift. The worths of the diluent materials were, as expected, quite low and therefore subject to large percentage uncertainties. There were, however, no major unexpected discrepancies in the data that could not be accounted for by the uncertainties.

An additional experiment was performed in relation to the massive control-rod mockups previously performed as part of a series of control-element studies. The original mockup rods were 4 x 4 in. in cross section, occupying four matrix tubes, and 6 ft long, penetrating equally into both halves of the reactor. The drawer loadings for each of the rods were:

Rod 1: 1/4 in. Na, 1/2 in. Ta, 1/2 in. Na, 1/2 in. Ta, 1/4 in. Na

Rod 2: 3/4 in. Na, 1/2 in. natural B_4C, 3/4 in. Na.

The new experiments used the same overall configuration, except that the internal drawer loadings were changed so that the poison materials were distributed more uniformly. The revised loadings were:

Rod 1a: 1/4 in. Na, 5/16 in. Ta, 1/4 in. Na, 6/16 in. Ta, 1/4 in. Na, 5/16 in. Ta, 1/4 in. Na.

Rod 2a: 1/2 in. Na, 1/4 in. natural B_4C, 1/2 in. Na, 1/4 in. natural B_4C, 1/2 in. Na.

Preliminary examination of the data indicates no change in the worth of the Ta/Na mockup rod and only a slight change in the B_4C rod, which may possibly be accounted for by the fact that the B_4C was distributed over a larger volume in Rod 2a than in the original rod.

b. Mockup Critical Experiments. W. P. Keeney (Last reported: ANL-7776, pp. 12-13, Jan 1971)

(1) Experimental Results, Assembly 63. Final processing of the data from all reference cores and from the substitution experiments in the ZPR-3 Assembly 63 series is awaiting the final β values being generated by the EBR-II Project. This report contains the results of the thermoluminescent gamma-dosimeter measurements in Assembly 63A.

(a) Thermoluminescent Dosimeter Measurements, Assembly 63A (G. G. Simons). Gamma-ray dose traverses were completed in ZPR-3 Assembly 63A (see Progress Report for November 1970, ANL-7758, for a description of the assembly) using thermoluminescent dosimeters. Solid 1 x 6-mm rods enriched to 99.993% in ^7Li encased in 2-in.-long, 0.035-in.-wall stainless steel sleeves were loaded into Half 1 of the assembly, 1 in. from the assembly interface. These capsules were exposed for a nominal 50 W-hr. The resulting relative dose traverses are shown in Fig. VII.10.

3. Planning and Evaluation of FFTF Critical Assembly Experiments (02-015; last reported: ANL-7776, p. 4, Jan 1971)

a. Comparison of Computed and Experimental Central Reaction-rate Ratios (A. Travelli and A. J. Ulrich)

Central reaction-ratio measurements have been reported for assemblies ZPR-3/51 (Progress Report for June 1968, ANL-7460, p. 22), ZPR-3/56B (Progress Report for April-May 1969, ANL-7577, p. 35), FTR-2 (Progress Report for December 1969, ANL-7655, p. 42), and FTR-3 (Progress Report for August 1970, ANL-7737, p. 25, and for February 1971, ANL-7783, p. 19). Computed central reaction ratios are compared to the experimental values in Table VII.2.

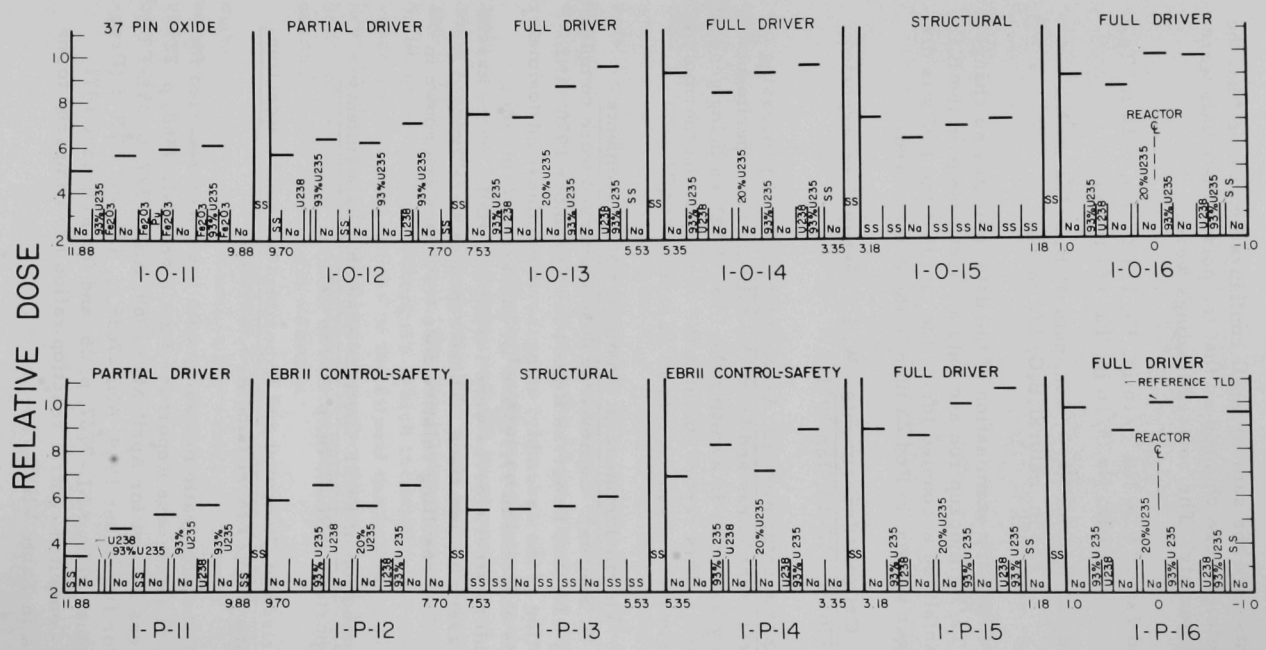

Fig. VII.10. ZPR-3 Assembly 63A, Partial TLD Traverse across the P and O Rows. ANL Neg. No. 103-A11650.

TABLE VII.2. Central Reaction Rates Relative to U-235 Fission Rates

Reaction	Ratio by Experiment	Calculation	C/E
FTR-3			
Pu-239 fission	0.984 ± 0.022	0.890	0.904
Pu-240 fission	0.256 ± 0.006	0.184	0.719
U-238 fission[a]	0.0250 ± 0.0006	0.0224	0.896
U-238 fission[a]	0.0234 ± 0.0013	0.0224	0.957
U-238 capture[a]	0.161 ± 0.009	0.135	0.839
FTR-2			
Pu-239 fission	0.973 ± 0.010	0.918	0.943
Pu-240 fission	0.227 ± 0.002	0.212	0.934
U-238 fission	0.0294 ± 0.0003	0.0273	0.929
ZPR-3/56B			
Pu-239 fission	1.028 ± 0.010	0.922[b]	0.897
Pu-240 fission	0.282 ± 0.003	0.214[b]	0.758
U-238 fission	0.0309 ± 0.0003	0.0274[b]	0.888
ZPR-3/51			
Pu-239 fission	1.003 ± 0.010	0.948	0.945
Pu-240 fission	0.240 ± 0.002	0.234	0.975
U-238 fission	0.0309 ± 0.0003	0.0300	0.971

[a] Measured by radiochemistry. All others were measured by detectors.

[b] Reactor Development Program Progress Report, ANL-7595, p. 16 (July 1969).

The cross-section sets used in the computations were taken from Set 29006 (Progress Report for August 1970, ANL-7737, p. 15) for FTR-3, from Set 29004.2 (Progress Report for December 1968, ANL-7527, pp. 9-10) for FTR-2 and ZPR-3/56B, and from Set 29005 for ZPR-3/51.

Set 29005 has the same 29 energy-group structure as the other two sets, and is also based on ENDF/B-I cross-section data. The core cross sections were averaged in the fundamental-mode spectrum for the core composition at criticality by the MC^2 code.* The cross sections of fissile and fertile core isotopes were averaged using the two-region heterogeneous treatment of MC^2. Radial and axial reflector cross sections were averaged in the spectrum of the radial and axial reflector compositions, respectively, with zero buckling and using the homogeneous treatment of MC^2.

*B. J. Toppel, A. L. Rago, and D. M. O'Shea, MC^2, A Code to Calculate Multigroup Cross Sections, ANL-7318 (June 1967).

The reaction rates were computed using central fluxes from diffusion theory for each assembly. The FTR-3 central flux was obtained from a representation in r,θ-geometry using the DIF2D code,* where the axial leakage was simulated by a DB_Z^2 absorber. The FTR-2 and ZPR-3/51 central fluxes were solutions of cylindrical problems using the MACH1 code,** which again simulated the axial leakage by a DB_Z^2 absorber. In the case of ZPR-3/56B, the central flux was taken from a diffusion-theory fundamental-mode calculation.

It would have been desirable to compute the reaction rates using cross sections with resonance self-shielding corrections for the spectrum intercepted by the counters or foils. In lieu of these cross sections, the most applicable cross sections available were employed. The cross sections used to compute reaction rates in the FTR-3 assembly were as follows: uranium isotopes, appropriate for the uranium in the ZPPR fuel plate in the inner core; plutonium isotopes, appropriate for plutonium of the inner core homogenized with all the inner core material, except for the U_3O_8 plates. All other reaction cross sections were appropriate (in the sense of MC^2) for the fuel plates, in the case of plutonium isotopes, or for the fertile plates, in the case of uranium isotopes.

*B. J. Toppel, Ed., The Argonne Reactor Computation (ARC) System, ANL-7332 (Nov 1967).

**D. A. Meneley, L. C. Kvitek, and D. M. O'Shea, MACH1, A One-dimensional Diffusion-theory Package, ANL-7223 (June 1966).

B. Support of ZPR Fast Critical Experiments

1. Fast Critical Experiments; Theoretical Support--Illinois (02-134)

a. Supplementary Analytical Interpretation of Integral Data. C. E. Till (Last reported: ANL-7765, pp. 7-8, Dec 1970)

(1) Calculation of the Doppler Effect in FTR (P. H. Kier). An isothermal Doppler coefficient in FTR based on beginning-of-equilibrium (BOE) cycle conditions has been calculated. For a uniform change in the temperature of the fuel pins from 1180 to 2180°K with other materials kept at 680°K, two-dimensional, R-Z, perturbation calculations were made of the total Doppler effect and the contributions to the Doppler effect from ^{238}U and ^{239}Pu. The results of these calculations, which used ENDF/B Version I data, are given in Table VII.3.

TABLE VII.3. Contributions to Doppler Effect in FTR by Isotope Using ENDF/B Version I Data. Temperature Change = 1180-2180°K

Isotope	Δk/k, %	α*
^{238}U	-0.29795	-0.00485
^{239}Pu	0.05729	
^{240}Pu		
^{235}U		
TOTAL	-0.24018	-0.00391

*[(1/k)(dk/dT)] = (α/T)

The reactivity effect of the change in fuel temperature was calculated to be -0.24% Δk/k. With the assumption that the Doppler effect has an inverse temperature dependence (i.e., dk/dT = -αk/T), the resulting Doppler coefficient was -0.00391. In interpreting this result, one must remember that the data for ^{239}Pu in ENDF/B Version I are of questionable accuracy as they yield positive calculated Doppler effects in contrast to recent experiments in which very small and probably negative Doppler effects in ^{239}Pu were measured. (See Progress Report for November 1970, ANL-7758, pp. 21-23.) A comparison of the total Doppler effect with the contributions from ^{238}U and ^{239}Pu shows that the contributions from ^{235}U and the higher isotopes of plutonium are negligible. Then, if on the basis of experimental results we take the contribution from ^{239}Pu to be small, the Doppler effect in FTR is well-approximated by the Doppler effect in ^{238}U.

The representation of the reactor in these calculations is shown in Fig. VII.11. Zones 1-6 represent the core homogenized by ring. In Zone 16, three partially inserted control rods are homogenized with fifth-ring fuel subassemblies. Zone 7 represents homogenized peripheral-control and radial-reflector subassemblies. Zones 8, 11, 14, and 15 represent the axial reflector, upper plenum, outer radial reflector, and radial shield regions, respectively. The withdrawn control rods are included in

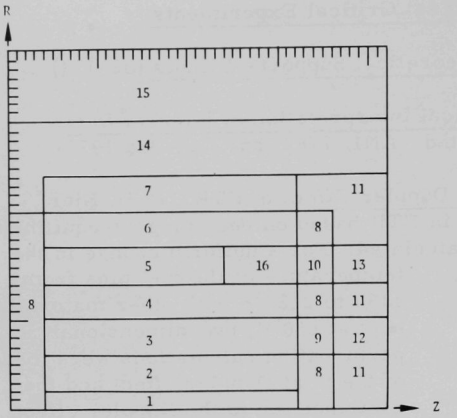

Fig. VII.11. Representation of FTR in 2-D Calculations

Zones 9, 10, 12, and 13. The types of subassemblies homogenized together in the various fuel-bearing zones are described* in Table VII.4.

The MC²** module within the Argonne Reactor Computation (ARC) System† was used to generate the cross-section set used in these calculations. Two MC² runs, which differed only in the temperature of the fuel pins, were used to obtain cross sections for the fuel zones. These problems, which were run heterogeneously to obtain proper resonance self-shielding, used an average core composition characteristic of the Engineering Mockup Criticals. Separate homogeneous MC² runs were made to obtain cross sections for the boron carbide control subassemblies

TABLE VII.4. Subassemblies Assigned to the Fuel-bearing Zones

Type	MWD/kg	Subassemblies Per Zone						
		1	2	3	4	5	6	16
Inner driver, i.d.	0		1	3	5			
	15		1	3	5			
	30	1	1	3	5			
Outer driver, i.d.	0					6	9	6
	15					7	9	7
	30					7	9	7
Special purpose closed loop					1		1	
General purpose closed loop			1		1			
Open loop, i.d.	15		1		1			
Open loop, o.d.	15						2	
Safety rod sodium channel				3				
Control rod sodium channel						4		1
Oscillator			1					
B_4C control rods								3
TOTAL		1	6	12	18	24	30	24

*L. E. Strawbridge to A. Travelli, personal communication (Dec 15, 1970).

**B. J. Toppel, A. L. Rago, and D. M. O'Shea, MC², A Code to Calculate Multigroup Cross Sections, ANL-7318 (June 1967).

†B. J. Toppel, Ed., The Argonne Reactor Computation (ARC) System, ANL-7332 (Nov 1967).

and the radial-reflector subassemblies. For the tantalum control subassemblies, the MC^2 run was heterogeneous to account for resonance self-shielding in the tantalum-tungsten rods, and a weighting spectrum characteristic of the core was used to collapse to broad-group cross sections.

b. Adjustment of Cross Sections on the Basis of Integral Measurements. C. E. Till (Last reported: ANL-7783, pp. 10-11, Feb 1971)

(1) Cross-section Sensitivity Studies (J. M. Kallfelz and M. Salvatores). The Italian zero-dimension perturbation code CIAP-O,* which calculates the sensitivities of k_{eff}, spectra, and reaction rates to various cross-section changes, has been implemented on the IBM 360/75. Preliminary sensitivity studies have been made for ZPR-6 Assembly 7. Standard perturbation theory was used to obtain the sensitivity coefficients for k_{eff}, and generalized perturbation methods** were used for other integral ratios. These sensitivity coefficients can be used in detailed analyses of group cross-section variations. Table VII.5 gives the energy breakdown of the sensitivity of k_{eff} in Assembly 7 to the differences between ENDF/B Versions I and II for important cross-section changes. Table VII.6 gives the sensitivity coefficients relevant to the ratio of the integral flux of the energy group including the 28-keV iron resonance, to the integral flux over the neighboring energy groups. The differences between Versions I and II of ENDF/B for the iron-scattering cross section in the energy range, lowered the ratio considered by about 2%.

The perturbation-theory code DUNDEE† has also been adapted to the IBM 360/75. This code calculates in transport theory the sensitivity of k_{eff} and the time constant λ to changes in various cross sections. For subcritical fixed-source systems, it can also calculate such sensitivities for spectra, reaction ratios, and other parameters of interest. The code, originally written for the IBM-7030, has been debugged so that a test problem prepared at Aldermaston has now run. Table VII.7 shows some results for this problem, which is the the British System I.2 (described by Hemment and Pendlebury††) a fully enriched ^{235}U core of 7.7-cm radius with a 1.8-cm-thick natural uranium blanket. In all cases, the elastic cross section has been changed to keep the partial and total cross sections consistent.

*G. P. Cecchini and M. Cosimi, The CIAP-O Program, CNEN Report RT/FI (69), 42 (1969).

**A. Gandini, A Generalized Perturbation Method for Bilinear Functionals of the Real and Adjoint Neutron Fluxes, J. Nucl. Energy 21, 755 (1967)

†P. C. E. Hemment et al., The Multigroup Neutron Transport Perturbation Program, DUNDEE, AWRE-0-40/66 (1966).

††P. C. E. Hemment and E. D. Pendlebury, "The Optimisation of Neutron Cross-section Data Adjustments to Give Agreement with Experimental Critical Sizes," Proceedings of the International Conference on Fast Critical Experiments and Their Analysis, October 10-13, 1966, ANL-7320, pp. 88-106.

TABLE VII.5. Energy Breakdown of the k_{eff} Sensitivity to the Change in Σ Going from Version I to Version II of ENDF/B (ZPR-6 Assembly 7)

Group j	$\Delta\nu\Sigma_f^j\phi^j$	$-\Delta\Sigma_a^j\phi^j\phi^{*j}$	$\Delta\Sigma_{j\to j+1}\phi^i(\phi^{*j+1} - \phi^{*j})$	$-B^2\Delta D\phi^j\phi^{*j}$
1	0.0	-0.00006	-0.00051	-0.00001
2	-0.00289	0.00031	-0.00006	0.00003
3	-0.00575	0.00147	-0.00050	0.00020
4	-0.00281	0.00095	-0.00089	0.00008
5	-0.00108	0.00077	0.00011	0.00022
6	-0.00147	0.00075	0.00012	0.00037
7	0.00062	0.00040	0.0	0.00024
8	0.00147	-0.00051	-0.00055	0.00039
9	-0.00060	-0.00016	0.00099	-0.00170
10	-0.00018	-0.00084	-0.00005	-0.00001
11	0.00358	-0.00396	-0.00078	0.00069
12	0.00120	-0.00125	0.00014	0.00107
13	0.00154	-0.00062	0.00005	0.00008
14	-0.00219	-0.00100	-0.00005	-0.00005
15	-0.00226	0.00029	0.00029	0.00008
16	-0.00195	0.00023	0.00018	0.00008
17	-0.00152	0.00043	0.00005	0.00004
18	-0.00209	-0.00060	0.00014	0.00011
19	0.00100	-0.00014	0.00023	0.00005
20	-0.00152	0.00046	0.00005	0.00002
21	0.00098	-0.00062	0.0	0.00001
22	-0.00010	0.00036	0.0	0.00001
23	0.0	0.00006	0.0	0.0
TOTAL	-0.01502	-0.00226	-0.00101	+0.00202

TABLE VII.6. ZPR-6 Assembly 7 Sensitivity Coefficients Relevant to the Ratio:

$$\frac{\phi_{12}}{\sum_{i=11,13}\phi_i}$$

Group	Scattering Sensitivity Coefficients, Relative to $\Delta\Sigma_{j\to j+1} = 1$	Absorption Sensitivity Coefficients, Relative to $\Delta\Sigma_a = 1$
11	14.81	+0.51
12	-21.32	-11.49
13	9.03	9.03

TABLE VII.7. Group Changes in $B = 1/k_{eff}$ for a 1% Increase in Various Cross Sections, for a Small, Hard ^{235}U Assembly (see text)

Group	E-Lower, MeV	Δu	$-10^4 \cdot \Delta B$ for Change in Listed Cross Section			
			$\sigma_f - {}^{235}U$	$\sigma_\gamma - {}^{235}U$	$\sigma_t - {}^{238}U$	$\sigma_{n,n'} - {}^{238}U$
1	2.4	1.52	11.6	0.014	0.69	0.55
2	1.1	0.78	14.5	0.307	1.80	0.61
3	0.55	0.69	12.8	0.914	2.32	0.37
4	0.26	0.75	10.5	1.26	2.18	0.14
5	0.13	0.69	5.3	1.06	1.19	0.033
6	0.043	1.11	3.0	0.88	0.67	0.003
7	0.010	1.46	0.58	0.25	0.11	0.0
8	0.0016	1.83	0.050	0.033	0.005	0.0

Work is now proceeding on changing the DUNDEE input subroutine to accept cross sections in the ARC format, and writing the interface code necessary between DUNDEE and the ARC 1-D transport code.

c. ZPR Heterogeneity Method Development. B. A. Zolotar (Last reported: ANL-7765, pp. 8-9, Dec 1970)

(1) Testing of MC^2-2 Heterogeneity Algorithms (M. Salvatores, B. A. Zolotar, and C. E. Till). The heterogeneity algorithms recommended for inclusion in MC^2-2 are being applied to the analyses of several recent critical experiments. Although the MC^2-2 coding is not yet available, many of the algorithms are contained in presently existing codes. This will allow separate studies of individual parts of the heterogeneity treatment. Some of the problems presently under study are:

(a) Analyses of pin-plate comparison measurements in ZPR-6 Assembly 7.

(b) Consistent comparisons of plate heterogeneity effects in ZPR-6 Assembly 6 (uranium fueled) and ZPR-6 Assembly 7 (plutonium fueled).

(c) Analyses of the measurements of reaction-rate cell traverses in ZPR-6 Assembly 7 using several calculational methods and leakage options.

2. Fast Critical Experiments; Experimental Support--Illinois (02-013)

a. Computer Applications. C. E. Cohn (Last reported: ANL-7783, pp. 12-13, Feb 1971)

(1) Improving the Efficiency of Direct-memory-access Output Operations on the SEL-840 Computer. Many reactor-physics measurements made with the ZPR facilities involve the SEL-840 computer. In particular, reactivity measurements using inverse-kinetics techniques are routinely made, and application of this computer to neutron time-of-flight experiments is planned. To optimize computer performance, the computer subroutines in current use were modified.

The disks and magnetic tapes attached to the SEL-840 computers are connected through direct-memory-access (DMA)* channels. In theory, DMA is supposed to increase throughput by overlapping input/output with computation. However, certain aspects of the simple software system supplied by the manufacturer prevented these benefits from being realized. The existing routines were altered to make available the full power of the DMA for output operations.

In the simple operating system used with the SEL-840 computers, programs communicate with peripherals by calls to input/output subroutines. Each such call passes the starting address of a data buffer area in memory and a count of words to be transmitted. The routine passes these parameters to the DMA channel and then commands the peripheral to initiate the input or output operation under DMA control. At this point, no further central-processor action is required to keep the operation going. Thus, in principle the subroutine could immediately return to the calling program, allowing the latter to go on with its tasks while the input or output operation proceeds automatically, preempting an occasional memory cycle for data transfer. For a variety of reasons, though, this efficient procedure is not feasible.

For output operations, one reason is the possibility that the calling program, in entering data into its buffer area for the next output operation, will overwrite the data for the current operation before being transmitted to the peripheral. The existing subroutines prevent that by deferring the return to the calling program until the output operation is complete. Clearly, such deferral nullifies the value of the DMA, making the system throughput no better than with just ordinary programmed data transfers.

*Called "Block Transfer Control" (BTC) in SEL-840 nomenclature.

The usefulness of the DMA may be realized at the cost of a small amount of core by providing the output subroutine with its own internal buffer area. The data to be output are moved to this buffer before output is started, and the DMA channel is addressed to it. Then there is no further need for the contents of the calling program's buffer, so control may return directly to the calling program, which may modify the contents of its buffer immediately. The desired overlap of computation and output is thus achieved. The time required to move the data to the internal buffer is normally a small fraction of the time required for the entire output operation, and thus does not detract appreciably from the gain in throughput.

It is clearly wasteful of core to provide a buffer area large enough for any conceivable requirement. Rather, the area should just be large enough for the record length most commonly employed, longer records being handled the old way. A buffer was provided only large enough for a card image on the magnetic tape and one sector on the disk. Figure VII.12 shows the flowchart for the disk subroutine operating in this way.

Some peripherals require a check on the correctness of data transmission after an output operation is complete. (Parity checking of magnetic tape is typical.) This is another reason why conventional routines defer the return. However, that deferral can be avoided if the parity check is postponed until the next time the subroutine is entered. Figure VII.13 shows how that was done for the magnetic-tape subroutine.

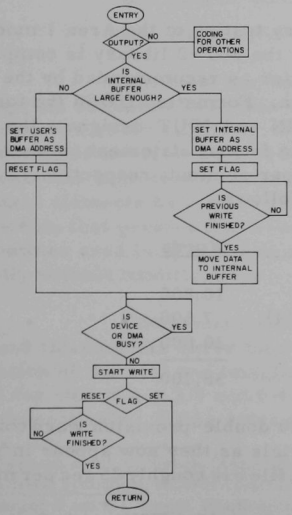

Fig. VII.12. Output Routine for a Device That Does Not Check Parity after Writing (e.g., disk). ANL Neg. No. 116-593.

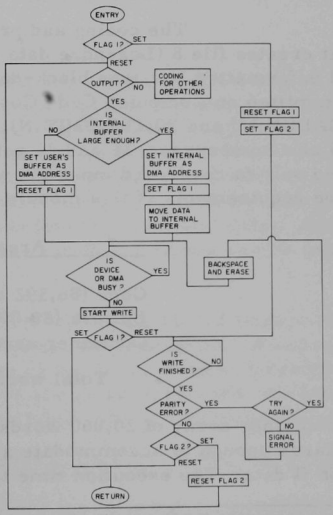

Fig. VII.13. Output Routine for a Device That Does Check Parity after Writing (e.g., magnetic tape). ANL Neg. No. 116-594.

C. Fast Reactor Analysis and Computational Methods

1. Theoretical Reactor Physics (02-081)

a. Reactor Computation and Code Development. B. J. Toppel (Last reported: ANL-7783, pp. 57-60, Feb 1971)

(1) Two-dimensional Transport Capabilities in the ARC System (W. L. Woodruff). A two-dimensional transport-theory capability* consisting of the ARC System standard path STP011 and catalogued procedure ARCSP011 (SNARC) is currently in the stage of user testing. In cooperation with the EBR-II program staff, a comparison with the results from the DOT code has been attempted. Some difficulty has been encountered in the convergence of a k-calculation in xy geometry for the EBR-II core. The problem seemed to stem from the original choice of negative-flux fixup used in SNARC. This testing is continuing. The current testing of k-calculations in rz geometry have not shown any difficulties.

(2) The MC^2-2 Code (H. Henryson, C. G. Stenberg, and B. J. Toppel). Coding is continuing on the new cross-section code MC^2-2 in the areas of: library preparation (Area 1); resolved resonance J integral calculations (Area 6); and macroscopic cross sections, continuous slowing-down moderating parameters, and Legendre elastic scattering matrix preparation (Area 7).

The coding and preliminary testing of the Area 1 module that creates file 8 (Legendre data file) for the MC^2-2 library is complete. All unformatted I/O uses block-data transfer as recommended by the Committee on Computer Code Coordination. Formatted I/O in the form READ(IN,M) and WRITE(IOUT,N), where IN and IOUT designate the logical unit numbers and M and N refer to the format statement numbers, are used only to read-card input and write-paper printout, respectively. The core requirements of this module are as follows:

Area	Words
Code (86,392 bytes/8)	10,800
Buffers (30,000 bytes/4)	7,500
Container array	20,000
Total words	38,300

A container array of 20,000 words (~11,000 double-precision word container) is large enough to accommodate all materials as they now appear in Version II data. The execution time to create file 8 is roughly 25 sec per material,

*W. L. Woodruff, 2-D Transport Capability in the ARC System Standard Path STP011 and the Catalogued Procedure ARCSP011, internal memorandum (Jan 7, 1971).

which includes a paper printout of all file 8 data in user-readable form and appropriate execution messages. Since this section of code has its own temporary input processor, it can stand alone to create an MC^2-2 library in this area. The user input options for this area include:

(a) The energy range of the library. The user specifies the maximum and minimum energy.

(b) The ultrafine-group lethargy width.

(c) The number of ultrafine groups per "block" of Legendre data.

(d) The maximum order of Legendre-polynomial expansion coefficients.

(e) Convergence criterion for elastic scattering angular data when ENDF/B data give tabulated distributions. If this convergence criterion cannot be met within the maximum order specified by item d, then an error message is printed out and execution continues.

(f) The highest order permitted for the extended transport approximation.

(g) Materials to be included in the library from the DAMMET* tape.

(h) Size of BPOINTER** container array.

(i) Print options.

The code has been variably dimensioned, and a search through the DAMMET tape (file 4) for the appropriate variable quantities is performed at the beginning of execution. The problem encountered in integrating products of high-order Legendre polynomials for the T matrix elements has been circumvented by generating the zero- and first-order T matrix elements by a recursive method. Coding is well under way in the module that creates file 5 (smooth-tabulated nonresonant data). Several subroutines used in ETOE† are appropriate for this area and can be used directly without modifications.

The structure of the second file of the MC^2-2 library that contains the complex error function W(x,y) has been modified. A coarse tabulation of the real and imaginary parts of the W function at increments of 0.1 for $-0.1 \leq x \leq 3.9$ and $0.4 \leq y \leq 3.0$ are given in records one and two, respectively. A fine structure of the tabulation of the real and imaginary

*J. Felberbaum and H. C. Honeck, Description of the ENDF/B Processing Codes CHECKER, CRECT, DAMMET, and Retrieval Subroutines, ENDF-110 (Sept 1967).

**H. Henryson II and B. J. Toppel, Modifications to BPOINTER--A Dynamic Storage Allocation Program Utilizing Bulk Memory, ANL internal memorandium (Oct 6, 1969).

†D. M. Green and T. A. Pitterle, ETOE, A Program for ENDF/B to MC^2 Conversion, APDA-219 (June 1968).

parts of the W function at increments of 0.1 for $-0.1 \leq x \leq 3.9$ and at increments of 0.02 for $-0.02 \leq y \leq 0.5$ are given in records three and four, respectively. The range and fineness of the tabulation in records three and four are given in order to obtain greater accuracy when table interpolation is used. In approximately half the calls to QUICKW for typical fast-reactor problems, the arguments of W fall in the range of the fine table. A six-point interpolation yields values of W accurate to at least five significant figures. The same six-point interpolation for values of y in the coarse table give four-figure accuracy.

The coding and compiling in the resolved resonance area (Area 6) is complete, but has not as yet been tested. A fast J integral calculation replaces the time-consuming integration over ultrafine groups used in MC^2 and should result in significant improvement in execution time in this part of the code. This area can accommodate homogeneous and heterogeneous options. The code treats either a multiregion slab cell or a two-region cylindrical geometry pin cell. Resonance integrals are generated for the homogeneous mixture and for each heterogeneous region.

A table of $E_3(x)$ has been generated for use in slab-geometry calculations. The tabulation is for $0 \leq x \leq 10.0$ at increments of 0.01.

The coding of the preparation of microscopic and macroscopic scattering matrices, macroscopic cross sections, fission spectra, extended transport cross sections, and moderating parameters (Area 7) is complete. Although the coding done thus far has compiled successfully, only a few areas have been tested with real data. These areas include:

(a) The generation of ultrafine-group unresolved resonance cross sections from the $\sigma(E^*)$ calculated in the unresolved calculation (successfully executed).

(b) The generation of chi vector from an analytical integration of formula (successfully executed for ^{239}Pu data; $\alpha = 0$, $\beta = 1.41 \times 10^6$).

(c) The generation of Legendre polynomials of the second kind for extended transport cross sections in B_1 or consistent B_1 option.

The extended transport cross sections depend on the term $Q_{N+1}(i\Sigma/B)/Q_N(i\Sigma/B)$, where

$\Sigma \equiv$ total cross section,
$B \equiv \sqrt{B^2}$ the buckling,
$Q_N \equiv$ Legendre function of the second kind,

and

$N \equiv$ order of extended transport approximation.

MC^2-2 will permit values of $1 \leq N \leq 9$. ($N = 1$ is the standard B_1 or consistent B_1 approximation.)

A function subprogram QL has been written which calculates the real or imaginary part of the ratio $Q_{N+1}(Z)/Q_N(Z)$ for $2 \leq N \leq 9$. Since the recursive relation for Q_N is not stable against roundoff errors for all values of $|Z|$, three relations are used in the routine Q_L.*

(a) Recursion Relation

$$nQ_n(Z) = (2n - 1)\, ZQ_{n-1}(Z) - (n - 1)\, Q_{n-2}(Z); \tag{1a}$$

$$Q_0(x) = \frac{1}{2} \ln \frac{1 + x}{1 - x}, \quad Q_1(x) = \frac{x}{2} \ln \frac{1 + x}{1 - x} - 1; \tag{1b}$$

$$Q_0(ix) = -i \tan^{-1}(1/x), \quad Q_1(ix) = x \tan^{-1}(1/x) - 1. \tag{1c}$$

(b) P_n Series Expansion

$$Q_n(Z) = P_n(Z)Q_0(Z) - \sum_{j=0}^{\frac{1}{2}(n-1)} \frac{2n - 1 - 4j}{(1 + 2j)(n - j)} P_{n-1-2j}(Z). \tag{2a}$$

$P_n(Z)$ is calculated from Eq. 1a with

$$P_0(Z) = 1, \quad P_1(Z) = Z. \tag{2b}$$

(c) Hypergeometric Series

$$Q_n(Z) = B(n,Z)F(\tfrac{1}{2},\tfrac{1}{2};\, n + \tfrac{3}{2};\, -t); \tag{3a}$$

$$t = \frac{Z - \sqrt{Z^2 - 1}}{2\sqrt{Z^2 - 1}}; \tag{3b}$$

$$B(n,Z) = \frac{\Gamma(\frac{1}{2})\,\Gamma(n + 1)}{\Gamma(n + \frac{3}{2})\,\sqrt{2}\,(Z^2 - 1)^{\frac{1}{4}}(Z + \sqrt{Z^2 - 1})^{n+\frac{1}{2}}}; \tag{3c}$$

$$F(\tfrac{1}{2},\tfrac{1}{2};\, n + \tfrac{3}{2};\, -t) = \sum_{k=0}^{\infty} \frac{\Gamma(k + \frac{1}{2})\;\Gamma(k + \frac{1}{2})\;\Gamma(n + \frac{3}{2})}{k!\,\Gamma(\frac{1}{2})\,\Gamma(\frac{1}{2})\,\Gamma(n + k + \frac{3}{2})}\,(-t)^k. \tag{3d}$$

Eleven terms are retained in Eq. 3d, and constants A are tabulated so that the evaluation of Eq. 3a takes the form

*Tables of Associated Legendre Functions, National Bureau of Standards, Columbia University Press, New York (1945).

$$Q_n(Z) = \frac{C_n(t)}{(Z^2 - 1)^{\frac{1}{4}}(Z + \sqrt{Z^2 - 1})^{n+\frac{1}{2}}} \tag{3e}$$

$$C_n(t) = A_0^n(1 - A_1^n t(1 - A_2^n t(1 \ldots (1 - A_{10}^n t)))))))))). \tag{3f}$$

The domains of use are as follows:

I. $Z^2 > 0$ ($B^2 < 0$, subcritical);

$Z = x$;

$x = 1$, QL = 1;

$x < 1$, recursion relation, Eq. 1;

$x > 1$, hypergeometric series, Eq. 3.

II. $Z^2 < 0$ ($B^2 > 0$, critical);

$Z = ix$;

$x \leq 0.45$, recursion relation, Eq. 1;

$x \leq 1$, $N \leq 3$, recursion relation, Eq. 1;

$0.45 < x \leq 1$, $N \geq 4$, P_n series expansion, Eq. 2;

$1 < x \leq 4$, $N \leq 3$, P_n series expansion, Eq. 2;

$x > 4$, hypergeometric series, Eq. 3;

$x > 1$, $N \geq 4$, hypergeometric series, Eq. 3.

The function QL has an accuracy of at least four significant figures (has been tested over the range $10 \geq |Z| > 0$) and an average timing for 2000 calls of 1.5 sec. The size of QL is 490 double-precision words.

In Area 7, several decisions have been made which will reflect on the speed of a particular calculation. A case in point is the form of the chi fission distribution. If the problem uses a single chi vector, as in the present version of MC^2, then that vector is calculated in Area 7 and no flux iteration is required in the spectrum calculation. On the other hand, MC^2-2 will permit the user to specify any number of chi vectors or matrices for the materials in the problem. If all materials have chi vectors, then Area 7 will calculate them once and they will be used in the spectrum calculation which will have a flux iteration. If any materials have chi matrices (energy-dependent), then those matrices must be recalculated during each flux iteration in the spectrum calculation. This decision is required because of storage capability.

A rather extensive restart capability has been built into the calculation of Legendre scattering matrices. The ground rules for using this capability are as follows:

The data set containing microscopic scattering arrays may be saved from a previous calculation. If this data set is provided in a second MC²-2 calculation, then those materials for which data are available (all materials in the reference problem) will not have the scattering arrays recalculated provided that:

(a) Both problems have the same number of groups.

(b) Both problems have the same maximum energy.

(c) If the second problem uses a consistent spectrum option, then the reference problem must also have used a consistent spectrum option.

If any of these conditions are violated, MC²-2 will generate a new set of microscopic scattering matrices. Caution must be taken in use of the transport approximation, as the code will permit the reference and restart problem to be inconsistent regarding this option (a warning message is printed). Thus, if, for example, the reference problem used one of the transport approximations and the restart problem does not, then the total cross section will be adjusted only for materials in the reference problem. The order of the extended transport approximation need not be the same in both problems. If higher-order scattering terms are required in the second problem which are not available on the restart data set, they will be generated.

2. Reactor Code Center. M. Butler (02-085; last reported: ANL-7783, pp. 60-61, Feb 1971)

In March, 11 new program packages were incorporated in the Code Center library. Three of these were revisions of existing library programs, and recipients of the earlier versions have been notified of the availability of new packages for FIGRO* (ACC 272), AIROS2A (ACC 326), and SUPERTOGII (ACC 431).

The new FIGRO package includes provision for the computation of time-dependent heat conduction for rapid transients, beginning with a fuel rod at operating power conditions. Other additions account for the effect on gap conductance of the release of volatile gases from the fuel, reduction of gap thickness due to cladding creep, ternary fission helium release, and the existence of cladding corrosion layers.

The revised AIROS2A code includes a contact resistance term in the overall heat-transfer-coefficient calculation and insertion of a subroutine to simulate setback or controller action of a single bank of control rods.

*I. Goldberg and L. L. Lynn, FIGRO (Addendum II): A CDC 6600 Computer Program for the Analysis of Fuel Swelling and Calculation of Temperature in Bulk-Oxide Cylindrical Fuel Elements, WAPD-TM-618, Addendum II (Apr 1970).

Facility to handle ENDF/B Version II data has been incorporated in the revised SUPERTOGII program.

Of the eight new programs, five were written for the UNIVAC 1108. Four of these contributions were from Gulf General Atomic and include:

SAFE-CRACK* (ACC 451), a FORTRAN V program in the SAFE finite-element series which performs a viscoelastic analysis of plane and axisymmetric composite concrete structures subject to transient temperature and mechanical loadings.

SHELL5** (ACC 452), a FORTRAN IV program using the finite-element method for analysis of smoothly curved, arbitrarily shaped, three-dimensional thin shells.

GAPER-2D† (ACC 471), a FORTRAN V two-dimensional, first-order, perturbation-theory program using the real and adjoint flux and current values calculated by 2DF in r-z or x-y geometry.

CAGE-BIRD-SPEC†† (ACC 476), a package of three codes designed for the reduction and processing of neutron time-of-flight spectra in pulsed assemblies.

Battelle Pacific Northwest Laboratories submitted the fifth UNIVAC 1108 package, BRT-1‡ (ACC 184), written in FORTRAN IV. The Battelle Revised Thermos program is that laboratory's version of the THERMOS thermalization transport-theory code developed by H. C. Honeck at Brookhaven National Laboratory. The program computes the space-dependent thermal neutron density, flux and current spectra over the energy range 0 to 0.683 eV in either slab or cylindrical geometry.

Three CDC 6600 packages complete this month's library acquisitions. These are:

3DDT‡‡ (ACC 463), a three-dimensional, multigroup diffusion-theory program prepared at Los Alamos Scientific Laboratory, which provides material burnup and fission-product buildup computations for specified time intervals. This program is an extension of the 2DB code written entirely in FORTRAN IV.

*Y. R. Rashid, Nonlinear Quasi-Static Analysis of Two-Dimensional Concrete Structures, Part I: Theory. Part II: Computer Program Manual, GA-9994 (Mar 23, 1970).

**N. Prince, SHELL5 SHELL-3D Version 5: A Computer Program for the Structural Analysis of Arbitrary Three-Dimensional Thin Shells, A User's Manual, GA-9952 (Jan 30, 1970).

†R. J. Archibald and D. A. Sargis, GAPER-2D, A Two Dimensional Transport Perturbation Theory Program, GA-10103 (Apr 29, 1970).

††P. d'Oultremont, D. Houston, and J. C. Young, CAGE-BIRD-SPEC, A Package FORTRAN-V System for the Reduction and Analysis of Neutron Time-of-Flight Spectra, Gulf-RT-10195 (Nov 18, 1970).

‡C. L. Bennett and W. L. Purcell, BRT-1: A Battelle-Revised-Thermos, BNWL-1434 (June 1970).

‡‡John C. Vigil, 3DDT, A Three-Dimensional Multigroup Diffusion-Burnup Program, LA-4396 (Sept 1970).

CRECT, CHECKER, RIGEL, LISTFC, DICTION, SLAVE3 and DAMMET (ACC 475), the FORTRAN IV processing package for the ENDF/B Version II data supplied by the National Neutron Cross Section Center.

ADLER, AVRAGE3, AVRAGE4, and SIGMA2 (ACC 465), a second NNCSC program package designed to calculate total, capture, or fission cross sections according to the Adler-Adler formalism using ENDF/B Version II file 2 parameters, to calculate scattering, capture, and fission cross sections from s-, p-, and d-wave data of the unresolved parameters of file 2 of ENDF/B, or to calculate scattering, capture, fission, and total cross sections from the resolved resonance parameter data.

PUBLICATIONS

The ARC System Neutronics Input Processor
E. A. Kovalsky and D. E. Neal
ANL-7713 (Jan 1971)

Comment on Resonance Averaging
P. A. Moldauer
Phys. Rev. C3, 948-949 (Feb 1971)

VIII. REACTOR SAFETY

A. Coolant Dynamics. H. K. Fauske (02-114)

1. Sodium Superheat. R. E. Henry, R. E. Holtz, and R. M. Singer (Last reported: ANL-7783, pp. 94-97, Feb 1971)

a. Incipient-boiling Tests with EBR-II Sodium

The incipient-boiling superheat tests with the EBR-II primary sodium have continued. These tests have used an electromagnetic pump to apply pressure to the sodium (i.e., no inert gas was introduced into the system). These data show considerable scatter (i.e., the pressure-temperature history is lost after a high-superheat run) unless the pressure-temperature history is reestablished for at least 20 min before conducting the test run.

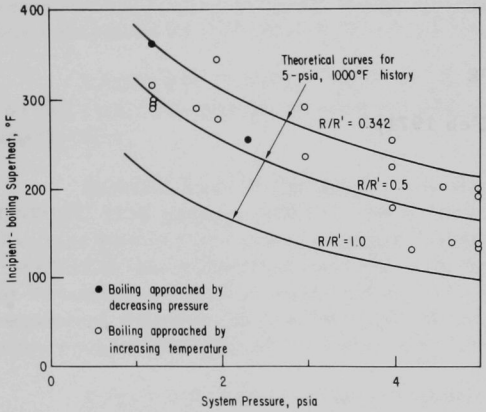

Fig. VIII.1. Experimental Data and Theoretical Predictions for a 5-psia, 1000°F Pressure-Temperature History

Figure VIII.1 shows the theoretical curves from the pressure-temperature history model for a 5-psia, 1000°F history and a ratio of receding-to-advancing radii of curvature (i.e., R/R') of 1.0, 0.5, and 0.342, as well as the corresponding data with the history applied for at least 20 min before conducting the test run.

Figure VIII.2 shows the data obtained with a 10-psia, 1000°F history and the theoretical curves for a ratio of receding-to-advancing radii of curvature of 1.0, 0.5, 0.342, and 0.174. For both histories, the data fall well above the theoretical curve for R/R' = 1.0 and are perhaps best represented by a R/R' ratio of about 0.34. This ratio for receding-to-advancing radii of curvature is in excellent agreement with recent contact-angle data.* The scatter in these data can be attributed to variations in the contact angle of the advancing liquid and variations in surface-cavity geometries.

Recent tests have been conducted with an argon cover gas as the means of applying pressure to the system. These tests have demonstrated that the presence of a partial pressure of inert gas in the surface cavities

*M. J. Todd and S. Turner, The Surface Tension of Liquid Sodium and Its Wetting Behavior on Nickel and Stainless Steel, TRD Report 1459(R), UKAEA (1968).

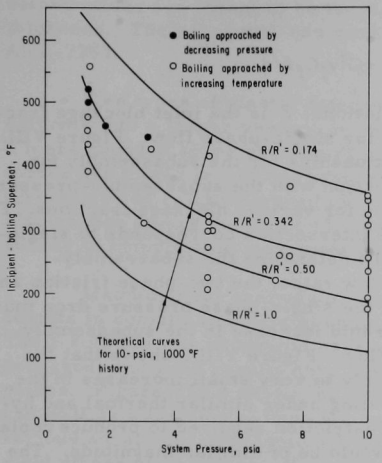

Fig. VIII.2. Experimental Data and Theoretical Predictions for a 10-psia, 1000°F Pressure-Temperature History

can significantly reduce the incipient-boiling superheat. With the assumptions of a partial pressure of inert gas in the surface cavities equal to the cover-gas pressure and an R/R' ratio of 0.34, the pressure-temperature-history model and the experimental data agree excellently.

2. Sodium Expulsion and Reentry: In-pile. M. A. Grolmes and H. K. Fauske (Last reported: ANL-7783, pp. 97-98, Feb 1971)

a. Planning of In-pile Test Vehicles

Integrated in-pile (TREAT Reactor) experiments are being planned to determine the overall consequences of coolant expulsion and reentry as they affect fuel failure and potential interactions of molten cladding, fuel, and coolant. For these tests, coolant expulsion will be specifically initiated by flow transients such as a coastdown and partial or complete blockage at steady power in a test vehicle that simulates current LMFBR design parameters. Near-term tests will be directed to simulation of FFTF parameters.

One of the loss-of-flow conditions of interest for in-pile testing is that arising from a partial inlet restriction. Beyond the extent of inlet blockage required for coolant boiling (see ANL-7783), it remains to be determined whether the resulting two-phase flow through the subassembly is stable or is unstable and leads to a boiling crisis in that assembly. A steady-state analysis of these conditions was carried out to determine the limits of stable two-phase flow for an increase in inlet blockage beyond that required for coolant boiling at the exit of the subassembly.

The typical LMFBR design is characterized by both a large subassembly pressure drop and exit subcooling under normal conditions. Reference conditions similar to current FFTF design were selected: a total pressure drop ΔP_0 = 130 psi, a flow rate G_0 = 1250 lb_m ft^{-2} sec^{-1} along the fuel pin, a sodium inlet temperature of 600°F, an average power of 7.61 kW/ft along a 3-ft heated length, and an exit pressure of 20 psia. The total pressure drop across the subassembly, ΔP_T, is made up of the pressure loss at inlet restriction, ΔP_i, plus the pressure drop for the subassembly, ΔP_0,

$$\Delta P_T = \Delta P_i + \Delta P_s \qquad (1)$$

where

$$\Delta P_i = \tfrac{1}{2}G^2 v_f (1-\beta)^{-2} \text{ and } \Delta P_s = \tfrac{1}{2}G^2 v_f C_f \ell/d$$

for single-phase flow. In the above relations, β is the inlet blockage fraction and C_f is the liquid friction factor for single-phase flow. Figure VIII.3 shows the pressure drop and flow relationships for the subassembly for various inlet restrictions. The intersection with the subassembly-pressure-drop curve gives the operating condition for various blockage fractions. For blockage fractions less than ≈ 0.95, the intersection corresponds to single-phase flow through the subassembly. To determine the subassembly-pressure-drop curve, ΔP_s, for lower flow rates, the two-phase friction and momentum pressure losses as well as the single-phase pressure drop must be accounted for. This results in the rapid increase in the subassembly-pressure-drop curve with decreasing flow. Figure VIII.3 shows that the two-phase flow is initially stable, but only to very small increases in the inlet blockage fraction. For in-pile testing under similar thermal and hydraulic conditions, the extent of inlet restriction required to produce coolant overheating and subassembly voiding would be of similar magnitude. The time scale and sequence of events following this overheating might be somewhat different from a sudden complete blockage because of different thermal conditions in the upper plenum region (as shown previously).

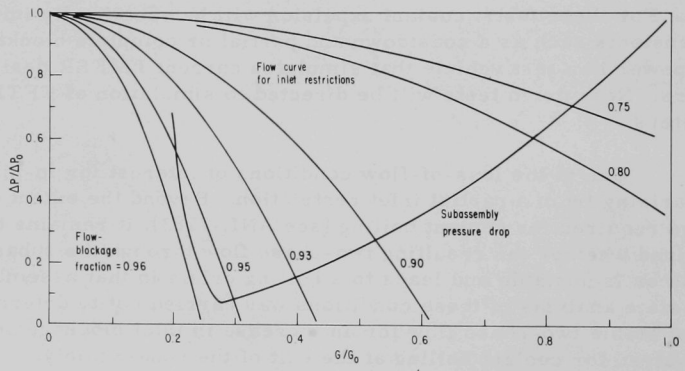

Fig. VIII.3. Flow and Pressure-drop Characteristics for LMFBR Subassembly of Approximate FFTF Design, ΔP_0 = 130 psi, G_0 = 1250 lb_m/ft^2-sec

B. Core Structural Safety. C. K. Youngdahl, ETD (02-115; last reported: ANL-7753, pp. 146-147, Oct 1970)

1. Dynamic Plasticity Analysis of Hexagonal Shells

To determine the containment capability of LMFBR hexagonal subassembly cans, a model was formulated for large dynamic plastic deformations of hexagonal cans subjected to internal impulsive pressures. Large

deformations are meant to be those deformations greater than the wall thickness. The hexagonal-can configuration is shown in Fig. III.A.1 of ANL-7753.

Two types of plastic deformation occur simultaneously. The hexagon deforms into a larger hexagon by stretching of the wall, and it distorts into a more rounded shape because of bending of the wall. These two deformation modes are mixed in varying proportions during the motion of the can. The directions and relative magnitudes of the stress resultants in the can wall also change during the motion because of the large deformation effects, resulting in complicated movement of the plastic zones.

Mathematical analysis of the large-deformation hexagonal-can model results in complicated sets of coupled nonlinear differential equations. Their solution was programmed for the computer. The program is now being debugged, and good results have been obtained for some simple pressure pulses. Figure VIII.4 shows the deformation of the center and corner of the can wall as a function of time for rectangular pulses of fixed magnitude and various durations. For typical LMFBR hexagonal-can dimensions and a yield stress of 35,000 psi, the applied pressure would be 220 psi as compared to a limit load of 135 psi; a dimensionless time of unity corresponds to about 0.2 msec. The corners of the can pull in slightly as the center of the wall deforms out. The most significant result is that the deformation stops at about three wall thicknesses for pulses that exceed 1.59 (dimensionless) units in duration. This means that the can has distorted into a shape that can statically contain the applied pressure. Of course, the increased containment potential is at the expense of considerable wall distortion.

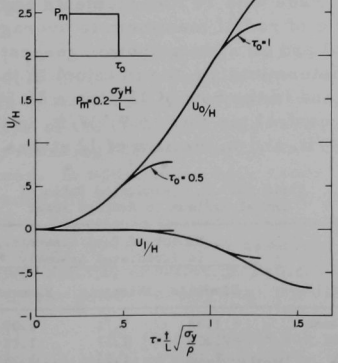

Fig. VIII.4

Hexagonal-can Plastic Deformation as a Function of Time for Pressure Pulses of Various Durations. U_0 = deformation at center of can wall, U_1 = deformation at corner, H = wall thickness, L = length of side of hexagon, P_m = applied pressure, t = time, τ = dimensionless time, τ_0 = duration of pulse, ρ = density, and σ_y = yield stress.

C. Fuel-element Failure Propagation. B. D. LaMar and R. O. Ivins (02-116)

1. In-pile Studies. R. O. Ivins and C. Bolta (Last reported: ANL-7776, pp. 104-106, Jan 1971)

a. Planning and Design of Experiments

A revised set of loop system design requirements is being developed. For the revised design requirements, several analyses and calculations are being performed to examine the needed simulation of FTR conditions for tests to be conducted in the FEFP loop.

Calculations have been made to compare the effects of filters in the design of the Fuel Element Failure Propagation Loop. Calculations were made for 7, 19, and 37 fuel elements. In each of the above calculations, results were found for the following cases: no neutron filter, an outside 40-mil-thick cadmium filter, an inner filter 0.125 in. thick of 2% natural boron in stainless steel, both the outer cadmium and inner boron filter, and an inner 40-mil-thick cadmium filter. When the boron filter was not used, it was replaced with sodium, and steel replaced the cadmium when no cadmium filter was required. Table VIII.1 lists the fuel-element enrichments. Tables VIII.2 and VIII.3 summarize the results of the calculations for various filter arrangements.

Conclusions that can be drawn thus far are: (a) Either the cadmium or boron filter alone would be sufficient to adequately flatten the average power, (b) using both filters gives the best power flattening, and (c) moving the location of the cadmium filter does not significantly change the power flattening or average linear power.

Additional calculations were made with 19 fuel elements and no filters. A final calculation gave a ratio of radial maximum to average fission power in the test assembly of 1.30 and an average power generated in a fuel element of 16.6 kW/ft. In this determination, the uranium in the row of six pins had a 69.4% enrichment, and in the row of 12 pins a 26.5% enrichment. The average power in each central pin was 15.9 kW/ft, in the elements of the row of six it was 16.9 kW/ft, and in the row of 12 it was 16.5 kW/ft.

TABLE VIII.1. Enrichment of Fuel Elements

Location of Fuel Elements	Enrichment, %		
	7 Elements	19 Elements	37 Elements
Center	93	93	93
Row of 6	78	80	82
Row of 12	--	65	70
Row of 18	--	--	55

TABLE VIII.2. Calculated Ratio of Radial Maximum to Average Power

Filter	Number of Fuel Elements in Irradiated Assembly		
	7 Elements	19 Elements	37 Elements
None	1.38	1.71	1.90
Cd	1.08	1.17	1.17
B	1.12	1.23	1.25
Cd and B	1.06	1.13	1.12
Cd inside	1.07	1.14	1.14

TABLE VIII.3. Calculated Average Linear Power

Location of Fuel Elements	Average Linear Power, kW/ft, with Various Filter Arrangements				
	None	Cd	B	Cd and B	Inside
With 7 Fuel Elements in Assembly					
Center	21.0	15.8	14.5	12.6	15.4
Row of 6	37.1	15.8	15.4	12.1	15.1
Average	34.6	15.8	15.2	12.2	15.1
With 19 Fuel Elements in Assembly					
Center	14.0	11.4	10.5	9.5	11.2
Row of 6	14.4	10.6	9.9	8.7	10.3
Row of 12	26.6	11.1	10.3	8.8	10.7
Average	22.0	11.0	10.7	8.8	10.6
With 37 Fuel Elements in Assembly					
Center	10.9	8.9	8.5	7.7	8.9
Row of 6	10.2	8.3	8.0	7.1	8.4
Row of 12	10.8	8.1	7.8	6.8	8.0
Row of 18	21.2	8.5	8.8	6.8	8.2
Average	15.8	8.3	8.2	6.9	8.2

The power densities reported previously (ANL-7776) and those calculated in the matrix of 15 cases (reported here), considering various numbers of fuel elements and various neutron filters, were based on an ETR core volume of 544 liters (an ETR core radius of 43.5 cm), giving an average power density of 0.322 MW/liter. ETR has a core volume of 354 liters (an ETR core radius of 35.1 cm), giving an average power density of 0.494 MW/liter. The ETRC experiment obtained an average power density of about 0.613 MW/liter in the region surrounding the experiment. With power peaking, a value around the experiment of 0.824 MW/liter might be obtained.

A calculation was performed using both a 43.5- and a 36.0-cm-radius core. The ratio of core volumes was 1.460. The ratio of the fraction of total fissions in the test region to total core fissions was 1.441. The shape of the neutron-energy spectrum in the region of the core immediately surrounding the test region was almost equivalent for both core-radius cases. In addition, in both cases, there was not significant power peaking around the test region. Thus, a good assumption is that the test linear power density is directly proportional to the average core power density. Thus, for the dual-filter case, the results can be modified for average core power density as shown in Table VIII.4. As can be seen, significant increases in linear power density over the values given in Table VIII.3 can be expected.

To form a basis for calculating the actual experiment power densities that can be obtained in FEFPL, experiments must be performed in the ETR critical facility. The experiments are to be performed using FTR-type fuel elements and a realistic mockup of the in-core portion of the FEFPL.

TABLE VIII.4. Modified Linear Power for Dual-filter Case

Enrichment; location	Average Linear Power, kW/ft, for Three Core Power Densities		
	0.322 MW/ℓ (calculated)	0.494 MW/ℓ (actual ETR)	0.613 MW/ℓ (critical)
93%; center	7.7	11.9	14.7
82%; row of 6	7.1	10.9	13.5
70%; row of 12	6.8	10.4	12.9
55%; outer row of 18	6.8	10.4	12.9

In general, a fuel element in a fast reactor can be expected to have a relatively uniform neutron flux in the fuel, and thus a relatively flat power generation. On the other hand, the same fuel element in a more thermalized reactor can be expected to exhibit self-shielding, giving a non-uniform flux in the fuel, and thus a skewed power generation in the fuel. This difference in internal power generation inside the fuel has suggested the use of a thermal-neutron filter to shape the neutron-flux energy spectrum inside a thermal reactor to more closely match that found in a fast reactor. To evaluate the importance of the neutron filter, calculations were made of the internal fuel-element temperatures for both flat and skewed internal fuel-power generations.

Under the assumption that the fuel element can be represented by a one-dimensional slab with no transverse heat transfer, and using both an exponential neutron flux and a flat neutron flux, only moderate differences in fuel temperatures (200°F) were obtained without a filter.

The effect of skewed power generation was also examined with respect to the surface heat flux and conductivity integral. A 10% skewing gave less than a 1/2% change in both the surface heat flux and conductivity integral.

In conclusion, power skewing is probably not as significant as previously suspected with respect to internal fuel-element temperatures and fuel restructuring. With the power flattening obtained by the dual neutron filter, quite good simulation of the fast-reactor environment can be obtained.

Additional improvements were made in the model and computer code used to simulate FEFPL transient thermal and hydraulic conditions. Specifically, changes were necessitated in the heat-exchanger representation when it was discovered that erroneous temperatures and energy balances occurred under conditions simulating mismatched mass flow rates of the coolants. The present improved model comprises four axial sections; temperatures are computed at five nodes in each relevant heat-exchanger material. Within the three fluids of the heat exchanger, the axial

temperature gradients were approximated using a mixed-differencing technique similar to that described by Gunby.* Results of steady-state calculations, representative of a variety of fluid flow rates, indicate satisfactory performance of the present model.

A similar treatment was also applied to modeling the active fuel and associated coolant. This improvement provides the capability for simulating nonuniform axial power profiles in the fuel and better resolution of potential thermal-crisis conditions in the coolant.

The foregoing changes in the FEFPL thermal-hydraulic model yield a net increase of 29 first-order differential equations plus a number of auxiliary algebraic relationships. The present version of the model now contains a total of 49 coupled differential equations, exclusive of those needed for control-systems simulation.

The model and the computer code that characterize sodium expulsion in the FEFPL continue to be developed. Equations of motion have been written for the two major fluid columns--one extending from the reservoir through the pump to the center of the test section, the other extending from the center of the test section to the reservoir through the heat exchanger. For these calculations, the loop was divided into approximately 40 regions. The equations treat two different methods for providing bypass coolant flow, i.e., that which does not pass through the test section.

If a neutron filter is located inside the loop primary containment, coolant flow between the test train and the flow divider must ensure continued cooling of the neutron filter. If a neutron filter is not located within the primary containment, bypass coolant might flow directly from the pump leg below the expansion device to the lower plenum of the heat exchanger. Estimates of the steady-state loop pressure drop for both types of coolant bypass of the test section have been made over a wide range of operating conditions. These data are needed as initial-condition information for the transient simulation of the FEFP loop using the Continuous System Modeling Program (IBM S/360-CSMP).

Pump operating characteristics under transient conditions, including reverse flow, have been estimated. These operating characteristics are included in the FEFP loop transient hydraulic model. Initial loop transient calculations have verified steady-state calculations. The transient calculations were performed for loop operation without coolant bypass of the test section. Loop operation with bypass flow will be simulated.

b. Loop Development

The ANL-INC task force preparing system-engineering requirements for the FEFPL began work. Features limiting the design of major

*A. L. Gunby, Intermediate Heat Exchanger Modeling for FFTF Simulation, BNWL-1367 (May 1970).

components of the system are being identified in view of functional range, physical-envelope restrictions, and facility operating restrictions. This information will be coordinated with experimental requirements to establish system capability.

Examination of a sodium-to-helium heat exchanger as an alternate to the present sodium-to-helium-to-water heat exchanger has continued. The helium supply rate might limit the performance of the two-fluid heat exchanger; the three-fluid heat exchanger is limited by available heat-transfer area. The existing helium system at the test-reactor site was designed for a gas-cooled experiment, and modifications to the system might be required to increase flow rate and pressure drop.

The annular linear-induction pump (ALIP) being tested at INC has been reworked to correct several deficiencies. An electrical imbalance was corrected by reversing one phase of the three-phase connection, and several mechanical problems were identified and corrected.

The model test-train design is being modified to accept a 37-pin fuel bundle instead of the original 19-pin bundle. Full-length FFTF pins will be used in the model.

Concept drawings of the hot-laboratory (FEF) handling equipment have been prepared. Studies of the cask requirements to interface with the test reactor and hot laboratory are continuing.

D. Fuel Dynamics Studies in TREAT. C. E. Dickerman (02-117)

1. Transient In-pile Tests with Ceramic Fuel. C. E. Dickerman (Last reported: ANL-7783, pp. 101-103, Feb 1971)

a. First Mark-II-loop Experiments (D1 and D2) on Effects of Release of a Small Amount of Molten Fuel, Using Pins with Local High-enrichment Sections

Preparation of the equipment for Test D1 has been completed. The pressure transducers, specified originally to be 1000-psi units, have been removed and replaced with 2500-psi units, which provide greater margin against diaphragm rupture. The transducer-to-loop seal was successfully leaktested with helium. A modification was made to the test train to limit the axial load it could exert on the loop closure in the event of excessive differential thermal expansion produced in a postulated accident. Following completion of this modification, the test train was installed in the loop. The main closure seal was successfully leaktested with helium. Pretest neutron radiography of the assembled equipment shows the test train to be properly seated in the loop. Pretest check of flow direction and instrument polarity have been completed.

The test specifications and safety analysis have been issued and safety review meetings held by the ICRS.

Test D1 is planned to take place as soon as final safety approval and availability of the TREAT control system permit. Experiment D1 requires operation of TREAT at a constant power for most effective results. The test is to be run using the new TREAT control system when it is available, which is expected soon.

2. Experimental Support. M. B. Rodin (Last reported: ANL-7783, pp. 103-104, Feb 1971)

a. Cask Fabrication

Material certifications for all materials for both casks have been received from the vendor and approved. (One cask was planned under this account; the other was added, at RDT request, to provide an increased general shipping capability.) All vendor quality-control and fabrication plans have been approved, except for one of the detailed procedures. An ANL inspector has visited the vendor's plant three times to witness critical production procedures and to verify quality-control measures. Delivery of the first cask is expected about June 1, 1971.

Before the Mark-II loop cask is ready, the existing 24-ton Yankee single-element cask will be used. The single-element shipping cask with its associated special-form container has been erected and opened for checkout. Certain features, principally external welds, have been inspected and found acceptable. As received, the cask was free of loose contamination on the external surfaces, but some was found on the exposed surfaces under the lid. This has been cleaned down to a safe working level. However, the special-form container was not removed from the cask, and it is assumed that some contamination remains in the cask cavity, but we believe that this remaining contamination will not interfere with handling of loops.

A trial assembly with a Mark-II loop has been made with the special-form container, but a bearing block of the clamping mechanism protrudes enough to prevent the loop from fully entering the cavity. After this is corrected, the special-form container will be checked to confirm that it can be properly closed with a loop inside.

b. Preparation of Last Six Mark-II Loops from FY 1970 Stocks

The Mark-II A4 integral loop assembly was completed and delivered for outfitting.

Assembly operations on the Mark-II 5A and 6A loop body weldments were suspended for lack of funds. The operations are limited to

preparing closure tubes for installation on both loops and preparing the pump flanges for installation on the A6 loop.

The ALIP A4 stator has been mechanically assembled. The final closure welds and inspection tests are scheduled for completion next month.

A new holder for the L2 test section is being designed to incorporate a prototype void-detection system. A layout has been completed, and detail design is proceeding. Purchase orders for long-lead items (metal-sheathed electrical conductors and thin-wall stainless steel tubing) have been initiated.

c. Preparation of Advanced Mark-II Loops for Use in Future Tests

The revised layout for the Mark-IIC (stretched Mark-II loops) has been completed. The layout is being reviewed by the experimenters before detailed design drawings are begun.

d. Preparation of Handling Equipment for Routine Alpha-cave Operations on Mark-II Loops

The transfer port for handling Mark-II sodium loops at the FEF glovebox has been given a preoperational checkout for proper operation. After being crated, it and the loop support table will be shipped to FEF for installation and final checkout.

3. Analytical Support. A. B. Rothman (Last reported: ANL-7783, pp. 104-106, Feb 1971)

a. Analysis of Transient In-pile Experiments

Experiment D1 is the first of the D series of experiments intended to investigate the actual fuel-release phase in studies of the behavior of small amounts of molten-oxide fuel released from a failed pin into the flowing liquid-sodium coolant. Survey-type fuel-pin performance calculations using the SAS1A-ASH code were reported (see Progress Report for September 1970, ANL-7742, pp. 138-140) for a "flattop" power rating of 40 kW/ft in the localized enriched-fuel section of the central pin of a seven-pin cluster arrangement. This power rating is about 23% higher than the 20% reactor overpower condition of FFTF. Therefore, results of SAS1A-ASH calculations for a power rating and experimental conditions representative of FFTF for two different transients are reported here.

Descriptions of the test pin and calculational procedure are in ANL-7742. Present calculations are based on an experimental calibration factor of 7.47 J/g of UO_2 for the 93%-enriched fuel section and 3.36 J/g of

UO_2 per MW-sec of TREAT energy for the 26%-enriched fuel, which differ appreciably (~15-20%) from the SNARG-2D-calculated values used earlier.

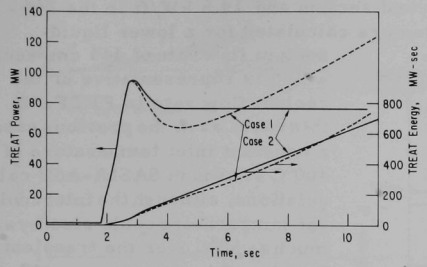

Fig. VIII.5. Point-kinetics-calculated Power and Energy Profiles

The first power transient (Case 1) considered corresponds to a reactivity step insertion of k_{ex} = 0.01 plus a ramp of 0.0034/sec at the peak power. The point-kinetics-calculated TREAT power and energy profiles are shown in Fig. VIII.5. Note that the temperature-feedback effect pulls down the power level to 64 MW from a peak power of 95 MW before the effect of reactivity-ramp insertion is felt. Results of SAS1A-ASH calculations for a liquid-sodium flow rate of 560 cm/sec at a constant inlet temperature of 400°C are shown in Fig. VIII.6. As expected, different temperature profiles follow the general trend of the power transient. More than 60% of the enriched UO_2 is estimated to be molten at the transient time of 12.8 sec, which corresponds to an integrated TREAT power of 1000 MW-sec. The centerline fuel temperature is calculated to be well in excess of its boiling point (~3550°C at STP) by neglecting fuel vaporization. In reality, the fuel temperature is not expected to exceed its boiling point, because the heat of vaporization is about 1800 J/g of UO_2. Both cladding and coolant are relatively cold. The strength of the stainless steel tube is demonstrated by a relatively small deformation (0.016 cm/cm at 11.0 sec) in the hot section of fuel. The effect of fuel vaporization, which is not considered in the SAS1A code, would be important in terms of loading on the cladding. At any rate, by the mere virtue of a large amount of fuel melting, it appears likely that the central pin would fail due to molten-fuel interaction with the cladding.

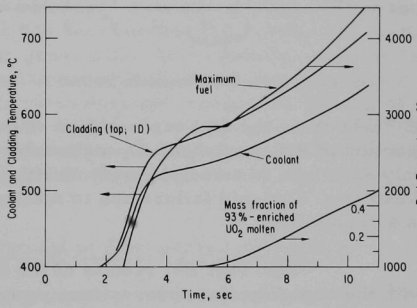

Fig. VIII.6. Calculated Parameters for Case 1

The second power transient (Case 2) considered here is similar to the first one, except that the reactivity-ramp insertion rate is 0.4%/sec and the feedback control system is used at 4.0 sec, so that a constant reactor power of 76 MW is attained (see Fig. VIII.5). This type power transient is perhaps more desirable to simulate the steady-state operation of the

FFTF reactor, granting, of course, that a fresh fuel pin is used here rather than a preirradiated element. Central-pin power for this constant power level is 32.4 kW/ft in the 93%-enriched section and 14.6 kW/ft in the 26%-enriched region. Fuel-pin conditions are calculated for a lower liquid-sodium flow rate of 445 cm/sec, which is representative of the coolant flow rate in FFTF. In this case, as in the previous case, a constant inlet temperature of 400°C is used in SAS1A-ASH calculations, although the inlet coolant temperature could rise by as much as 50°C over the transient. Results of temperature profiles and mass fraction of molten UO_2 in the hot section are shown in Fig. VIII.7. Note that all curves tend to reach their asymptotic values. Here again, the cladding is rather cold and strong--the maximum calculated strain is only 0.012 cm/cm. The fuel peak temperature in this case does exceed its boiling point by about 400°C because the fuel vaporization effect has been neglected. The maximum fraction of 93%-enriched UO_2 molten during the transient is calculated to be only 32%, i.e., to a radial extent of 56% or up to 0.14 cm of its radius of 0.246 cm. Fuel-pin failure due to molten-fuel interaction with the cladding is a possibility.

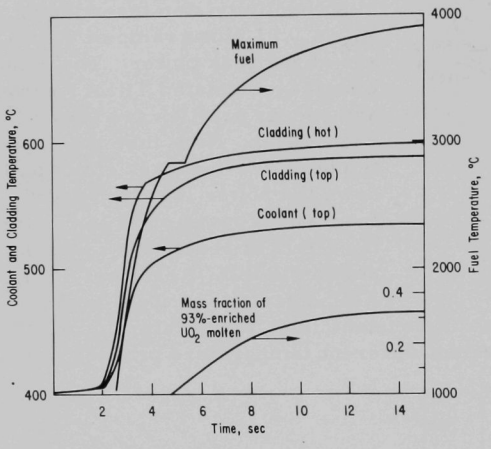

Fig. VIII.7. Calculated Parameters for Case 2

For Test E4, results of the SAS1A-ASH code were compared with the experimental observations reported previously. (See Progress Report for January 1971, ANL-7776, pp. 107-109.) Test E4 is the first Mark-II-loop experiment on fuel movement in the failure of a mixed-oxide fuel element during a power-excursion accident. The SAS1A-ASH code uses a two-phase slip-flow model for coolant hydrodynamics. Although this coolant-hydrodynamics module predicted the initial time for the onset of sodium boiling, the calculated rate of void growth was lower by a factor of two. Calculations for this test have been repeated with the currently incorporated slug-ejection coolant module in the SAS code system. Preliminary results indicate the initiation of sodium boiling at about 1.5 cm below the top of the mixed-oxide pellet at 1.9644 sec, which is roughly 15 msec later than the time predicted by the SAS1A-ASH code. This discrepancy is associated with the assumption of constant power generation across the test pin in the current calculations.

Figure VIII.8 shows preliminary results for the formation and destruction of sodium vapor bubbles for 50°C superheat with an initial

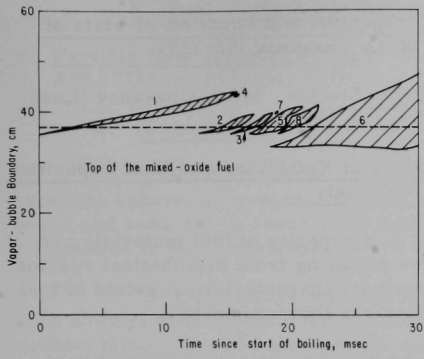

Fig. VIII.8. Preliminary Results of Slug-ejection Coolant Module for Test E4

liquid-film thickness of 0.03 cm. The initial vapor bubble (slug) is formed at about 1.5 cm below the top of the fuel. This bubble is pushed upward into the cooler plenum region. An intermediate liquid slug is created when a second vapor bubble is formed below the first one. The vapor pressure in the lower vapor bubble exceeds that in the upper one, so the intermediate liquid slug is accelerated upwards, until the upper vapor bubble collapses. In addition to creation and collapse of these large bubbles, some 10-12 smaller bubbles are also formed and destroyed almost instantaneously. A pressure pulse should be associated with each bubble collapse. The time of the first bubble collapse cannot be compared directly with the time of the first measured pressure spike (~1.978 sec) because the present calculations are based on uniform radial power generation. More detailed analysis is under way. These calculation results were obtained with the current version of the multiple-bubble model, which does not incorporate effects of pressure gradients within a bubble or friction between vapor and liquid film on the cladding and walls. Those effects (now being incorporated into SAS under Accident Analysis and Safety Evaluation) might make significant differences.

b. Evaluation and Development of Fuel-movement Models

Analyses of in-pile experiments performed using the DEFORM module of SAS have been reviewed.

E. High-temperature Physical Properties and Equation-of-state of Reactor Materials. M. G. Chasanov (02-119)

1. High-temperature Physical-property Studies. M. G. Chasanov (Last reported: ANL-7783, pp. 107-108, Feb 1971)

a. Experimental Determination of Enthalpies and Heat Capacities of Molten $(U_{0.8},Pu_{0.2})O_2$ Materials

Data on the enthalpy and heat capacity of fuel materials are needed to calculate fuel temperatures resulting from hypothetical reactor accidents. Evaluation of Doppler shutdown characteristics, extent of fuel melting, and cladding interactions requires this information.

The technique we are using to measure enthalpies and heat capacities is based on the method of mixtures. The encapsulated sample is equilibrated at the desired temperature and dropped into an adiabatic calorimeter. From the temperature rise of the calorimeter, the enthalpy of the sample plus the capsule can be calculated. Then the measurement is repeated with an empty capsule, and the enthalpy of the sample is found by difference.

The calorimeter system previously used for measurements of the enthalpy, heat of fusion, and heat capacity of UO_2 has been modified for work with $(U,Pu)O_2$ mixed-oxide fuel. However, before work was begun on the plutonium-containing material, an additional high-temperature measurement was performed at 3523°K with UO_2. All the data we have obtained on liquid UO_2, along with some of the higher-temperature values on solid UO_2, are shown in Fig. VIII.9. As can be seen, the highest temperature point is in good agreement with the other data. Also shown in the figure are the liquid data of Hein and Flagella,* which agree well with the present values. The heat capacity of liquid UO_2 determined from our data is 32.5 cal/mol-°K.

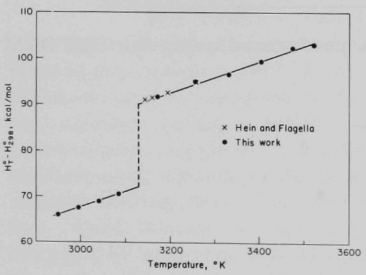

Fig. VIII.9. Enthalpy of UO_2 as a Function of Temperature

We have begun measurements on $(U,Pu)O_2$ mixed-oxide fuel and have completed experiments to 3041°K. We are evaluating the data and performing chemical and metallographic analyses on the heated samples.

*R. A. Hein and P. N. Flagella, GEMP-578 (1968).

F. Fuel-Coolant Interactions. R. W. Wright (02-164)

1. Particle Heat-transfer Studies. D. R. Armstrong (Last reported: ANL-7726, p. 159, July 1970)

a. Experiments Immersing Single Sphere in Sodium

The experimental study of transient-boiling heat transfer from tantalum spheres to sodium has been completed, and data are being analyzed and reduced. A theoretical model that explains the sphere-sodium interaction is being developed.

In a qualitative way, the experimental results show that stable film boiling, under natural-convection conditions, takes place when the sodium temperature is above 850°C and the surface temperature is above 1550°C. As the surface temperature drops below that level, the sodium film breaks and transition boiling takes over.

The magnitude and frequency of the pressure pulses constitute a useful means for identifying the various boiling regimes. In this manner, the onset of transition boiling is easily described. The same phenomenon was also observed in preliminary experiments in water using stainless steel spheres.

Violent transition-type boiling with expulsion of sodium occurs when the sodium temperature is in the range of 750-840°C and the initial sphere temperature is about 2300°C. At sodium temperatures below 830°C, transition boiling lasts only a short time and is followed by nucleate boiling.

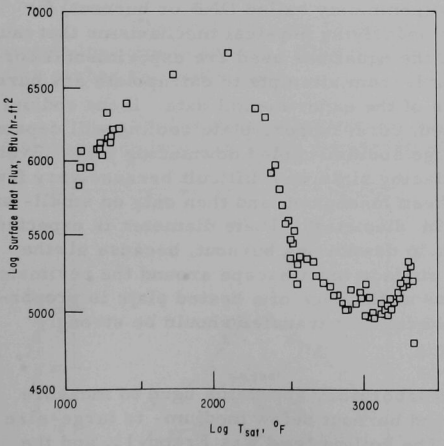

Fig. VIII.10. Surface Heat Flux from Tantalum Sphere to Sodium. The sodium was at 1607°F (875°C); initially, the 1.00-in.-dia sphere was at 3894°F (2145°C).

A finite-difference technique was used to solve the heat equation and obtain the temperature distribution in the sphere as a function of time. The surface heat flux and heat-transfer coefficient are calculated using the temperature distribution. The results from one of the runs in which stable film boiling took place are shown in Fig. VIII.10. The surface heat flux is plotted against log T_{SAT}, where T_{SAT} is the difference between the sphere-surface temperature and the

saturation temperature of sodium. The three boiling regimes (film boiling, transition boiling, and nucleate boiling) are apparent in the figure.

G. Post-accident Heat Removal. R. W. Wright (02-165)

1. Core-debris Retention within the Reactor or Guard Vessel. R. P. Anderson and L. Bova (Last reported: ANL-7776, pp. 122-123, Jan 1971)

a. Experiments

One of the major unknown factors in evaluating meltthrough of the core debris from a reactor accident is the ability of containment vessels and plates to transfer heat downward into a coolant beneath the plate. Whether the debris bed will melt through the core support plate depends on the balance between the heat conducted into the plate from the debris and the heat lost from the plate to the coolant. Heat-transfer calculations (see Progress Report for April-May 1970, ANL-7688, p. 248) show that, 4 hr after an accident, the coolant needs to dissipate about 100,000 Btu/hr-ft^2 from the plate bottom to prevent melting. With sufficient bypass coolant flow, this heat load can be transferred by natural convection. If the bypass flow is insufficient, the sodium in the plenum will slowly heat up and eventually begin to boil. After boiling starts, the integrity of the support plate will depend on the maximum boiling heat-transfer rate.

Numerous equations have been proposed for calculating maximum boiling heat-transfer rates (commonly called DNB or burnout) for various conditions. Because the underlying physical mechanisms that cause burnout are not well understood, the equations used are experimental correlations. Large errors can result from attempts to extrapolate any burnout equation far beyond the range of the experimental data. If the sodium saturation temperature is reached, core-support-plate cooling will depend on the burnout heat flux for a large sodium-cooled downfacing plate. Evaluating the effect of a large downfacing plate was difficult because very few downfacing burnout points have been measured, and then only on small- and medium-size heated plates ($\leq$2-in. diameter). Plate diameter is expected to be a major determining factor in downfacing burnout, because all the vapor generated over the entire surface must escape around the perimeter. Since the average vapor thickness at the edge of a heated plate is proportional to the diameter, the peripheral heat transfer should be strongly decreased in large plates.

Figure VIII.11 shows laboratory apparatus used to measure downward boiling heat transfer and burnout below medium- to large-size plates (2-in. to 2-ft diameter). The boiling fluid was Freon-11, and the heat was supplied by circulating hot water across the top of the plate.

A flow distributor provided an adequate supply of hot water to all portions of the plate, and maximum temperature deviation across the plate was kept below 2°C.

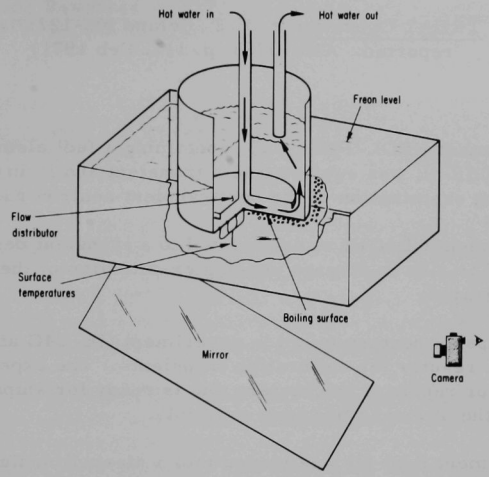

Fig. VIII.11. Experimental Apparatus for Measurement of Downfacing Heat Transfer

The heat flux was back-calculated from the rate of Freon weight loss due to boiling. This method necessarily gives an average heat flux across the whole plate.

Preliminary experimental results are shown in Fig. VIII.12. The heat-removal capability decreased strongly with increasing plate

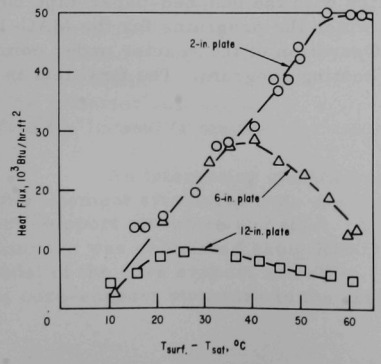

Fig. VIII.12

Boiling Heat Flux vs Difference between Surface Temperature and Saturation Temperature for Freon-11 for Plates of Three Diameters

diameter. For the 2- and 12-in. plates, the maximum heat flux was proportional to the reciprocal of the plate diameter. These initial results show that boiling beneath large plates is an inefficient cooling mechanism.

H. TREAT Operations. J. F. Boland (02-122; last reported: ANL-7783, p. 111, Feb 1971)

1. Operations

Experiment HEDL-PNL-2-10, containing a fuel element previously irradiated in EBR-II, was subjected to a transient and is in storage at TREAT pending examination of the posttransient neutron radiographs.

Experiment GE-C4H was subjected to a transient designed to cause pin failure and is also in storage pending examination of the posttransient neutron radiographs.

The capsule heaters failed in experiment GE-C4G after it had been loaded into the reactor for calibration transients. The experiment was returned to GE for repair of the heaters and is ready for shipment back to TREAT when the T-2 cask becomes available.

Experiment RAS-D1 was loaded into a Mark-II sodium loop, radiographed, and placed in storage until the automatic power-level control system becomes operational.

Neutron radiographs were made of elements from EBR-II experimental subassemblies X054 and X108.

a. Automatic Power Level Control System

Computer control of the hydraulic rod-drive system was found satisfactory during preoperational tests. Completion of this phase of system checkout was delayed by difficulties with the punched-paper-tape output from the central IBM 360 system (on which the programs for the MAC-16 computer at TREAT are compiled). Operation of the reactor under computer control is the next phase of the testing program. The first test is scheduled for early April.

I. Reactor System and Containment Structural Dynamic Response. S. H. Fistedis (02-126)

1. Hydrodynamic Response of Primary Containment to High-energy Excursion. Y. W. Chang (Last reported: ANL-7776, pp. 124-134, Jan 1971)

a. Parametric Studies of System Geometries and Excursion Magnitudes and Durations to Assist FFTF Accident Analysis. T. J. Marciniak, J. Gvildys, and Y. W. Chang (Last reported: ANL-7776, pp. 124-125, Jan 1971)

As part of an FFTF postaccident heat-removal (PAHR) study, the condition of the reactor internals following a postulated flow coastdown accident was evaluated. The accident analyzed a zone involving approximately 60% of the core in which 60% of the fuel was melted. Sodium was assumed to be present in the zone due to reentry and was mixed with the molten fuel. The P-V curve for this zone was determined using two models:

(1) A modified Hicks-Menzies calculation, in which molten fuel is mixed with the coolant and reaches thermodynamic equilibrium. The sodium is allowed to expand adiabatically to about 11 atm while decoupled thermodynamically from the fuel. The total work calculated was 152-MW-sec.

(2) A finite-rate heat-transfer model with sodium expansion to about 10 atm, in which the total work done is 27.2 MW-sec.

A model was devised to use REXCO-H radial strain data in the originally unaffected core region to evaluate the amount of flow blockage during the calculation. Since the REXCO-H code is based on a hydrodynamic model, the deformation in the region of the fuel and reflector subassemblies is conservative in that the mechanical strength of these structures is ignored. However, the regions are represented by P-V curves which take into account all the materials present in a subassembly in their correct proportions and weight, so that inertia effects are considered correctly. Results show that flow blockage in a subassembly may be expected at about 8 msec in Model 1 and at 16 msec in Model 2. Deformations in the region of the reflector subassemblies indicate possible shear of the flow tubes on which the Inconel is stacked and subsequent blockage of these areas.

An interesting application of REXCO-H and the NASTRAN finite-element structural code was made in evaluating the response of the core-support structure and skirt. A load-time history on the core-support structure was calculated using REXCO-H, and this was applied to a NASTRAN model of the core support and skirt. Of prime interest was the deflection of the core-support structure in the region of the support lugs. Calculations

indicate that although the dynamic loading did exceed the static yield load in the core-support skirt, it was for very short times and the structure will survive the postulated accident. Deflection of the core support at the lugs was about 0.02 in.

Since the time of the completion of this study in which the load-time history was hand-integrated over the surface of the core support structure, a feature has been added to the program which allows direct integration and graphical output of the loading.

A detailed report has been prepared as part of the postaccident heat-removal study.

b. Insertion of Heat Transfer into Codes. T. J. Marciniak (Last reported: ANL-7776, p. 133, Jan 1971)

Work is continuing on the inclusion of heat-transfer effects in postburst accident analysis on essentially two fronts. The first, and primary purpose, is to develop dissipative heat-transfer models; the second is concerned with the inclusion of pressure-producing heat-transfer phenomena.

The dissipative mechanisms would include conductive, radiative, and convective effects that would transfer heat energy from hot, high-pressure regions to relatively cool regions, thus reducing the amount of work damage to the reactor structure. Of immediate concern would be mechanisms that would transfer heat from the hot, high-pressure core region, whether the high-pressure vapor is fuel or sodium; of secondary concern would be condensation effects in the upper region of the reactor due to the presence of a large mass of relatively cool sodium and structural components. These condensation effects might reduce the damage potential of vessel-head movement and subsequent sodium spillage.

To incorporate these various modes of heat transfer into REXCO-H, numerical techniques compatible with the Lagrangian coordinate system must be devised. The most obvious mode amenable to such treatment is the heat-conduction equation in cylindrical coordinates, which is given as

$$\rho c \frac{dT}{dt} = k\left(\frac{\partial^2 T}{\partial r^2} + \frac{1}{r}\frac{\partial T}{\partial r} + \frac{\partial^2 T}{\partial z^2}\right). \qquad (1)$$

By application of the midpoint method, used in the development of the differencing technique for the REXCO-H hydrodynamic equations,* the

*Y. W. Chang, J. Gvildys, and S. H. Fistedis, Two-dimensional Hydrodynamic Analysis for Primary Containment, ANL-7498 (Nov 1969).

difference equations for the various quantities shown in the parentheses on the right side of Eq. (1) are given as follows (for clarification of the nomenclature, see Fig. VIII-13:

$$\left(\frac{\partial T}{\partial r}\right)_{I,J} = \frac{1}{8A_{I,J}}\left[\left(T_{I,J} - T_{I-L,J-1}\right)\left(z_{I,J+1} + z_{I-1,J} - z_{I,J-1} - z_{I+1,J}\right)\right.$$

$$\left. - \left(T_{I-1,J} - T_{I,J-1}\right)\left(z_{I,J+1} - z_{I-1,J} - z_{I,J-1} + z_{I+1,J}\right)\right], \qquad (2)$$

where

$$A_{I,J} = \frac{1}{8}\left[\left(r_{I,J+1} - r_{I,J-1}\right)\left(z_{I+1,J} - z_{I-1,J}\right) - \left(z_{I,J+1} - z_{I,J-1}\right)\left(r_{I+1,J} - r_{I-1,J}\right)\right], \qquad (3)$$

and

$$\left(\frac{1}{r}\frac{\partial T}{\partial r}\right)_{I,J} \simeq \frac{1}{4R_{cent}}\left[\left(\frac{\partial T}{\partial r}\right)_{I,J} + \left(\frac{\partial T}{\partial r}\right)_{I+1,J} + \left(\frac{\partial T}{\partial r}\right)_{I+1,J+1} + \left(\frac{\partial T}{\partial r}\right)_{I,J+1}\right], \qquad (4)$$

where R_{cent} is the centroidal radius of the cell. Extending the technique further yields

$$\left(\frac{\partial^2 T}{\partial r^2}\right)_{I,J} \simeq \frac{}{2A_{I,J}}\left\{\left[\left(\frac{\partial T}{\partial r}\right)_{I,J+1} - \left(\frac{\partial T}{\partial r}\right)_{I+1,J}\right]\left(z_{I+1,J+1} - z_{I,J}\right)\right.$$

$$\left. - \left[\left(\frac{\partial T}{\partial r}\right)_{I+1,J+1} - \left(\frac{\partial T}{\partial r}\right)_{I,J}\right]\left(z_{I,J+1} - z_{I+1,J}\right)\right\}. \qquad (5)$$

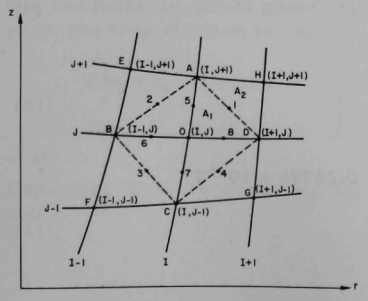

Fig. VIII.13. Typical Mesh Point (I,J), Illustrating Finite-differencing Notation

The term

$$\left(\frac{\partial^2 T}{\partial z^2}\right)_{I,J}$$

is derived in a similar manner.

To determine the validity of the set of difference equations in solving the conduction equation, a test case was defined for which an analytical solution and other numerical solutions exist. The test problem was defined as an infinitely long cylindrical steel rod of

radius a, with an initial uniform temperature of 1000°C with the wall held at 0°C. This transient problem was solved analytically and numerically by using the THTB heat-transfer code. The THTB and analytical solutions agreed very well. However, with the above differencing technique, comparable solutions were not obtained. Near the wall, the response was comparable, but near the centerline, the temperature apparently remained constant. A modification of the differencing technique might be needed because the Laplacian (the term in parentheses in Eq. 1) becomes identically zero for the central zone. Investigation of this fault is continuing.

Work has also resumed on the incorporation of a fuel-coolant interaction model into REXCO. One aspect of this work involves the development and inclusion of a two-phase equation of state for sodium that would allow for expansion of the liquid phase during heating, vaporization of sodium, and finally expansion of the sodium vapor, all as part of a continuous calculational procedure. The equation of state for the liquid expansion has already been formulated. (See Progress Report for October 1970, ANL-7753, pp. 167-168.) Presented here is a technique for determining the quality and temperature of a sodium vapor-liquid mixture given the enthalpy and specific volume of the mixture.

The equations describing the two-phase sodium mixture are

$$h_g = 0.77881 \times 10^{11} - 6.14965 \times 10^{7}T + 0.43455 \times 10^{5}T^2 - 9.7274T^3, \quad (6)$$

$$h_f = -3.8566 \times 10^{10} + 8.13507 \times 10^{7}T - 0.4399 \times 10^{5}T^2 + 9.3842T^3, \quad (7)$$

$$P_{sat} = 1.01325 \times 10^{6}T^{-0.61344} \exp\left(15.3838 - \frac{12767.8}{T}\right), \quad (8)$$

$$v_g = 3.6132 \times 10^{6} \frac{zt}{P_{sat}}, \quad (9)$$

$$v_f = v_{\ell 0} \exp\left[\int_{T_0}^{T} \alpha(T)\, dT\right], \quad (10)$$

$$z = -0.97258 + 0.42417 \times 10^{-2}T = 0.28996 \times 10^{-5}T^2 + 0.55424 \times 10^{-9}T^3, \quad (11)$$

and

$$\alpha(T) = 0.21968 \times 10^{-3} + 0.81226 \times 10^{-7} + 0.97135 \times 10^{-11} T^2 + 0.68998 \times 10^{-15} T^3, \quad (12)$$

where T is temperature in °K, h_g is vapor enthalpy in dyne-cm/g, h_f is liquid enthalpy in dyne-cm/g, p_{sat} is saturation pressure in dyne/cm^2, v_g is vapor specific volume in cm^3/g, v_f is liquid specific volume in cm^3/g, z is the compressibility factor, and $\alpha(T)$ is coefficient of thermal expansion in °C^{-1}.

The specific volume and enthalpy of a liquid-vapor mixture of sodium are given as

$$v = xv_g + (1 - x) v_f \quad (13)$$

and

$$h = xh_g + (1 - x) h_f, \quad (14)$$

where x is the quality of the mixture. The known quantities in the above at any given iteration of REXCO-H are the specific volume and the enthalpy. The unknown quantities are the quality and temperature of the mixture. To solve the set of equations, a Newton-Raphson technique for a set of two nonlinear algebraic equations has been applied.

In general, if one has two simultaneous nonlinear equations of the form

$$\left.\begin{aligned} F(x,T) &= 0, \\ G(x,T) &= 0, \end{aligned}\right\} \quad (15)$$

one can make an initial guess (x_0, T_0) as the solution of the equations. However, the true solution is $(x_0 + \delta_0, T_0 + \epsilon_0)$, so that

$$\left.\begin{aligned} F(x_0 + \delta_0, T_0 + \epsilon_0) &= 0; \\ G(x_0 + \delta_0, T_0 + \epsilon_0) &= 0. \end{aligned}\right\} \quad (16)$$

Expanding Eqs. 16 about (x_0, T_0) and neglecting higher-order terms, one gets

$$\left.\begin{aligned} F(x_0 + \delta_0,\ T_0 + \epsilon_0) &= F(x_0, T_0) + \delta_0\left(\frac{\partial F}{\partial x}\right)_0 + \epsilon_0\left(\frac{\partial F}{\partial T}\right)_0 = 0; \\ G(x_0 + \delta_0,\ T_0 + \epsilon_0) &= G(x_0, T_0) + \delta_0\left(\frac{\partial G}{\partial x}\right)_0 + \epsilon_0\left(\frac{\partial G}{\partial T}\right)_0 = 0. \end{aligned}\right\} \quad (17)$$

It is straightforward to solve Eqs. 17 for δ_0 and ϵ_0 and make a second guess $(x_1, T_1) = (x_0 + \delta_0, T_0 + \epsilon_0)$. One can continue this process until one gets sufficiently close to the solution for a given error criterion.

By application of the above to Eqs. 13 and 14, one gets

$$F(x,y) = v - xv_g - (1 - x)\, v_f = 0$$

and

$$G(x,y) = h - xh_g - (1 - x)\, h_f = 0. \quad (18)$$

It is straightforward to calculate $\partial F/\partial x$, $\partial F/\partial T$, $\partial G/\partial x$, and $\partial G/\partial T$ to solve for δ and ϵ.

Several test cases were run using the above technique; convergence was quite rapid for an error of 0.001 in quality and 1°C in temperature. For example, in an initial guess of (0, 273.1), the solution converged in eight steps to the correct x and T for a specific volume of 5882 cm^3/g and an enthalpy of 4.67×10^{10} dyne-cm/g (x = 0.489, T = 1030°K). It is expected that convergence will be much more rapid during an actual case because initial guesses will be closer to the solution.

The above subroutine has been added to the heat-transfer version of REXCO and is being debugged.

Development of the above models will be useful in calculating both dissipative heat-transfer phenomena and pressure-producing phenomena. The first model, that of conduction heat transfer, is a model numerically compatible with the present REXCO-H Lagrangian technique. It might be possible to apply thermal conductivities in the regions of contact between gaseous and liquid or solid phases that simulate the heat-transfer rate, if not the precise mechanism of energy transfer. The second model is useful in the overall program development, because it supplies a two-phase equation of state for sodium that can be used not only for pressure-producing phenomena, such as the fuel-coolant interaction, but also for dissipative phenomena, such as condensation of sodium vapor in relatively cold regions, as in the sodium pool above the reactor core.

c. General Improvement of Codes. Y. W. Chang (Not previously reported)

The constitutive relations used in the REXCO-H computer code have been improved. For elastic-plastic material, the Mises-Hencky yield criterion is used, namely,

$$\Phi = \sigma_\phi^2 - \sigma_\phi \sigma_\theta + \sigma_\theta^2 - \sigma_0 = 0,$$

where σ_ϕ and σ_θ are the principal stresses, and σ_0 is the yield stress of the given material under uniaxial stress conditions. Assume that, at time t^{n+1}, the stresses σ_ϕ^n and σ_θ^n, strains ϵ_ϕ^n and ϵ_θ^n, and strain increments $\Delta\epsilon_\phi^{n+1}$ and $\Delta\epsilon_\theta^{n+1}$ are known. To compute the stresses σ_ϕ^{n+1} and σ_θ^{n+1}, first the trial stresses are calculated from

$$\sigma_{\phi_T}^{n+1} = \sigma_\phi^n + \frac{E}{1 - \nu^2}\left(\Delta\epsilon_\phi^{n+1} + \nu\Delta\epsilon_\theta^{n+1}\right)$$

and

$$\sigma_{\theta_T}^{n+1} = \sigma_\theta^n + \frac{E}{1 - \nu^2}\left(\Delta\epsilon_\theta^{n+1} + \nu\Delta\epsilon_\phi^{n+1}\right),$$

where E is Young's modulus and ν is Poisson's ratio. Then the trial stresses are substituted into the above yield function to produce

$$\Phi_T^{n+1} = \left(\sigma_{\phi_T}^{n+1}\right)^2 - \left(\sigma_{\phi_T}^{n+1}\right)\left(\sigma_{\theta_T}^{n+1}\right) + \left(\sigma_{\theta_T}^{n+1}\right)^2 - \sigma_0^2.$$

If $\Phi_T^{n+1} < 0$, there has been no plastic flow and the stresses are simply their trial values. If Φ_T^{n+1} is greater than or equal to zero, plastic yielding has occurred and the stresses are

$$\sigma_\phi^{n+1} = \sigma_{\phi_T}^{n+1} - \bar{\lambda}\left(\bar{\sigma}_\phi^n + \nu\bar{\sigma}_\theta^n\right)$$

and

$$\sigma_\theta^{n+1} = \sigma_{\theta_T}^{n+1} - \bar{\lambda}\left(\bar{\sigma}_\theta^n + \nu\bar{\sigma}_\phi^n\right),$$

where

$$\bar{\sigma}_{\theta}^{n} = \left(2\sigma_{\theta}^{n} - \sigma_{\phi}^{n}\right)$$

and

$$\bar{\sigma}_{\phi}^{n} = \left(2\sigma_{\phi}^{n} - \sigma_{\theta}^{n}\right),$$

and $\bar{\lambda}$ is calculated from

$$\bar{\lambda} = -\frac{B}{2A} + \left[\left(\frac{B}{2A}\right)^2 - \frac{C}{A}\right]^{1/2},$$

where

$$A = \left(\bar{\sigma}_{\phi}^{n} + \nu\bar{\sigma}_{\theta}^{n}\right)^2 + \left(\bar{\sigma}_{\theta}^{n} + \nu\bar{\sigma}_{\phi}^{n}\right)^2 - \left(\bar{\sigma}_{\theta}^{n} + \nu\bar{\sigma}_{\phi}^{n}\right)\left(\bar{\sigma}_{\phi}^{n} + \nu\bar{\sigma}_{\theta}^{n}\right),$$

$$B = -\left[\left(\bar{\sigma}_{\phi}^{n} + \nu\bar{\sigma}_{\theta}^{n}\right)\bar{\sigma}_{\phi_T}^{n+1} + \left(\bar{\sigma}_{\theta}^{n} + \nu\bar{\sigma}_{\phi}^{n}\right)\bar{\sigma}_{\theta_T}^{n+1}\right],$$

and

$$C = \Phi_{T}^{n+1}.$$

Preliminary results indicate that a better energy balance was obtained by using these constitutive equations, particularly when the containment vessel has undergone large deformations.

2. Dynamic Response of Core Subassemblies. J. M. Kennedy (Last reported: ANL-7776, pp. 133-134, Jan 1971)

a. Development of Mathematical Model

A model that accounts for material plasticity in the static case has been developed by using a layered-membrane concept; it is being modified to have capability in dynamic problems.

b. Use of NASTRAN Code

The MacNeal-Schwendler Corporation was consulted for information concerning troubles encountered with the various options and formats of NASTRAN needed for the modeling work. A better understanding of how material plasticity operates in the code was gained for static and dynamic transient analysis; the various ways it can be employed were discussed.

c. Experimental Verification of Mathematical Model.
J. M. Kennedy, T. J. Marciniak, and G. Nagumo

Preliminary tests have been initiated to provide experimental verification of the NASTRAN hexagonal-subassembly-can model for two cases. They are: (a) external loading across two flats and (b) internal pressure loading. An initial, exploratory test has been performed in which a 6-in.-long EBR-II hexagonal-can section was loaded across two opposite flats. One goal was to determine the yield point of the hexagonal can and determine deflection as a function of load. Initially, the hexagonal can was loaded to about 300 lb (Load 1) and released; a slight permanent set was taken by the specimen. The loading was repeated to 400 lb (Load 2) and again released; the permanent set increased, and there was indication that the yield strength was exceeded. Next, the load was increased to its maximum, 484 lb (Load 3), and continued until the deflection reached 0.3 in., an arbitrary deflection chosen for convenience, and then had dropped 4 lb. Figure VIII.14 shows the load-deflection curves for these three loading sequences.

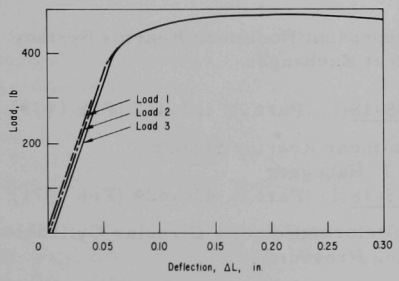

Fig. VIII.14

Load-deflection Curve for Hexagonal Cylinder Loaded across Flats. Deflection rate was 0.03 in./min.

Figure VIII.15 shows the deflection pattern for this particular hexagonal-can section. The deformation was quite symmetrical and followed the general shape predicted by NASTRAN. Upon inspection, it appeared that the basic assumption of rigidity at the corners is justified. For the next test, strain gauges will be placed at the positions indicated in order to quantitatively verify NASTRAN calculations.

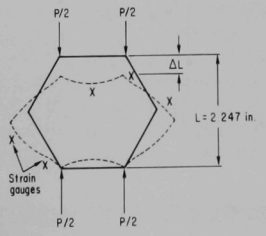

Fig. VIII.15

Hexagonal-can Deflection ΔL due to Total Load P Applied as Shown

PUBLICATIONS

DBLSCAT--A Computer Code for Double Scattering Corrections
A. K. Agrawal and S. G. Das
Nucl. Sci. Eng. 44, 113-114 (Apr 1971)

Bubble Growth and Collapse in Narrow Tubes with Nonuniform Initial Temperature Profiles
W. D. Ford
ANL-7746 (Dec 1970)

Spatial Effects in Transfer-Function Measurements of Large Nuclear Reactor Power Systems
L. J. Habegger and C. Hsu
IEEE Trans. Nucl. Sci. NS-18(1) (Part I), 418-425 (Feb 1971)

Experimental Study of a Gas Jet Penetrating a Liquid Coolant and Impinging on a Heated Surface
B. M. Hoglund, R. P. Anderson, and L. Bova
ANL-7734 (Mar 1971)

Lyapunov Stability of Spatially-Dependent Nonlinear Reactor System Including an External Primary Heat Exchanger
C. Hsu and L. J. Habegger
IEEE Trans. Nucl. Sci. NS-18(1) (Part I), 412-417 (Feb 1971)

Parameter Identification in a Nonlinear Reactor System
W. S. Roman, C. Hsu, and L. J. Habegger
IEEE Trans. Nucl. Sci. NS-18(1) (Part I), 426-429 (Feb 1971)

Correlating the Dynamic Plastic Deformation of a Circular Cylindrical Shell Loaded by an Axially Varying Pressure
C. K. Youngdahl
ANL-7738 (Oct 1970)

IX. ENVIRONMENTAL STUDIES

A. Thermal-plume Dispersion Studies. B. Hoglund (02-166)

1. Sinking-plume Experiment. B. Hoglund, G. Romberg, D. Nelson, S. Spigarelli, W. Prepejchal, and A. Frigo (Not previously reported)

The purpose of the sinking-plume experiment was to make exploratory measurements of the lake water temperature on the lake bottom to determine the degree to which this water might be heated as a result of a sinking thermal plume. The experiment is relevant to the behavior of waste-heat inputs during winter conditions. The Lake Michigan Enforcement Conference Technical Committee on Thermal Discharges has expressed concern* that "Bottom layering of warm water might occur over relatively large areas, having its chief effects on bottom fauna and the disruption of fish reproduction." The premature hatching of fish eggs resulting from exposure to warmer than normal ambient water is an item of particular concern.

The phenomenon of a sinking thermal plume occurs when the lake temperature is less than 39°F. The heated water discharged from the power plant entrains and mixes with the cold lake water. When the discharged and entrained water cools to 39°F, it achieves its maximum density, and gravitational forces cause it to sink through the colder, more buoyant lake water. This slightly denser mass of water should flow along the lake bottom until additional mixing further reduces the temperature.

The site chosen for the experiment was the Wisconsin Electric Power Company's Point Beach Nuclear Generating Plant, at Point Beach, Wisconsin. This plant utilizes a pressurized-water reactor to generate 500 MWe. The nominal condenser discharge flow is 270,000 gpm with a nominal temperature rise of 20°F. The instruments were placed in the lake on March 11 and 12. The lake temperature at that time was 0.5°C.

The experiment consists of placing 11 temperature recorders on the lake bottom in an area expected to be influenced by the thermal plume. (These instruments were obtained on loan from the Environmental Protection Agency, Great Lakes Region.) The instruments were bolted to 800-lb steel anchors, so the temperature sensor would be about 6 in. above the lake bottom. Nine of the instruments were placed in a 3 x 3 grid, slightly south of the plant, an area where the plume was observed to flow most often. Three instruments were placed in 15-ft-deep water, approximately 1000 ft offshore; three in 23-ft-deep water, approximately 2000 ft offshore; and three in 30-ft-deep water, approximately 3500 ft offshore. Two of the

*Recommendations of the Lake Michigan Enforcement Conference Technical Committee on Thermal Discharges to Lake Michigan (Jan 1971).

instruments were placed 2 miles north to provide measurements of ambient lake conditions. They were placed at depths of 20 and 30 ft.

The instruments were deployed by lowering them from a 90-ft vessel, the Telson Queen. A diver observed the placement of the instruments on the bottom to see that they were upright and not setting on rocks. While on the bottom, he described bottom conditions and reported seeing numerous crayfish, sculpins, and rocks covered with a dense growth of periphyton.

The temperature sensors are set to record the water temperature every 10 min for approximately 2 months. The position of the sensors was determined by triangulation from sightings from two surveyor's transits located on shore, about one-half mile apart.

Current plans are to recover the instruments during the first week in May.

2. Correlation of Far-field Plume Data. J. Asbury and A. Frigo (Not previously reported)

A phenomenological approach was adopted in attempting to find a relationship that would be used to predict lake-plume surface areas. The approach was based upon two considerations: (a) The behavior of lake plumes beyond the zone of flow establishment is governed by lake processes for which adequate models do not exist, and (b) there does exist a published set of lake-plume temperature measurements which can be examined for relationships among the plume variables.

Seven useful sets of plume data were identified during a literature survey. After examining the data, we concluded that they could be best displayed on an Edinger and Polk* type plot of θ/θ_0 versus A/A_n, where θ/θ_0 is the fractional excess temperature, A is the plume area within the θ isotherm, and A_n is a scaling area. The best parameterization for A_n was found to be $A_n = Q$, where Q is the volumetric discharge flow rate.

Figure IX.1 summarizes the results of the investigation. The data key for Fig. IX.1 is given in Table IX.1. All the buoyant-plume data are reasonably well described by the curve drawn through the data points. The curve thus represents a phenomenological fit relating fractional excess temperature to the quotient of plume surface area and volumetric-discharge flow rate.

*J. E. Edinger and E. M. Polk, Initial Mixing of Thermal Discharges into a Uniform Current, Report No. 1, Dept. of Environmental and Water Resources Engineering, Vanderbilt University.

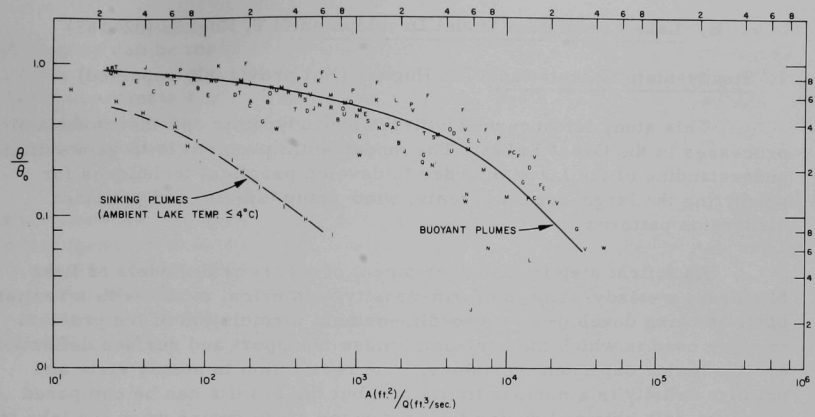

Fig. IX.1. Fractional Excess Temperature vs Surface Area/Flow Rate

TABLE IX.1. Data Key for Fig. IX.1

Data Points	Power Plant	Source
A,B,C,D,E	Waukegan, Illinois	Romberg et al.
F	Big Rock, Michigan	Krezoski
G,H,I	Millikan, N. Y.	Sundaram
J.K	Michigan City, Mich.	Ayers et al.
L	Waukegan, Illinois	Ayers et al.
M,N,O,P,Q R,S,T,U	Allen S. King, Minn.	Fitch
V,W	Douglas Point, Ontario	Csanady et al.

All the plume data shown in Fig. IX.1 refer to channel outfall geometries. The fit, therefore, may not be applicable to other outfall geometries in regions where $\theta/\theta_0 \gtrsim 0.5$. Allowing for this restriction, we believe that the curve represents a useful rule of thumb for predicting surface areas of thermal plumes in lakes.

B. Lake Circulation Model Development. T. Hughes (02-185)

1. Steady-state Calculations. T. Hughes (Not previously reported)

This study is concerned with the hydrodynamic and thermodynamic processes in the Great Lakes. The fundamental problem is to gain sufficient understanding of the lakes in order to develop practical techniques for predicting the large-scale currents, wind-setup effects, and pollutant dispersion patterns.

As a first step in the development of theoretical models of Lake Michigan, a steady-state, uniform-density, numerical model with a realistic basin is being developed. A two-dimensional formulation of the problem is being used in which the horizontal mass transport and surface deflections are the major dependent variables. The restriction to steady state and uniform density is a serious limitation, but the results can be compared with lake data obtained during the winter and early spring when the lake is essentially uniform and there are periods of steady winds. Motions in the system, driven by wind stresses, will be calculated using both idealized wind fields and also some examples from weather charts.

The major programs have been written, and the first circulation pattern has been calculated. A major problem has been to understand why the SOR (successive over-relaxation) iteration would not converge. This difficulty is basically due to the irregular region (Lake Michigan) in which the calculations were performed. There were three significant factors involved in eliminating this difficulty. (a) Standard methods for estimating the optimum SOR parameter gave a value such that the calculation did not converge. After many trials to determine whether there was a bug in the code, we found that the correct SOR parameter was much lower than the estimates. This can be explained by the irregular pattern in the linear equations needed to accommodate the Lake Michigan shoreline. (b) Difficulty occurs due to the differencing method used for certain first derivative terms. A change was made to "upwind" differencing rather than the usual centered differencing. (c) The accuracy of the values used for the bottom slope of the lake played an important role in the convergence of our calculations. We are currently exploring numerical smoothing of the bottom topography data.

To perform numerical calculations or hydraulic laboratory studies using a realistic basin for Lake Michigan, the shoreline and depths below mean water level must be conveniently available. What was needed was the intersections of the shoreline with a regular grid and the average depth at each grid intersection. The data were obtained from 13 major navigation charts covering Lake Michigan plus some field sheets obtained from the Corps of Engineers. A 2-min grid size was chosen (approx 5000 points) as appropriate to the density of sounding data on the charts and also to be consistent with the finest likely calculation grid.

The programs to produce the computer displays are about complete. A display can be made of any one of the forty-five 30- by 30-ft data blocks or any portion of the lake with linearly interpolated bottom contours. The basic coordinate system is minutes longitude and latitude. To properly account for the convergence of the meridians, a sinusoidal or Mercator equal-area map projection was incorporated into the routines.

The average depths at the 2-ft grid intersections are rather choppy, and questions concerning adequacy of representation and stability and convergence of numerical calculations have arisen. Numerical experiments to resolve this problem are being conducted utilizing the techniques in use to initialize data for numerical weather forecasting. This work will be reported upon at the 14th Great Lakes Research Conference in Toronto on April 21, 1971.

PUBLICATION

A Photographic Method for Determining Velocity Distributions within Thermal Plumes
J. G. Asbury, R. E. Grench, D. M. Nelson, W. Prepejchal, G. P. Romberg, and P. Siebold
ANL/ES-4 (Feb 1971)

B